

ÉCOLE DE TECHNOLOGIE SUPÉRIEURE
UNIVERSITÉ DU QUÉBEC

THÈSE PAR ARTICLES PRÉSENTÉE À
L'ÉCOLE DE TECHNOLOGIE SUPÉRIEURE

COMME EXIGENCE PARTIELLE
À L'OBTENTION DU DOCTORAT EN GÉNIE
Ph.D.

PAR
Daniel COUTU

CONCEPTION ET EXPLOITATION D'UNE STRUCTURE ACTIVE POUR UNE AILE
LAMINAIRE ADAPTATIVE EXPÉRIMENTALE

MONTRÉAL, LE 25 OCTOBRE 2010

© Tous droits réservés, Daniel Coutu, 2010

PRÉSENTATION DU JURY

CETTE THÈSE A ÉTÉ ÉVALUÉE

PAR UN JURY COMPOSÉ DE :

M. Vladimir Brailovski, professeur titulaire, directeur de thèse
Département génie mécanique à l'École de technologie supérieure

M. Patrick Terriault, professeur titulaire, codirecteur de thèse
Département génie mécanique à l'École de technologie supérieure

Mme Ruxandra Botez, professeure titulaire, présidente du jury
Département du génie de la production automatisée à l'École de technologie supérieure

M. Martin Viens, professeur titulaire, membre du jury
Département génie mécanique à l'École de technologie supérieure

M. Éric Laurendeau, membre du jury externe
Bombardier aéronautique

M. Jean-Yves Trépanier, examinateur externe indépendant
Département de génie mécanique à l'École polytechnique de Montréal

ELLE A FAIT L'OBJET D'UNE SOUTENANCE DEVANT JURY ET PUBLIC

LE 2 SEPTEMBRE 2010

À L'ÉCOLE DE TECHNOLOGIE SUPÉRIEURE

AVANT-PROPOS

Les Alliages à Mémoire de Formes (AMF) sont fascinants et peuvent être préparés pour manifester un comportement particulier en vue d'être mis en œuvre pour apporter une solution simple et efficace à un problème d'ingénierie.

Après mes études de premier cycle en génie mécanique, j'ai joint le Laboratoire sur les Alliages à Mémoire et les Systèmes Intelligents (LAMSI) afin d'y réaliser des travaux de maîtrise concernant des actionneurs utilisant la technologie des AMF. Passionné de l'aéronautique, ma principale motivation consistait à entrevoir la possibilité d'utiliser ces actionneurs pour modifier la forme d'une aile d'avion. Ces travaux ont mené à la mise en place d'une méthodologie de dimensionnement optimal des AMF. La méthode s'appuie sur un diagramme de design expérimental et elle a fait l'objet d'une publication à la conférence « ACTUATOR 2006 » en Allemagne (2006).

Puis, en octobre 2006, le projet CRIAQ 7.1 visant « l'amélioration de l'écoulement laminaire sur une voilure aéroélastique » a été inauguré officiellement (CRIAQ, 2006). Ce projet multidisciplinaire de grande envergure a été initié par le Consortium de Recherche et d'Innovation en Aérospatiale au Québec (CRIAQ) et fait intervenir différents partenaires et organismes subventionnaire tels que :

- **Partenaires industriels** : Bombardier Aéronautique et Thales Canada;
- **Partenaires universitaires** : École Polytechnique de Montréal (EPM), École de technologie supérieure (ETS-LAMSI et ETS-LARCASE) et
- **Partenaire institutionnel** : Institut de Recherche en Aérospatiale du Conseil National de Recherche du Canada (CNRC-IRA);
- **Organismes subventionnaires** : Conseil de Recherche en Sciences Naturelles et en Génie (CRSNG) et Consortium de Recherche et d'Innovation en Aérospatiale au Québec (CRIAQ).

Alors que l'EPM fut en charge de l'exécution des calculs aérodynamiques, le LABoratoire de Recherche en Commande active, avionique et en AéroServoÉlasticité de l'ÉTS (ETS-LARCASE) travailla à l'asservissement et au contrôle de l'aile. Le ETS-LAMSI et le CNRC-IRA se partagèrent le mandat de concevoir et fabriquer l'aile expérimentale au profil adaptatif en vue d'améliorer l'écoulement laminaire sur sa surface supérieure. Étant donné l'ampleur de la tâche, j'ai réalisé dès lors le passage accéléré de la maîtrise au doctorat afin de débuter la conception de la structure active destinée à procurer à l'aile expérimentale son comportement adaptatif désiré. Par le fait même, j'ai passé le relais du développement des actionneurs AMF au nouvel étudiant à la maîtrise, Thomas Georges. Dans la première année, il me fallut collaborer étroitement avec l'équipe de l'EPM qui procéda à de nombreuses simulations numériques en dynamiques des fluides afin de peaufiner le cahier des charges. Cette collaboration m'introduisit aux fonctionnalités du logiciel de simulation aérodynamique XFOIL. En parallèle, le LAMSI fabriqua un pré-prototype à l'aide d'associés de recherche et d'étudiants stagiaires pour se familiariser au concept de structure active et aux procédés de mise en forme. Ce pré-prototype fut également utilisé pour la validation d'un modèle d'éléments finis que j'ai développé afin de décrire le comportement structural de la structure active (Coutu *et al.*, 2007).

La diffusion des travaux et des résultats de cette recherche a fait l'objet de nombreuses publications à titre de premier auteur et de co-auteur. Les références sont fournies ci-dessous :

Revue scientifique (premier auteur)

Ces articles de revues, publiés ou sur le point de l'être, sont intégrés dans cette thèse sous forme de chapitres distincts :

- Coutu, D., V. Brailovski, P. Terriault, M. Mamou, Y. Mebarki, É. Laurendeau. « Real-Time Optimization of a Morphing Laminar Wing in a Wind Tunnel ». Version révisée soumise au *Journal of Intelligent Material Systems and Structures*, juillet 2010.

- Coutu, D., V. Brailovski, P. Terriault, M. Mamou, Y. Mebarki. « Aero-Structural Model for Morphing Laminar Wing Optimization in a Wind-Tunnel ». Version révisée soumise au *Journal of Aircraft*, juillet 2010.
- Coutu, D., V. Brailovski, P. Terriault. 2010. « Optimized design of an active structure for an experimental morphing laminar wing ». *Journal of Aerospace Science and Technology*, vol. 14, n° 7, p. 451-458.

Comptes rendus de conférence avec comité de lecture (premier auteur)

- Coutu, D., V. Brailovski, P. Terriault, M. Mamou, É. Laurendeau. 2009. « Real-Time Optimization of a Research Morphing Laminar Wing in a Wind Tunnel ». In *ASME Conference on Smart Material, Adaptive Structures and Intelligent Systems*. (Oxnard, USA, 21-23 sep. 2009).
- Coutu, D., V. Brailovski, P. Terriault, C. Fischer. 2007. « Experimental validation of the 3D numerical model for an adaptive laminar wing with flexible extrados ». In *Proceedings of 18th International Conference on Adaptive Structures and Technologies (ICAST '07)*. (Ottawa, Canada, 3-5 oct. 2007).

Note d'ingénierie (premier auteur)

- Coutu, D., V. Brailovski, P. Terriault. 2009. « Promising benefits of an active-extrados morphing laminar wing ». *Journal of Aircraft*, vol. 46, n°2, p. 730-731.

Revue scientifique (co-auteur)

- Georges, T., V. Brailovski, E. Morellon, D. Coutu, P. Terriault. (2009). «Design of Shape Memory Alloy Actuators for Morphing Laminar Wing with Flexible Extrados». *ASME Journal of Mechanical Design*, vol. 131, n°9.

Comptes rendus de conférence avec comité de lecture (co-auteur)

- Georges, T., V. Brailovski, É. Morellon, D. Coutu, P. Terriault. 2009. « Wind-tunnel testing of shape memory alloys actuators as morphing wing driving systems ». In *ASME*

Conference on Smart Material, Adaptive Structures and Intelligent Systems. (Oxnard, USA, 21-23 sept. 2009).

- Sainmont, C., I. Paraschivoiu, D. Coutu. 2009. « Multidisciplinary Approach for the Optimization of a Laminar Airfoil Equipped with a Morphing Upper Surface ». In *AVT-168 NATO Symposium on the Morphing Vehicles.* (Evora, Portugal, 20-23 avr. 2008).
- Sainmont, C., I. Paraschivoiu, D. Coutu, V. Brailovski, É. Laurendeau, M. Mamou, Y. Mébarki, M. Khalid. 2009. « Boundary Layer Behaviour on a Morphing Airfoil: Simulation and Wind Tunnel Tests ». In *Canadian Aeronautics and Space Institute AERO'09 Conference: Aerodynamics Symposium.* (Kanata, Ontario, 7-9 mai 2009).
- Brailovski, V., P. Terriault, D. Coutu, T. Georges, É. Morellon, C. Fisher, S. Bérubé. 2008. « Morphing laminar wing with flexible extrados powered by shape memory alloy actuators ». In *ASME Conference on Smart Material, Adaptive Structures and Intelligent Systems.* (Elicott City, USA, .28-30 oct. 2008).
- Georges, T., V. Brailovski, D. Coutu, P. Terriault. 2007. « Design diagram for linear SMA actuators integrated in a morphing wing structure ». In *Proceedings of the International Conference on Shape Memory and Superelastic Technologies (SMST'07).* (Tsukuba, Japon, 3-5 déc. 2007), p. 455-462.
- Mamou, M., Y. Mébarki, M. Khalid, M. Genest, D. Coutu, A.V. Popov, C. Sainmont, T. Georges, L. Grigorie, R.M. Botez, V. Brailovski, P. Terriault, I. Paraschivoiu, E. Laurendeau. 2010. « Aerodynamic performance optimization of a wind tunnel morphing wing model subject to various cruise flow conditions ». In *27th International Congress of the Aeronautical Sciences.* (Nice, France, 19-24 september 2010), paper 496.

REMERCIEMENTS

Je tiens à remercier en premier lieu le professeur Vladimir Brailovski qui m'a invité à faire le passage accéléré pour entreprendre des études doctorales afin d'œuvrer à la réalisation de l'aile adaptative, mandat confié à son laboratoire, le LAMSI. Son soutien constant et son soucis de l'excellence manifestés dans la direction de mes travaux m'ont aidé à soutirer le meilleur de moi-même. Je remercie également la présence du professeur Patrick Terriault au dynamisme inspirant. Ses interventions en tant que codirecteur ont toujours été grandement appréciées pour éclaircir et clarifier des idées et des concepts nouveaux.

Un merci particulier va à mon collaborateur immédiat Thomas Georges pour sa présence amicale, son aide technique valeureuse et son soutien moral. Je lui souhaite beaucoup de découvertes et de plaisir dans la poursuite de son projet de doctorat actuellement en cours. Ce bonheur de travailler au développement d'une aile adaptative aurait demeuré sur papier si ce n'eut été de la participation de professionnels de recherches doués et débrouillards : Charles Fischer, Sébastien Bérubé et Jean-Sébastien Ratelle. La contribution d'Émeric Morellon à titre d'étudiant en maîtrise est à souligner également, apportant une aide significative aux travaux d'expérimentation. Enfin, je remercie également tous les autres collègues du LAMSI qui m'ont permis de travailler dans un environnement favorisant l'entraide et stimulant la créativité : Vincent, Yannik, Pierre-Luc, Karina, Alexandre Dominique, Maxime et les autres de passage que je ne peux tous nommer. Je n'oublierai pas les bons rires qui ont résonnés entre les murs du LAMSI et ces « midis de qualité ».

Vue la multidisciplinarité de ma recherche, je me dois de remercier les collaborateurs universitaire de l'École Polytechnique de Montréal, Dr. Octavian Trifu et Corentin Sainmont tout comme ceux au Laboratoire de recherche en commande active, avionique et en aéroservoélasticité, professeure Botez (chef du projet CRIAQ 7.1) et Andrei Vladimir Popov. Enfin, je remercie également le personnel attitré aux essais en soufflerie au CNRC-IRA, en particulier Brian Jahraus, Youssef Mekarbi et Mahmoud Mamou pour leur aide. Du côté des industriels, je remercie Éric Laurendeau et Philippe Molaret pour leurs interventions

constructives aux réunions d'étape. D'un point de vue personnel, je remercie le support financier du FQRNT et de la Fondation J. Armand Bombardier de même que toutes les personnes qui se sont impliquées dans la préparation de mes demandes de bourse qui se sont avérées fructueuses.

Enfin, je tiens à ne pas passer sous ombre le support de ma famille, en particulier celui de mes parents qui m'ont toujours encouragé à foncer dans ce que j'aime, tant par leurs valeurs transmises que par leur dévouement. Finalement, un merci particulier va à ma chère Sandra pour sa présence aimante source de réconfort, d'équilibre et de bien-être dans l'accomplissement de ce travail.

CONCEPTION ET EXPLOITATION D'UNE STRUCTURE ACTIVE POUR UNE AILE LAMINAIRE ADAPTATIVE EXPÉRIMENTALE

Daniel COUTU

RÉSUMÉ

Cette thèse a contribué au succès du projet CRIAQ 7.1 démontrant la faisabilité d'une aile laminaire adaptative capable de réduire la consommation de carburant des avions. En particulier, les travaux de recherche ont permis la conception de l'aile expérimentale et son exploitation en soufflerie subsonique (nombres de Mach compris entre 0.2 et 0.3 avec des angles d'attaques compris entre -1 et 2°).

Tout d'abord, le principe d'adaptation de l'aile repose sur un laminé en matériau composite lié à un système d'actionnement permettant la modification géométrique de la surface supérieure de l'aile. Cette structure active fut conçue à l'aide d'une méthodologie de design spécialement développée pour les problèmes aéro-structuraux. Sous ANSYS, la méthode des éléments finis permit de modéliser les différentes configurations potentielles de structures actives. Le chargement aérodynamique appliqué de même que les profils cibles à reproduire ont été fournis par les collaborateurs de l'École Polytechnique de Montréal. Ensuite, le solveur aérodynamique Xfoil 6.96 a été employé pour évaluer l'augmentation du régime d'écoulement laminaire que chacune des configurations permettraient. Afin de poser le meilleur compromis entre la performance aérodynamique et l'énergie d'actionnement nécessaire, une optimisation multi-objective a été réalisée. Finalement, parmi les configurations offrant une performance aérodynamique stable, la structure composite constituée de 4-pli de renfort et de 2 lignes d'action a été retenue.

Par la suite, les travaux de recherche ont visé à exploiter le comportement adaptatif de l'aile, à savoir déterminer les courses optimales des actionneurs pour différentes conditions de vol testées. Ainsi, une fois le prototype fabriqué, le modèle structural a été revu, calibré et couplé au solveur aérodynamique afin de prédire avec précision le comportement aéro-structural en soufflerie. À l'aide d'un algorithme de recherche par motifs généralisés suivi d'un code pour raffiner la solution, les meilleurs profils adaptés ont été déterminés pour chacune des conditions d'écoulement. Ces efforts permirent de maintenir l'écoulement laminaire sur l'extrados à une distance supplémentaire moyenne de 25% de la corde de l'aile. Conséquemment, une réduction moyenne de 18.5% de la traînée de profil a pu être observée.

Malgré ces résultats satisfaisants, les limitations du modèle couplé ont été décelées lors de la comparaison des prédictions numériques avec la réponse expérimentale de l'aile en soufflerie. Pour cette raison, l'optimisation de la forme adaptée a été réalisée en temps réel (contrôle en boucle fermée) afin d'exploiter le plein potentiel de l'aile. Pour ce faire, la balance de la soufflerie a été employée afin de fournir instantanément une mesure de la

finesse de l'aile à l'optimiseur. Afin de minimiser le temps de recherche, l'algorithme d'optimisation spécialement conçu pour cette application commande des trajectoires de recherche minimisant les allers-retours des actionneurs. Aussi, pour accélérer la recherche, les prédictions du modèle couplé (boucle de contrôle ouverte) sont utilisées en tant que formes adaptées initiales. Ainsi, en comparaison avec l'approche en boucle ouverte, l'amélioration de la finesse de l'aile mesurée à la balance passa de 11 à 12.2% en moyenne. Également, pas plus de 4 minutes supplémentaires ont été nécessaires pour la convergence vers le profil optimisé en temps réel, ce qui est acceptable pour la durée d'un vol de croisière. Finalement, pour le bénéfice du projet CRIAQ 7.1, la réciprocité de la relation entre la finesse de l'aile et l'augmentation de l'étendue de l'écoulement laminaire a pu être confirmée expérimentalement à l'aide de mesures infrarouges réalisées par l'équipe du CNRC-IRA.

Mots-clés: aile laminaire adaptative, élément finis, structure active, conception, matériau composite, essais en soufflerie, optimisation multi-objective, optimisation en temps réel, actionneurs, alliages à mémoire de forme.

DESIGN AND OPERATION OF AN ACTIVE STRUCTURE FOR AN EXPERIMENTAL MORPHING LAMINAR WING

Daniel COUTU

ABSTRACT

This doctoral research contributed to the success of the project CRIAQ 7.1, demonstrating the capability of a morphing laminar wing to reduce fuel consumption. Respectively, this thesis shows the design of the experimental wing and its operation in a subsonic wind tunnel (Mach numbers of 0.2 to 0.3 with angles of attack between -1 and 2°).

First of all, the morphing wing is formed of a composite laminate linked to an actuation system to build an active structure capable of modifying the wing upper surface geometry. The design was performed using a new developed methodology to solve aero-structural problems. Using ANSYS software, the finite elements method was applied to model the different possible active structure configurations Aerodynamic loads applied over the active structure as well as targeted morphed geometries have been provided by the École Polytechnique team. Next, laminar flow enhancements allowed by each active structure configuration were evaluated using the aerodynamic solver XFOIL 6.96. A best trade-off between aerodynamic performance and energy needed for wing morphing was found using a multi-objective optimization technique. Among the retained stable configurations, a 4-ply composite laminated shell driven by 2 actuation lines was retained.

Thereafter, the research effort focused on the exploitation of the morphing capabilities of the experimental wing over each given set of flow conditions. Therefore, once the prototype was built, the structural model was refined, calibrated and coupled with the aerodynamic solver to accurately predict the aero-structural behavior in the wind tunnel. Optimal morphing wing shapes were numerically calculated using a generalized pattern search algorithm and a local search routine to refine the solution. In the wind tunnel, this open-loop control approach allowed an average 25% laminar flow regime extension over the wing prototype upper surface. Consequently, an average 18.5% profile drag reduction was measured by the pressure survey rake across the wake.

Although these results were satisfactory, limitations in the aero-structural coupled model were observed when comparing numerical and experimental responses of the prototype. For that reason, the research continued with the development of a real-time optimization strategy in closed loop to exploit the complete potential of the morphing laminar wing. The wind tunnel balance was used as a hardware-in-the-loop returning the instantaneous lift-to-drag ratio to the optimizer. An optimization algorithm has been built to minimize the actuation required and thus reduce the time period until convergence to the optimal shape. To accelerate the search, numerically predicted actuation strokes (open loop) were used as initial

modified shapes. As measured in the wind tunnel, the use of the closed-loop control strategy resulted in an average lift-to-drag ratio increase from 11 to 12.2% as compared to the open-loop approach. No more than 4 additional minutes were required to converge to the real-time optimized shapes, an acceptably small time delay on the cruise flight period time scale. Finally, infrared measurements performed by the IAR-NRC team allowed experimental demonstration of the reciprocity between the laminar flow improvement and the lift-to-drag ratio increase.

Keywords: morphing laminar wing, finite elements, design, active structure, composite structure, wind tunnel tests, multi-objective optimization, real-time optimization, actuators, shape memory alloy.

TABLE DES MATIÈRES

	Page
INTRODUCTION	1
CHAPITRE 1 MISE EN CONTEXTE	1
1.1 L'aviation et l'environnement.....	1
1.1.1 Mobilisation et moyens financiers	2
1.1.2 Progrès et intérêts économiques.....	3
1.2 Présentation du projet CRIAQ 7.1	7
1.2.1 Notions aérodynamiques et motivations.....	10
1.2.2 Terminologie aéronautique	11
1.2.3 Description sommaire du projet CRIAQ 7.1	13
1.2.4 Cahier des charges « adaptatif » du projet CRIAQ 7.1.....	16
1.2.5 Les outils de calculs numériques	20
1.2.6 La soufflerie subsonique du CNRC-IRA.....	20
1.3 Problématique de la recherche	22
1.4 Objectifs de la recherche.....	23
1.5 Déroulement et contributions au projet.....	23
CHAPITRE 2 REVUE DE LA LITTÉRATURE SUR LES AILES ADAPTATIVES	27
2.1 Les concepts.....	28
2.1.1 <i>Belt-rib</i> (adaptation de la cambrure du profil)	30
2.1.2 Structure active (adaptation du bord d'attaque).....	30
2.1.3 Structure compliante (adaptation du bord de fuite)	31
2.2 Les méthodologies de design	32
2.2.1 Approche simultanée	32
2.2.2 Approche séquentielle.....	33
2.3 L'exploitation optimale du caractère adaptatif	34
2.3.1 Optimisation numérique (boucle ouverte)	35
2.3.2 Modélisation expérimentale (boucle ouverte)	36
2.3.3 Optimisation en temps réel (boucle fermée)	37
CHAPITRE 3 ARTICLE#1 « OPTIMIZED DESIGN OF AN ACTIVE EXTRADOS STRUCTURE FOR AN EXPERIMENTAL MORPHING LAMINAR WING ».....	41
3.1 Introduction.....	43
3.1.1 Morphing wing concepts and technologies.....	44
3.1.2 Morphing wing design methodologies.....	46
3.2 CFD optimization of the MLW.....	47
3.2.1 The CRIAQ 7.1 MLW	47
3.2.2 Aerodynamic solver.....	48
3.2.3 CFD-optimized wing shape database.....	49
3.3 Active structure modeling.....	51

3.3.1	Flexible extrados constituents and properties	51
3.3.2	Structural FE modeling	52
3.4	Sensitivity analysis.....	53
3.4.1	Simplification of the loading conditions.....	53
3.4.2	Design parameters of the active structure.....	57
3.5	Multi-objective optimization	59
3.5.1	Formulation of the objective function.....	60
3.5.2	Configuration evaluation	62
3.5.3	Configuration selection.....	63
3.6	Conclusion	65
3.7	Acknowledgments.....	65
3.8	References.....	66
CHAPITRE 4 ARTICLE#2 « AERO-STRUCTURAL MODEL FOR MORPHING LAMINAR WING OPTIMIZATION IN A WIND-TUNNEL »		69
4.1	Nomenclature.....	70
4.2	Introduction.....	71
4.3	Overview of the CRIAQ7.1 morphing laminar wing project	72
4.3.1	Morphing wing control approaches	73
4.4	Overview of the CRIAQ7.1 morphing laminar wing project	75
4.4.1	Validation of the reference prototype geometry	75
4.4.2	Force-displacement actuator diagrams	76
4.4.3	Validation of the FEM shape modification response under actuation	77
4.5	Aerodynamic effects of the deviations between FEM predictions and experiments...79	79
4.6	The aero-structural model and its wind tunnel validation	80
4.6.1	Preliminary works.....	80
4.6.2	Aero-structural interaction	81
4.6.3	Empirical correlation for pressure loading	82
4.6.4	Empirical correlation for pressure loading	83
4.6.5	Validation of the coupled model - pressure distribution calculations.....	84
4.7	Actuator strokes' optimization.....	85
4.7.1	Optimization problem:	85
4.7.2	Global optimization	86
4.7.3	Local optimization	87
4.7.4	Optimization results	88
4.8	Wind-tunnel validation	89
4.8.1	Experimental set-up	89
4.8.2	Morphing wing performance	90
4.9	Discussion of the comparison of the experimental and numerical results.....	92
4.9.1	Beyond the prototype's physical limitations.....	93
4.10	Conclusion and recommendations	95
4.11	Acknowledgments.....	96
4.12	References.....	96

CHAPITRE 5 ARTICLE#3 « LIFT-TO-DRAG RATIO MORPHING LAMINAR WING CONTROL USING WIND-TUNNEL BALANCE AS HARDWARE-IN-THE-LOOP »	99
5.1 Introduction.....	101
5.1.1 Morphing wing shape optimization	103
5.1.2 Morphing wing control	104
5.1.3 Proposed control approach for the MLW performance optimization.....	106
5.2 Presentation of the MLW.....	108
5.2.1 The MLW concept	108
5.2.2 MLW aerodynamic performance.....	109
5.3 MLW controller development for shape optimization.....	109
5.3.1 The numerical optimized wing shape database	109
5.3.2 Design-of-Experiment (DOE).....	110
5.3.3 Pattern Search Algorithm.....	112
5.3.4 Pattern Search Implementation and Calibration	114
5.3.5 MLW Controller Wind Tunnel Setup with Hardware-in-the-Loop.....	115
5.4 Wind-tunnel optimization results.....	116
5.5 Discussion	117
5.6 MLW controller wind-tunnel behavior.....	117
5.6.1 Open-loop versus closed-loop.....	121
5.6.2 Objective Function: L/D vs x_{tr}	125
5.7 Conclusion	126
5.8 Recommandations	127
5.9 Acknowledgments.....	129
5.10 References.....	129
CONCLUSION.....	132
RECOMMANDATIONS	134
ANNEXE I EXPERIMENTAL VALIDATION OF THE 3D NUMERICAL MODEL FOR AN ADAPTIVE LAMINAR WING WITH FLEXIBLE EXTRADOS	137
ANNEXE II PROMISING BENEFITS OF AN ACTIVE-EXTRADOS MORPHING LAMINAR WING	148
LISTE DE RÉFÉRENCES BIBLIOGRAPHIQUES.....	151

LISTE DES TABLEAUX

	Page
Tableau 1.1 Potentiel de réduction de consommation en carburant associé aux structure d'aéronefs en développement	9
Tableau 1.2 Matrice des noms de profils pour les conditions d'écoulement du projet CRIAQ 7.1	17
Tableau 2.1 Méthodes d'exploitation (et de contrôle) d'une aile adaptative.....	35
Tableau 3.1 Optimization flow cases.....	50
Tableau 3.2 Elastic constants from testing and approximation	52
Table 4.1 Computation time for optimization	88
Table 5.1 Algorithm parameters	114
Table 5.2 Wind-tunnel MLW shape optimization results.....	116

LISTE DES FIGURES

	Page	
Figure 1.1	Moyenne du carburant brûlé par les nouveaux avions, 1960-2008.	4
Figure 1.2	Proportion du coût en carburant dans les frais d'exploitation totaux des avions de lignes aux États-Unis.	5
Figure 1.3	Réduction en consommation de carburant des nouveaux avions et ceux à venir.....	6
Figure 1.4	Technologies probablement disponible au cours des prochaines années. ...	8
Figure 1.5	Aperçu des différents niveaux de l'échelle d'avancement technologique...9	
Figure 1.6	Transition de l'écoulement laminaire à turbulent dans la couche limite..10	
Figure 1.7	Schéma explicatif d'une aile 2D et son profil.....	12
Figure 1.8	Forces principales sur (a) l'avion et (b) l'aile.....	12
Figure 1.9	Comparaison des bords de fuite du profil WTEATE1 original et modifié pour l'analyse aérodynamique.....	14
Figure 1.10	Schéma de l'aile aéroélastique du projet CRIAQ 7.1 : principe de fonctionnement et composantes.....	15
Figure 1.11	Schéma du système de contrôle de l'aile aéroélastique du projet CRIAQ 7.1	16
Figure 1.12	Analyse de courbure profil WTEATE1 : (a) original, (b) avec polynôme de régression.	18
Figure 1.13	Résultats de l'équipe de l'EPM fournis au LAMSI : (a) espace de travail, (b) 1 ^{ère} série de profils optimisés (novembre 2007) et (c) 2 ^e série de profils optimisés (mai 2008).	19
Figure 1.14	Maquette de la soufflerie de 2 m sur 3 m du CNRC-IRA utilisée pour tester l'aile laminaire adaptative.	22
Figure 1.15	Déroulement et contributions au projet de recherche présentées dans les différentes sections de la thèse.	25
Figure 1.16	Polaire de traînée obtenue en soufflerie : (a) octobre 2008, (b) février 2009.....	25

Figure 2.1	Bec (<i>slat</i>) et volet (<i>flap</i>) de l'airbus A300.....	27
Figure 2.2	Avion des frères Wright lors du premier envol historique de 1903.....	29
Figure 2.3	Triplan Fokker Dr-1, premier avion de guerre à utiliser un profil épais....	29
Figure 2.4	Design optimisé du <i>belt rib</i> concept.....	30
Figure 2.5	Détails de construction du modèle de profil à bord d'attaque déformable de façon dynamique.....	31
Figure 2.6	<i>Mission Adaptative Compliant Wing</i>	32
Figure 2.7	Aile adaptative utilisant des alliages à mémoire de formes.....	33
Figure 2.8	MACW prototype installé sous l'avion Scaled Composite White Knight.....	37
Figure 2.9	Vol de l'avion F111 TACT au dessus du désert de Mojave en Californie.....	39
Figure 2.10	Aile adaptative d'un MAV exploitée en HIL avec deux variables de design.....	40
Figure 3.1	Experimental MLW setup in the subsonic wind tunnel.....	44
Figure 3.2	Conceptual design of the MLW.....	45
Figure 3.3	CFD-optimized profiles of the MLW: (a) shape modification envelope; (b) drag coefficient as a function of the extrados transition point location for the CFD-optimized and the WTEATE1 reference profiles. (C25 flow case is taken as an example.)	50
Figure 3.4	Flexible extrados with steel stiffeners (manufacturing setup)	51
Figure 3.5	Numerical model of the active structure using ANSYS software ($Na = 2$ and $Np = 3$).	53
Figure 3.6	Chord-wise shifts of the actuation lines during morphing of the “3-ply and 4 actuators” active structure according to the C25 optimized profile.....	55
Figure 3.7	Evolution of aero-structural parameters for each coupled iteration for the 3-ply and 2-actuator active structure under the C49 flow condition case.....	56

Figure 3.8	Shape deviation of the FE-modeled in respect to the CFD-optimized C25 profile (horizontal solid line): a) 5-ply with 2, 4 and 7 actuators; b) 4 actuators with 3, 5 and 8 plies.	58
Figure 3.9	Variable design parameters of the flexible extrados: number of actuators (Na) and plies (Nb).	59
Figure 3.10	Nested loops for all active structure performance evaluation.....	62
Figure 3.11	Laminar gain deviation (RMSD) and mean laminar flow gain for all FE-modeled active structure configurations.	63
Figure 3.12	Objective plot for all active structure configurations (the three best configurations are encircled by a dotted line).....	64
Figure 3.13	Evaluation of Pareto solutions over a range of tradeoffs.....	64
Figure 4.1	MLW concept with active extrados [6].	72
Figure 4.2	Structural FEM.....	75
Figure 4.3	Unmorphed profile characterization: (a) coordinate measuring machine setup and (b) deviation of the manufactured from the designed (targeted) reference profile	76
Figure 4.4	Force-displacement test bench for the active structure.....	76
Figure 4.5	Force-displacement diagrams comparison: (a) first and (b) second actuation lines; EXP –experimental, FE – calculated data.	77
Figure 4.6	Validation of the shape modification for two sets of actuators' displacements: (a) bench test setup and (b) comparison of the numerical and experimental thickness modifications.....	78
Figure 4.7	The effects of modeling error on the predicted aerodynamic performance for the 1st and 2nd sets of actuator displacements (see also Figure 4.6b).	80
Figure 4.8	Aero-structural interaction of the coupled model.....	81
Figure 4.9	Wind tunnel pressure variations and empirical correlation.	82
Figure 4.10	Aero-structural convergence study: (a) maximum absolute variation of the pressure load and shape modifications and (b) absolute variation of the drag coefficient and location of the laminar/turbulent transition. ...	83

Figure 4.11	Numerical and experimental pressure differentials over the flexible extrados for two aerodynamic cases: (a) Mach 0.2 and Alpha -1° and (b) Mach 0.3 and Alpha 2°.....	85
Figure 4.12	Numerical drag coefficient response for: (a) Mach 0.25 & Alpha -1° and (b) Mach 0.25 & Alpha 0.5°.....	86
Figure 4.13	Two-step optimization method for: (a) Mach 0.25 & Alpha -1° and (b) Mach 0.25 & Alpha 0.5°	87
Figure 4.14	Optimum strokes for actuator 1 and 2 resulting from the centers of the optimal zones.....	88
Figure 4.15	Optimization results as a function of the Mach number and the angle of attack.....	89
Figure 4.16	(a) Experimental MLW in the wind tunnel, (b) open-loop control.....	90
Figure 4.17	Numerical and experimental morphing effect over the aerodynamic lift vs drag coefficients (a, b) and over the laminar flow transition (c, d) for flow conditions ranging from alpha -1 to 2° (1° increments) at given Mach number: (a, c) Mach 0.2; (b, d) Mach 0.3.....	91
Figure 4.18	Laminar/turbulent flow transition over the active structure using infrared thermography visualization for Mach 0.2 and Alpha 2°: (a) unmorphed profile; (b) morphed profile.....	92
Figure 4.19	Optimum strokes for actuator 1 and 2 with no physical limitations of the actuation strokes (to be compared with Figure 4.14).....	93
Figure 4.20	Optimization results as a function of the Mach number and the angle of attack without consideration of the prototype's physical limits	94
Figure 4.21	Relative drag reduction upon morphing from the unmorphed profile for limited and unlimited actuator strokes: (a) Mach number variation at 2° angle of attack (b) Angle of attack variation at Mach number 0.3	94
Figure 5.1	MLW setup in the 2 x 3 m IAR-NRC wind tunnel: (a) inside and (b) outside view.....	103
Figure 5.2	Closed-loop controller for morphing shape optimization of the MLW in a wind tunnel.....	107
Figure 5.3	MLW wing concept using an active extrados structure. Adapted from Coutu et al. (2009a).....	108
Figure 5.4	Aero-structural coupled model of the MLW active structure.....	110

Figure 5.5	Lift-to-drag ratio response surfaces for Mach=0.2, Alpha=-1° (a, c) and Mach=0.3, Alpha=2° (b, d); (a, b) DOE, (c, d) calculations.....	111
Figure 5.6	Pattern search actuator strokes' optimization algorithm: a) flowchart and b) simulation example for Mach=0.2 and Alpha=0.5°.....	113
Figure 5.7	Stroke optimization for Mach=0.275 and Alpha= 0.5°: (a,c) resulting pattern search and (b,d) performance change upon actuation; (a,b) experimental results and (c,d) numerical prediction using response surfaces.	118
Figure 5.8	Stroke optimization for Mach=0.275 and Alpha=-2°: (a) first and (b) second try.....	123
Figure 5.9	Transition point detection using (a) IR thermography visualization over the active extrados for: (b) unactuated shape $\delta = \{0; 0\}$; c) open-loop optimization $\delta = \{5.21; 7.85\}$ and d) closed-loop optimization $\delta = \{4.87; 7.09\}$	124
Figure 5.10	Stroke optimization for Mach=0.2 and Alpha=0.5 using two different feedback signals: (a, b) L/D from balance and (c, d) Xtr from IR; (a, c) resulting pattern search and (b, d) performance change upon actuation.....	126

LISTE DES ABRÉVIATIONS, SIGLES ET ACRONYMES

2D	Bidimensionnel
3D	Tridimensionnel
ACARE	Advisory Council for Aeronautics Research in Europe
AMF	Alliage à mémoire de forme
CLEEN	Continuous Lower Energy, Emissions and Noise Technology Program
CNRC-IRA	Conseil National de Recherche du Canada - Institut de Recherche en Aérospatiale
CRIAQ	Consortium de Recherche et d'Innovation en Aérospatiale au Québec
CRSNG	Conseil de Recherche en Science Naturel et en Génie
EPM	École polytechnique de Montréal
ETS	École de technologie supérieure
FAA	Federal Aviation Administration
FQRNT	Fonds Québécois de la Recherche sur la Nature et les Technologies
GARDN	Groupement Aéronautique de Recherche et Développement en eNvironnement
GIEC	Groupe d'expert Intergouvernemental sur l'Évolution du Climat
HIL	Hardware In the Loop
IATA	International Air Transport Association
ICCT	International Council on Clean Transportation
LAMSI	Laboratoire sur les alliages à mémoire de forme et les systèmes intelligents
MACW	Mission Adaptive Compliant Wing
NASA	National Aeronautics and Space Administration
NLF	Natural Laminar Flow

OACI	Organisation de l'aviation civile internationale
PARTNER	Partnership for AiR Transportation Noise and Emissions Reduction
TACT	Transonic AirCraft Technology
TERESA	Technology Roadmap for Environmentally Sustainable
TRL	Technology Readiness Level

LISTE DES SYMBOLES ET UNITÉS DE MESURE

%c	pourcentage de la corde du profil, sans unité
C _D	coefficient de traînée, sans unité
C _L	coefficient de portance, sans unité
gal	gallon US
km	kilomètre
L	litre
L/D	Finesse aérodynamique
Mach	Vitesse du son
X _{tr}	Position du point de transition le long de la corde (%c)
°	degré (angle)

INTRODUCTION

Cette thèse présente les connaissances développées et les résultats obtenus en ce qui concerne la conception et l'exploitation d'une structure active pour une aile laminaire adaptative. Cette structure est responsable du caractère adaptatif de l'aile expérimentale découlant du grand projet multidisciplinaire CRIAQ 7.1. Lors d'essais en soufflerie, ce projet vise à démontrer la faisabilité d'une aile laminaire capable de modifier la géométrie de son extrados afin d'en accroître la performance. Les conditions de vols considérées sont celles du vol en croisière avec des angles d'attaques variant de -1 à 2°. Bien que les avions de ligne volent en régime transsonique, le projet se réalise au régime subsonique étant donné le type de soufflerie disponible. Avec un nombre de Mach variant de 0.2 à 0.3, cette décision a l'avantage de simplifier les travaux numériques et expérimentaux tout en réduisant leur coût d'exécution.

Le chapitre 1 situe le contexte des travaux en dressant le portrait des préoccupations environnementales et économiques du secteur aéronautique. Les exigences du cahier des charges y sont également présentées avant que le chapitre 2 ne fasse l'état de l'art sur la conception et l'exploitation des ailes adaptatives. Par la suite, le chapitre 3 expose la méthodologie de conception développée et appliquée pour déterminer la configuration optimale de la structure active. Une fois le prototype fabriqué, les essais de soufflerie viseront à tester deux approches permettant l'exploitation du caractère adaptatif de l'aile. La première approche est expliquée au chapitre 4 où la modélisation numérique de l'interaction aéro-structurale permet une optimisation multidisciplinaire des modifications de profils à générer. Il faudra attendre les derniers essais en soufflerie afin d'exploiter le plein potentiel de l'aile laminaire adaptative. Le chapitre 5 en présente les résultats et la stratégie utilisée, soit l'optimisation en temps réel de la forme du profil en soufflerie.

En terminant, les grands thèmes de cette recherche sont rappelés dans la conclusion suivie de recommandations formulées en vue d'une application éventuelle du concept de l'aile adaptative laminaire sur un avion réel.

CHAPITRE 1

MISE EN CONTEXTE

Les travaux de conception et d'exploitation liés au développement de l'aile laminaire adaptative contribuent à l'avancement de solutions technologiques permettant de réduire l'empreinte écologique des avions de même que leurs coûts d'exploitation. La première section de ce chapitre est consacrée aux préoccupations environnementales toujours grandissantes du secteur aéronautique. Dans cette section, il est également démontré comment l'enjeu environnemental relève également d'un intérêt économique lié au coût en carburant. Afin de présenter en détail le grand projet multidisciplinaire de l'aile adaptative laminaire, ce dernier est d'abord situé à l'égard des nombreuses initiatives technologiques entreprises par les constructeurs d'avions. Ensuite, sa raison d'être ainsi que son principe de fonctionnement sont abordés à l'aide de notions et de termes aéronautiques expliqués et schématisés. Finalement, le cahier des charges du projet de l'aile laminaire adaptative est parcouru avant que ne soient formulés la problématique et les objectifs visés par cette recherche doctorale.

1.1 L'aviation et l'environnement

Selon un rapport du Groupe d'Expert Intergouvernemental sur l'évolution du climat (GIEC, 1992), le secteur aéronautique est responsable de 2% des émissions de dioxyde de carbone d'origine humaine et contribue à 3,5% du forçage radiatif potentiellement lié au réchauffement planétaire¹ (Info.effeserre.free.fr, 2005). Alors que les voyages de passagers dans le monde augmentent d'environ 5% à chaque année, la prédiction des augmentations des émissions est limitée à 3% par année étant donné l'amélioration continue de l'efficacité des aéronefs. En utilisant le scénario médian IS92a, le GIEC prévoit qu'en 2050,

¹Le forçage radiatif désigne tout phénomène affectant l'équilibre énergétique de la planète par son influence sur le comportement du rayonnement. Par exemple, les gaz à effet de serre ont un forçage radiatif positif puisqu'ils augmentent la température au sol en empêchant les infrarouges de rayonner vers l'espace.

l'aviation sera responsable de 1,7 à 11% des émissions de carbone avec une contribution de 3,5 à 14,7% au forçage radiatif (GIEC, 1999). En réponse à cette prise de conscience environnementale, plusieurs organisations se sont mobilisées afin que la responsabilité environnementale devienne prioritaire au cœur des activités aéronautiques, au même titre que la sécurité.

1.1.1 Mobilisation et moyens financiers

Financé conjointement par la *Federal Aviation Administration* (FAA), la *National Aeronautics and Space Administration* (NASA) ainsi que par Transport Canada, un centre d'excellence appelée PARTNER pour «*Partnership for AiR Transportation Noise and Emissions Reduction*» a vu le jour en septembre 2003. PARTNER aborde les questions sur l'environnement et l'aviation en utilisant les ressources universitaires et industrielles disponibles. Jusqu'à maintenant, il a fourni une appréciable quantité d'information sur le défi environnemental posé par la croissance des activités du secteur de l'aviation (Bernhard, 2005). En 2007, soit 4 ans plus tard, l'*International Air Transport Association* (IATA) a déployé un plan stratégique mobilisant l'industrie, les gouvernements et les organismes de réglementation dans la réduction des émissions de carbone. Sous l'acronyme TERESA pour «*Technology Roadmap for Environmentally Sustainable Aviation*», ce projet a été initié pour motiver les constructeurs d'avion à atteindre le zéro-émission dans les 50 prochaines années (IATA, 2009). Par ailleurs, en 2009, l'Organisation de l'aviation civile internationale (OACI) a emboité le pas en adoptant «comme objectifs ambitieux mondiaux des améliorations annuelles de 2 % du rendement en carburant jusqu'en 2050» (ICAO, 2009).

De l'autre côté de l'Atlantique, en 2001, un groupe d'experts définissait la vision de l'Europe à l'égard de l'aéronautique : devenir un leader mondial en satisfaisant conjointement la demande en matière de sécurité, d'environnement et de mobilité d'ici 2020 (ACARE, 2001). Parmi les nombreux objectifs pour 2020, la réduction de la consommation en essence des avions a été fixée à 50%. L'une des recommandations du groupe contribua à la création du conseil ACARE pour «*Advisory Council for Aeronautics Research in Europe*» chargé de

développer et de maintenir une stratégie de recherche aéronautique en Europe (ACARE, 2009).

Conséquemment, pendant les 3 dernières années, de nombreux centres d'excellence et regroupements disposant d'importants moyens financiers ont vu le jour afin de couvrir la recherche et le développement sur l'aspect environnemental de l'aviation. À cet effet, l'initiative technologique européenne commune *Clean Sky* (Brusati, 2007) est l'un des plus grands projets de recherche européens avec un budget prévu de 1,6 milliards d'euros partagés entre la commission européenne, les industriels et les universitaires entre 2008 et 2013 (CLEANSKY, 2008). Aux États-Unis, sous l'égide de la FAA et avec l'aide de la NASA, le programme CLEEN pour « *Continuous Lower Energy, Emissions and Noise Technology Program* » dispose d'un budget de 123 millions \$US réparti de 2009 à 2014 (Skalecky, 2008). Au Canada, sous l'acronyme GARDN pour « Groupement Aéronautique de Recherche et Développement en eNvironnement », ce nouveau Réseau des centres d'excellence est dirigé par les entreprises et est doté d'un budget initial de 22 millions de dollars pour quatre ans (de 2009 à 2013) (GARDN, 2009). De plus, en mars 2010, le gouvernement québécois annonçait la mise en place de SAGE, à l'aide d'un :

« [...] soutien financier accordé aux initiatives industrielles de démonstration de technologies en matière d'avion « vert ». Une enveloppe de 150 millions de dollars, échelonnés sur 4 ans pour le secteur, contribuera à maintenir la compétitivité de l'industrie par rapport à la concurrence internationale » (Aéro-Montréal, 2010).

1.1.2 Progrès et intérêts économiques

Au cours de ses 100 ans d'histoire, l'aviation a démontré une capacité surprenante à réaliser de gigantesques exploits. La Figure 1.1 tirée d'un rapport de l'*International Council on Clean Transportation* (ICCT) (Rutherford and Zeinali, 2009) montre que de 1960 à 2008, la consommation en carburant par passager transporté sur un kilomètre a été réduite de 51%. Pour chacune des décennies, l'augmentation de l'efficacité en carburant n'a pas toujours été constante. Elle fut notamment très élevée au cours des années '60 et '80, avant de devenir très faible dans les années '90, pour pratiquement stagner jusqu'en 2008. Selon les auteurs du rapport, l'augmentation de la taille des avions au cours des années '60 a permis de réaliser

une économie d'échelle en augmentant le nombre de passagers prenant place à bord. Pour les années '80, l'amélioration est attribuable à l'introduction des avions de transport de moyenne distance utilisant des nouveaux moteurs à double flux présentant un taux de dilution plus élevé. En dépit de l'absence de la préoccupation environnementale lors de ces deux périodes, l'ICCT attribut le progrès en efficacité énergétique à la hausse du prix du baril de pétrole. Ainsi, en considérant le temps nécessaire à un appareil pour être conçu, testé, certifié et mis en production, la Figure 1.2 permet de corrélérer la stagnation en efficacité avec la période où la proportion du coût en carburant à l'intérieur des frais d'exploitation des avions était à son minimum.

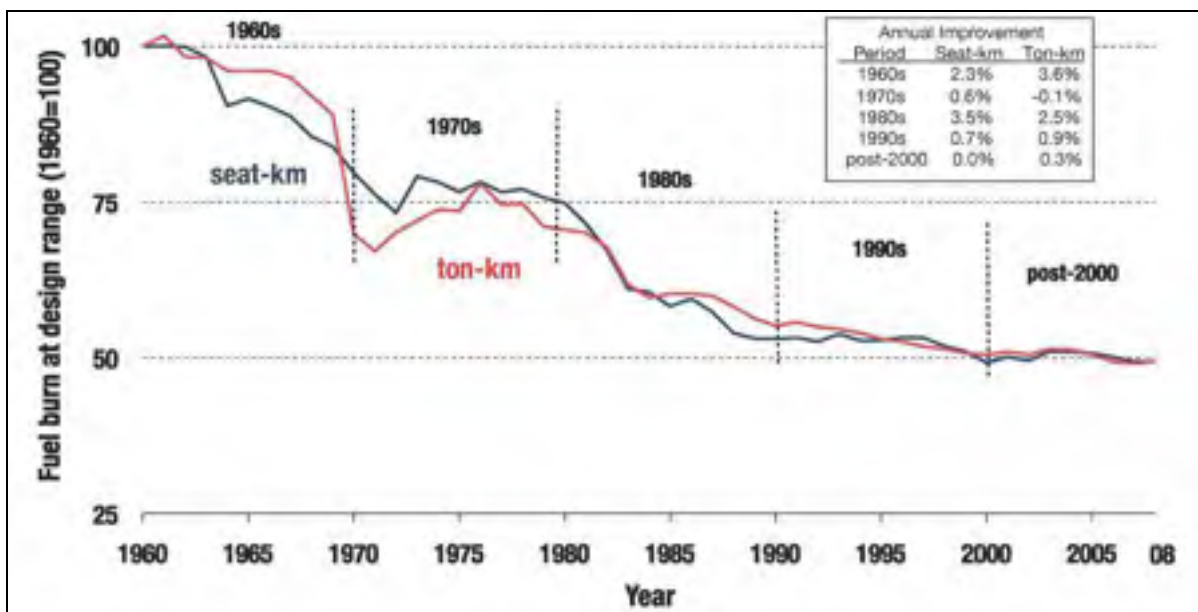


Figure 1.1 Moyenne du carburant brûlé par les nouveaux avions, 1960-2008.
Tirée de Rutherford and Zeinali (2009)



Figure 1.2 Proportion du coût en carburant dans les frais d'exploitation totaux des avions de lignes aux États-Unis.
Tirée de Rutherford and Zeinali (2009)

Or, depuis 2004, le prix du baril de pétrole a suivi une hausse, atteignant un pic record de 147\$ US avant le crash économique de juillet 2008. Vue l'aspect limité de cette ressource, il est attendu qu'elle devienne de moins en moins abordable. Maintenant, lors de l'achat d'une flotte d'avions, les compagnies aériennes accordent une plus grande place à l'efficacité en carburant. Comme le montre la Figure 1.3, les nouveaux avions et ceux à venir présentent et présenteront des réductions en consommations de carburant allant jusqu'à 30% en comparaison avec les avions similaires existants. D'ailleurs, à l'égard de la nouvelle génération de gros transporteurs (Airbus 380 et Boeing 787), une consommation inférieure à 3 litres de carburant par passager transporté sur 100 km est prévue (Enviro.aero, 2008), soit un taux comparable à une petite voiture économique. Alors que l'éveil de la conscience environnementale coïncide avec la hausse du prix du pétrole, l'avancement du concept de l'avion « vert » est devenu un investissement à long terme prometteur à tous les niveaux: économique, social et environnemental.

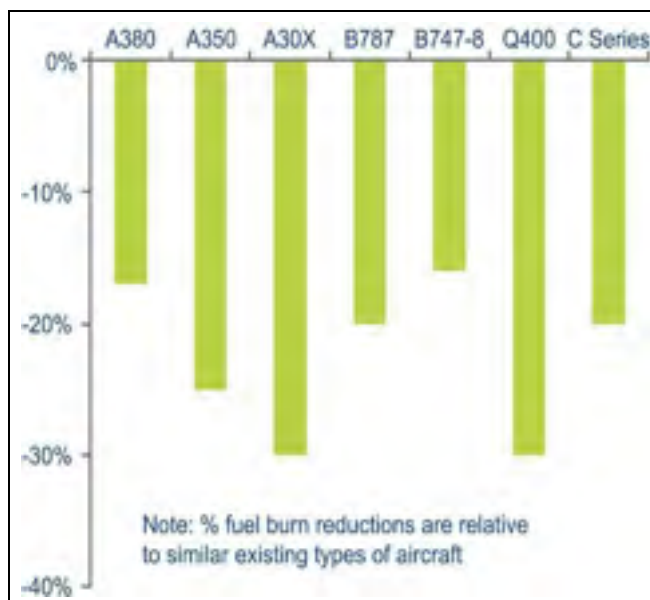


Figure 1.3 Réduction en consommation de carburant des nouveaux avions et ceux à venir.

Tirée de l'IATA (2009)

Selon l'IATA, pour un avion de transport typique comptant 120 passagers, chaque 1% d'économie en carburant permet une réduction proportionnelle des émissions de gaz carboniques et l'économie de 250 litres (65,5 Gallons US) de carburant par vol. Selon le prix moyen du gaz d'avion aux États-Unis de 2000 à 2008 (ATA, 2008), ceci représente une économie moyenne par vol de 54 \$US (82.4¢/gal*65.5gal) à 201\$US (306.8¢/gal*65.5gal). En supposant que cet avion typique effectue deux vols en moyenne par jour, c'est environ 40 000\$ de carburant en 2000 et 147 000\$ en 2008 qui auraient pu être économisés annuellement pour chaque 1% d'économie en carburant. Compte tenu qu'en 2008 seulement, la consommation d'essence d'avion au États-Unis représentait près de 58 milliards \$US (1% = 580 millions \$US/an) (ATA, 2008), les efforts liés aux développements de l'avion vert sont destinés à être largement récompensés du point de vue économique.

Enfin, toujours selon l'IATA, le grand défi environnemental auquel est confrontée l'aviation ne peut être relevé qu'avec la coopération de tous les acteurs techniques, économiques et législatifs du secteur (IATA, 2009). Le plan TERESA initié par l'IATA prévoit l'utilisation de 4 piliers stratégiques pour y parvenir : technologie, exploitation, infrastructure et

instrument économique positif. Parmi ces piliers, la technologie a le plus haut potentiel pour réduire l'empreinte écologique de l'activité aéronautique.

1.2 Présentation du projet CRIAQ 7.1

Ainsi, dans les années à venir, les nouvelles technologies seront appliquées pour une gestion plus économique des trajectoires de vols, pour augmenter la performance des moteurs, alléger le poids des avions et améliorer leur efficacité aérodynamique. Parmi ces axes de recherche technologique, l'amélioration de l'efficacité aérodynamique des avions est l'aspect le plus prometteur pour réduire la consommation d'essence. En fait, selon les données de Braslow (1999), 50% du carburant brûlé en régime de croisière d'un avion de transport sert à vaincre la friction de l'air. Bien que les premières recherches visant à réduire la traînée de friction des avions remontent aux années 1930, l'implémentation de ces technologies au sein des avions de transport civils est encore très peu avancée. Il reste beaucoup de problèmes d'intégration et de prédiction des performances à résoudre avant de convaincre les compagnies de transport aérien, exigeantes en matière de garantie de bénéfices, de fiabilité et de sécurité. Le développement de prototypes à grande échelle est nécessaire afin d'étudier la faisabilité des concepts et leur potentiel d'application. C'est dans ce contexte scientifique et politique que le CRIAQ a inauguré en 2006 le projet 7.1 intitulé « Amélioration de l'écoulement laminaire sur une voilure aéroélastique ». Ce projet multidisciplinaire fait intervenir des partenaires universitaires (ÉTS et EPM), institutionnel (CNRC-IRA) et industriels (Bombardier et Thalès) ainsi que des organismes subventionnaires (CRSNG et CRIAQ). D'une durée de trois ans, son budget total est de 1 329 951 \$ (Dion *et al.*, 2007).

Bombardier Aéronautique de même que le Groupe Thalès font tous deux partis des 20 partenaires ayant participé à l'élaboration du plan d'action TERESA de l'IATA. La Figure 1.4 montre la liste des technologies en développement bientôt disponibles que ces derniers ont identifiées afin de relever le défi environnemental.

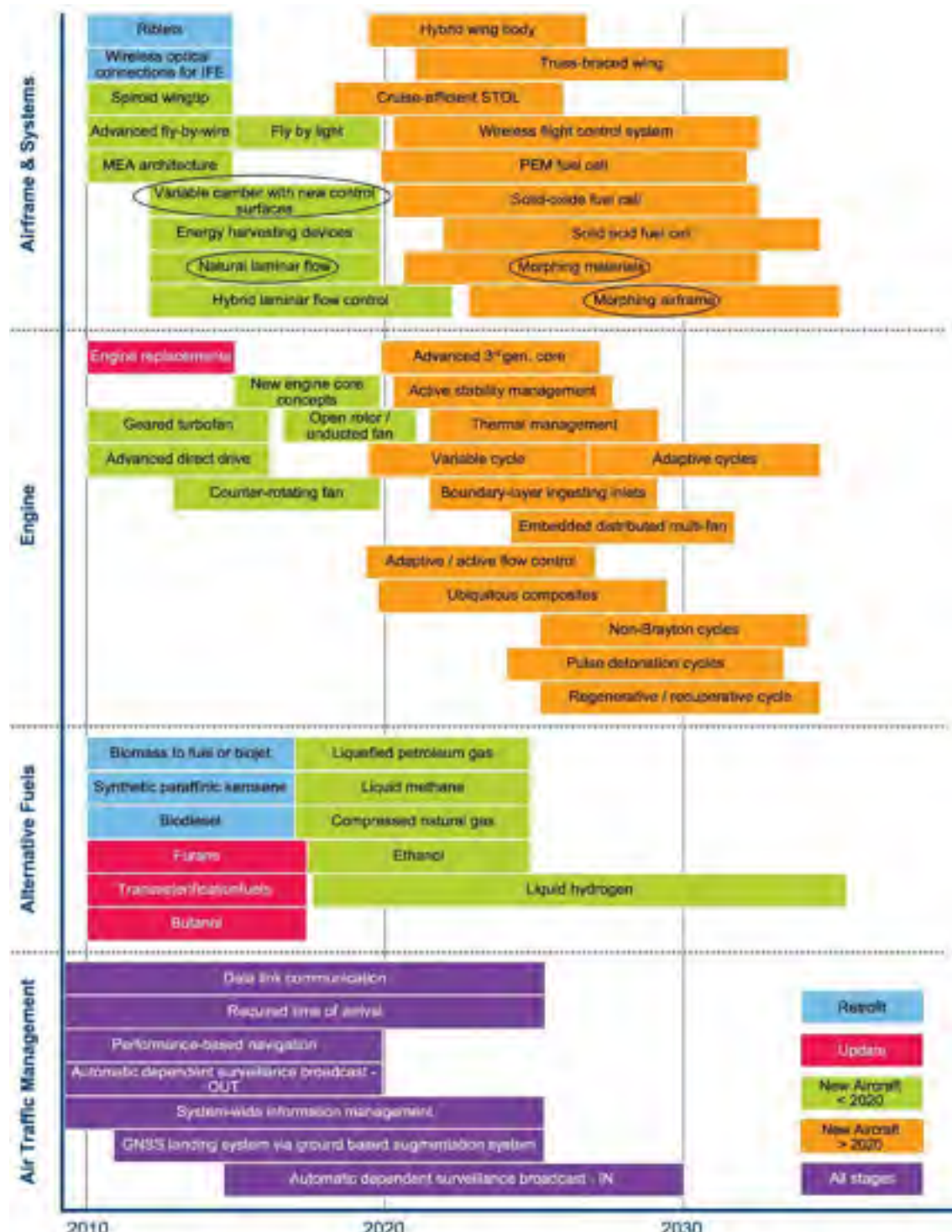


Figure 1.4 Technologies probablement disponible au cours des prochaines années.
Adaptée de l'IATA (2009)

Le projet CRIAQ 7.1 se situe dans le secteur technologique des structures d'aéronefs, permettant l'avancement de plusieurs technologies (encerclés sur la Figure 1.4) associées à l'aile adaptative laminaire. En utilisant l'échelle *Technology Readiness Level* (TRL) illustrée et expliquée en Figure 1.5, le Tableau 1.1 présente leur niveau d'avancement technologique de 2007. Compte tenue du large potentiel de réduction en consommation de carburant associés à ces technologies (Tableau 1.1), la réalisation du projet CRIAQ 7.1 relève à la fois d'intérêts économiques et environnementaux.

Tableau 1.1
Potentiel de réduction de consommation en carburant
associé aux structure d'aéronefs en développement
Adapté de l'IATA (2009)

Airframe Technologies	Fuel burn reduction	TRL
Natural laminar flow	5 à 10%	6
Variable camber with new control surface	1 à 5%	5
Morphing airframe	5 à 10%	3
Morphing material	1 à 5%	3

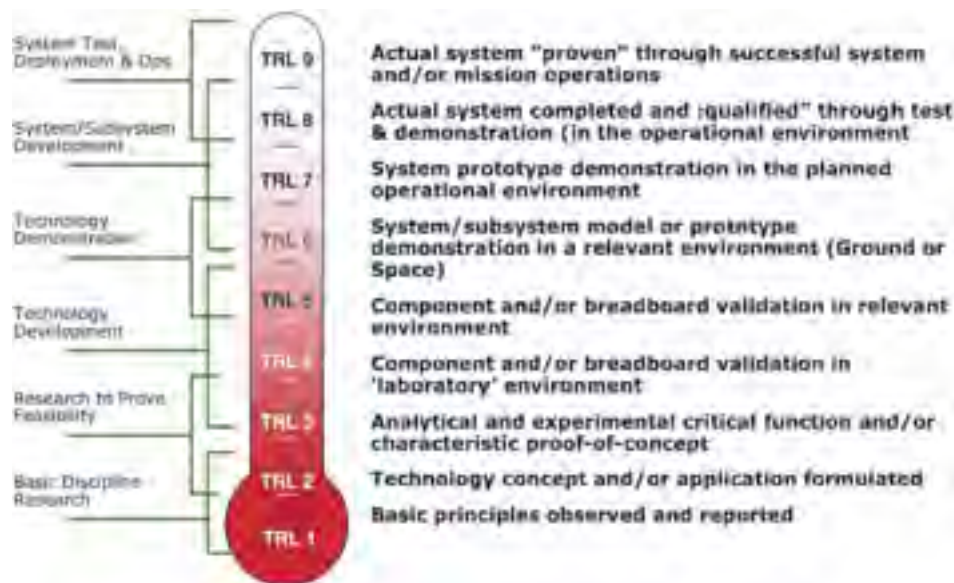


Figure 1.5 Aperçu des différents niveaux de l'échelle d'avancement technologique.
Tirée de (Mankins, 2009)

1.2.1 Notions aérodynamiques et motivations

En 1904, Ludwig Prandtl a démontré que l'écoulement d'air autour d'un corps peut être divisé en deux régions d'analyse. À proximité de la surface, il y a une zone mince nommée « couche limite » dans laquelle la friction de l'air est importante alors qu'en dehors de cette zone, la friction peut être négligée. Or, à l'intérieur de la couche limite tel qu'illustrée à la Figure 1.6, l'écoulement transite d'un état laminaire à turbulent. L'écoulement laminaire est constituée de couches se cisaillant les unes par rapport aux autres alors que l'écoulement turbulent se caractérise par un mélange chaotique complet des particules d'air. La friction entre l'air et la surface, communément appelée traînée de friction (qui représentent environ 80% de la traînée visqueuse) est beaucoup plus importante lorsque la couche limite est turbulente. Sur les avions de transport civil actuel, la majorité de la couche limite est turbulente. La réduction de la traînée visqueuse par le contrôle de l'écoulement laminaire dans la couche limite offre un potentiel de réduction de la consommation de carburant de 30% (Braslow, 1999).

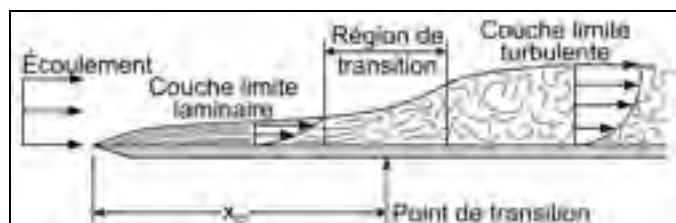


Figure 1.6 Transition de l'écoulement laminaire à turbulent dans la couche limite.
Adaptée de Anderson (2001)

Actuellement, les techniques à l'étude pour favoriser l'écoulement laminaire dans la couche limite sont le refroidissement de la surface, l'aspiration, les jets synthétiques, et le *Natural Laminar Flow* (NLF). Un profil NLF favorise naturellement l'extension du régime laminaire du bord d'attaque vers le bord de fuite. Par sa forme, l'accélération de l'écoulement est graduelle, évitant ainsi la formation d'un gradient de pression inverse qui déclencherait la transition (Braslow, 1999). Le développement de la technologie NLF est attribuable en partie à Liebeck (Liebeck and Ormsbee, 1970) et à la NASA qui, suite à l'embargo du pétrole en 1973, chercha des solutions pour améliorer l'efficacité énergétique des avions. Dans des

conditions favorables, un profil NLF peut conserver l'état laminaire de la couche limite jusqu'à 60-70% de la corde sur la surface supérieure et 50% de la corde sur la surface inférieure. L'extension laminaire de la couche limite permet de réduire d'au moins 50% la traînée qui serait générée par une couche limite turbulente (Eggleston *et al.*, 1987).

L'inconvénient des ailes d'avion NLF est que leur performance peut être compromise facilement dès que la vitesse ou l'angle d'attaque diffèrent du point de design. À l'égard de cette problématique, le projet CRIAQ 7.1 innove avec l'utilisation d'une aile à géométrie variable permettant de générer une panoplie de profils laminaire pour chacune des conditions de vol rencontrées. Bien que le concept même de réduction de la traînée par modification du profil remonte aux années 1980, aucune aile adaptative n'a encore atteint le niveau commercial. Ceci indique que la création d'une structure adaptative viable constitue un défi technologique majeur, ce qui a été réalisé dans le cadre du projet CRIAQ 7.1.

1.2.2 Terminologie aéronautique

Afin de faciliter la compréhension, la terminologie aéronautique utilisée dans la thèse est introduite dans cette section. Un profil se caractérise par une corde, une cambrure, une épaisseur, un bord d'attaque et un bord de fuite tels que présentés à la Figure 1.7. L'extrados et l'intrados désignent respectivement les sections supérieures et inférieures du profil. La corde est utilisée comme longueur de référence pour exprimer des dimensions relatives en %, par exemple, une épaisseur de 16%c. La vitesse relative de l'écoulement par rapport à l'aile est exprimée en nombre de Mach, soit le nombre de fois la vitesse à laquelle se déplace les ondes sonores dans cet écoulement d'air. L'angle d'attaque se défini entre la direction de l'écoulement et celle de la corde du profil.

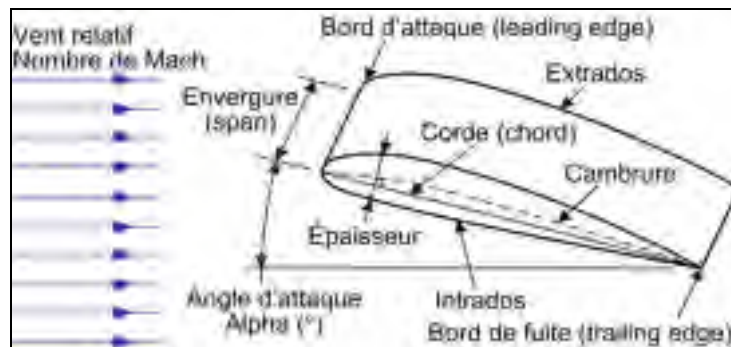


Figure 1.7 Schéma explicatif d'une aile 2D et son profil.
Adaptée de (Transport Canada, 1998)

La physique du vol identifie quatre principales forces agissantes sur un avion telles qu'illustrées à la Figure 1.8a. La portance est générée principalement par l'aile, permettant ainsi à l'avion de voler. La traînée freine le déplacement de l'aéronef et se présente sous diverse formes. En vol rectiligne à vitesse constante comme en régime de croisière par exemple, la force de traînée est annulée par la force de traction alors que la pesanteur est équilibrée par la force de portance. Au niveau de l'aile (Figure 1.8b), on distingue la traînée de forme que Transport Canada (1998) définit comme « [...] la résistance qu'offre l'air à la forme même d'un corps qui s'y déplace ». Pour sa part, la traînée de friction est engendrée par le frottement de l'air à la surface du profil. Dans le cas d'une aile d'avion, la traînée de friction est beaucoup plus importante que la traînée de forme. C'est précisément ce type de traînée que le projet CRIAQ 7.1 vise à réduire par l'amélioration du régime d'écoulement laminaire dans la couche limite.

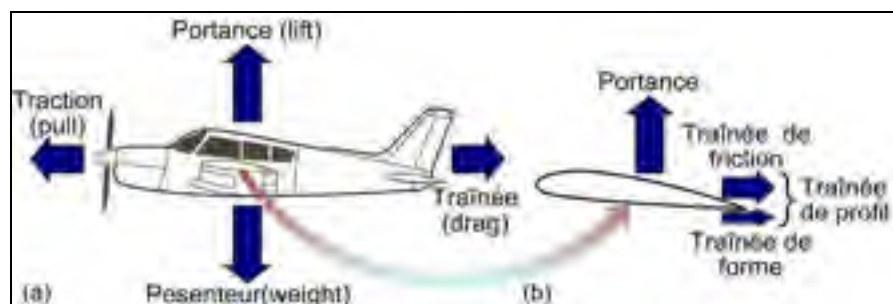


Figure 1.8 Forces principales sur (a) l'avion et (b) l'aile.
Adaptée de (Transport Canada, 1998)

La réduction de la traînée de l'avion a l'effet d'augmenter non seulement son efficacité énergétique mais également ses performances en vol comme, par exemple, la distance franchissable, l'endurance de vol (temps maximal en vol) et le taux de montée. Le gain en performance qu'offre une aile laminaire adaptative doit être évalué en considérant non seulement son impact sur la traînée, mais également celui sur la portance. Ainsi, dans le cadre de cette recherche doctorale, deux indicateurs ont été employés pour quantifier la performance de l'aile du projet CRIAQ 7.1 : 1) la réduction de la traînée en condition de portance constante et 2) la finesse de l'aile (ratio portance/traînée). La condition de portance constante se réalise par l'ajustement adéquat de l'angle d'attaque lors de l'adaptation du profil.

1.2.3 Description sommaire du projet CRIAQ 7.1

Le projet CRIAQ 7.1 a pour objectif de vérifier la faisabilité d'une aile au profil adaptatif capable de réduire la traînée de friction par l'amélioration de l'écoulement laminaire à sa surface supérieure. Pour y parvenir, un prototype est conçu, fabriqué et testé en soufflerie. Puisque l'étude se réalise en deux dimensions (2D) seulement, le profil de l'aile expérimentale est constant sur toute l'envergure. Ce profil de référence s'appelle WTEATE1 (pour *Wind Tunnel Experimental Airfoil with Trailing Edge 1*) et a été fourni par le CNRC-IRA. Avec son épaisseur maximale de 16% c , il est semblable à une famille de profils supercritiques naturellement laminaires ayant fait l'objet d'études passées (Eggleston *et al.*, 1987). Une particularité du profil WTEATE1 est son bord de fuite cassé. Or, à des fins de simulation aérodynamique seulement, le bord de fuite du profil est modifié pour en faciliter l'analyse, passant d'une terminaison cassée à pointue. À l'aide du logiciel Fluent, des analyses numériques en dynamique des fluides ont été réalisés au LARCASE afin de s'assurer que cette modification n'altère pas le comportement aérodynamique du profil (Benkemoun, 2006).

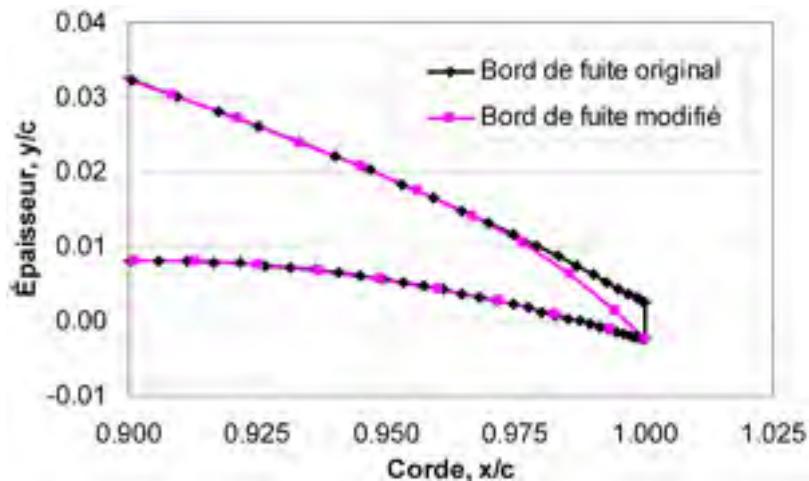


Figure 1.9 Comparaison des bords de fuite du profil WTEATE1 original et modifié pour l’analyse aérodynamique

Les composantes principales du prototype, de même que son principe de fonctionnement, sont schématisés à la Figure 1.10. Le caractère adaptatif de l’aile est attribuable à une structure active constituée d’un extrados flexible en matériau composite dont la géométrie peut être modifiée par le déplacement contrôlé des lignes d’actions fixées sous ce dernier. La structure active intègre des capteurs de pression à haut taux d’échantillonnage capable de localiser la position du point de transition de l’écoulement laminaire/turbulent. Sur la section rigide de l’aile, des pores de pression statiques permettent de compléter la mesure de la distribution de pression sur le contour du profil.

Le fonctionnement de l’aile aéroélastique repose sur un contrôleur commandant les actionneurs soit en boucle de contrôle ouverte ou fermée. Pour plus d’information, le schéma du contrôle de l’aile est détaillé en Figure 1.11. En boucle ouverte, seulement les conditions de l’écoulement (nombre de Mach, angle d’attaque) sont acheminées au contrôleur afin que ce dernier, par l’entremise d’une base de données, puisse générer les commandes optimales aux actionneurs. En boucle de contrôle fermée, l’optimisation du profil de l’aile s’effectue en temps réel à l’aide d’une rétroaction d’une mesure de la performance de l’aile acheminée au contrôleur. Cette rétroaction peut provenir de la mesure à la balance (A) permettant de déterminer la finesse de l’aile (L/D). Autrement, il est possible d’évaluer la transition de l’écoulement laminaire/turbulent par les capteurs de pressions (B) ou par la discontinuité de

température observée sur l'extrados à l'aide d'une caméra infrarouge (C). C'est ainsi que l'avion muni d'une telle innovation devrait voir sa traînée réduite puisque le profil de l'aile s'adaptera aux conditions de vol changeantes afin de demeurer optimal.

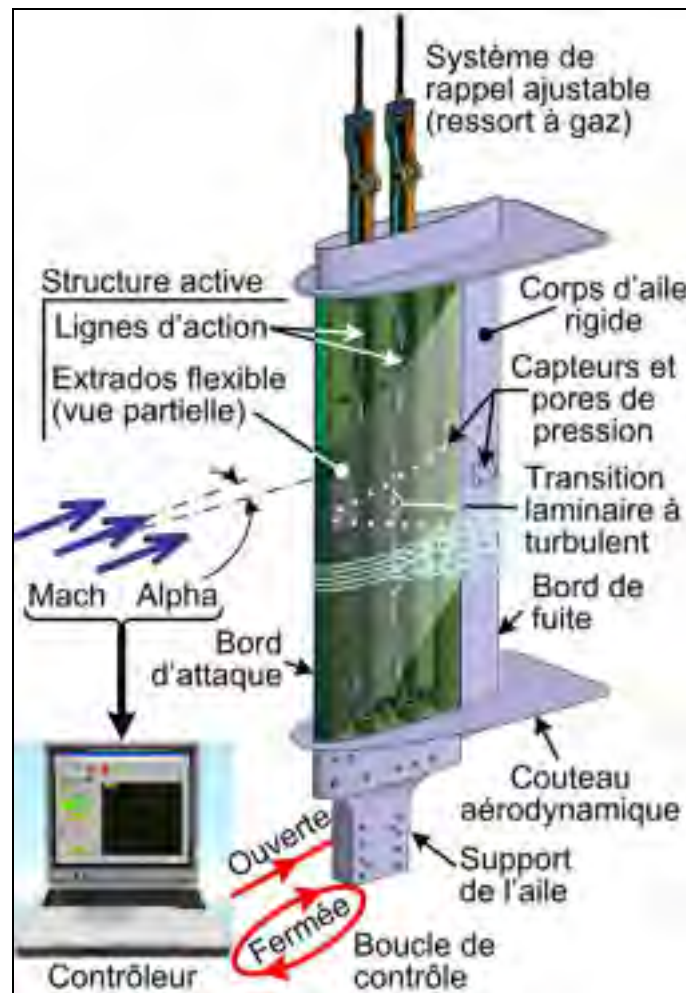


Figure 1.10 Schéma de l'aile aéroélastique du projet CRIAQ 7.1 : principe de fonctionnement et composantes

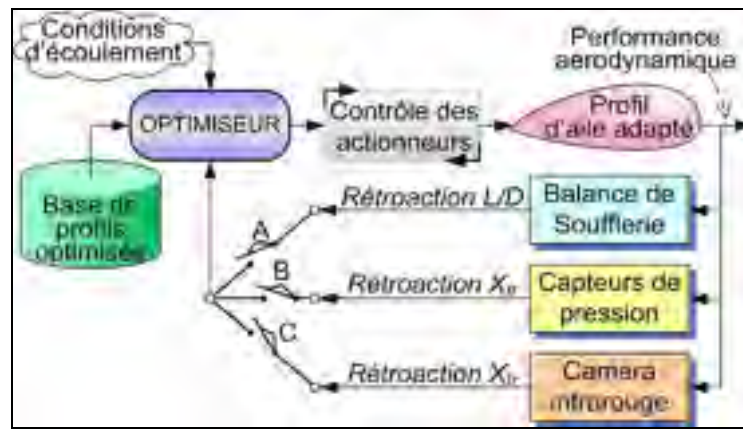


Figure 1.11 Schéma du système de contrôle de l'aile aéroélastique du projet CRIAQ 7.1

1.2.4 Cahier des charges « adaptatif » du projet CRIAQ 7.1

Le cahier des charges du projet CRIAQ 7.1 se précisa au fur et à mesure des différentes interactions entre les équipes multidisciplinaires. Tel que présentées au Tableau 1.2, 49 cas aérodynamique ont été définies par une matrice faisant varier le nombre de Mach entre 0.2 et 0.35 (pas de 0.025) et les angles d'attaque de -1° et 2° (pas de 0.5°). Afin de permettre l'adaptation de l'extrados du prototype à l'égard des différentes conditions d'écoulement, un espace pour le design et la fabrication des actionneurs de la peau flexible fut réservé au LAMSI tel que présenté à la Figure 1.13a. Le CNRC, chargé de la fabrication de la section rigide, utilisa la corde du profil pour établir le plan d'interface avec le module adaptatif du LAMSI. Les limites de la zone de travail furent établies entre 3 et 70 %c par l'équipe de l'EPM qui procéda à de nombreuses simulations numériques en dynamique des fluides. Selon leur calcul, cette zone de variation géométrique de l'extrados est suffisante pour améliorer le régime d'écoulement laminaire à la surface supérieure du profil.

Tableau 1.2
Matrice des noms de profils pour les conditions d'écoulement
du projet CRIAQ 7.1

Nombre de Mach	Angle d'attaque, deg						
	-1.0	-0.5	0.0	0.5	1.0	1.5	2.0
0.200	C1	C2	C3	C4	C5	C6	C7
0.225	C8	C9	C10	C11	C12	C13	C14
0.250	C15	C16	C17	C18	C19	C20	C21
0.275	C22	C23	C24	C25	C26	C27	C28
0.300	C29	C30	C31	C32	C33	C34	C35
0.325	C36	C37	C38	C39	C40	C41	C42
0.350	C43	C44	C45	C46	C47	C48	C49

Tel que présenté à la Figure 1.13b, en novembre 2007, l'équipe de l'EPM fournit au LAMSI et au LARCASE 47 profils adaptés suggérant des variations de l'épaisseur de l'aile allant de +8.1 mm (près du bord d'attaque) à -1.8 mm (près du bord de fuite). Pour deux des 49 cas aérodynamiques, C1 et C8, aucune adaptation n'a pu améliorer le régime d'écoulement laminaire déjà bien développé. À titre informatif, cette optimisation de profils a été réalisée en utilisant une courbe de Bézier (*B-Spline*) contrôlée par deux points mobiles limités en déplacement suivant la direction de la corde ($3.3\%c \leq x_1 \leq 35.7\%c$; $37.3\%c \leq x_2 \leq 69.7\%c$) et suivant la direction de l'épaisseur ($-.06\%c \leq y_i \leq 1\%c$). La fonction objective utilisée a visé à minimiser l'augmentation du régime d'écoulement laminaire tout en conservant les coefficients de portance et de moment constants. Plus de détails sont fournis dans le rapport interne d'Octavian Trifu (2007). Dans les travaux de conception de la structure active présentés au chapitre 3, ces données sont utilisées en tant que variations géométriques cibles.

Pendant la fabrication du prototype au mois de mai 2008, une seconde série de profils optimisés a été fournie par l'équipe de l'EPM en vue des premiers essais en soufflerie d'octobre 2008. Ces profils présentés en Figure 1.13c sont supérieurs aux précédents au niveau de l'augmentation du régime d'écoulement laminaire sur la surface supérieure de l'aile et ce, pour plusieurs raisons. D'abord, entre les deux optimisations, des polynômes de

régression ont été utilisés pour redéfinir le profil de référence qui présentait d'importantes discontinuités de courbures tel que présentés à la Figure 1.12. Également, après une recommandation d'Éric Laurendeau de Bombardier Aéronautique, les premiers 10%c de l'extrados ont été modifiés afin de diminuer l'accélération de l'écoulement et, d'un même coup, la probabilité de déclencher une transition laminaire/turbulent prématurée. De nouvelles limites du déplacement des points mobiles de la *B-Spline* ont été définies comme suit suivant les directions de la corde ($3.1\%c \leq x_i \leq 69.9\%c$) et de l'épaisseur ($-0.6\%c \leq y_1 \leq 1\%c$; $-0.6\%c \leq y_2 \leq 1,7\%c$). La fonction objective demeura la même que pour l'optimisation antérieure (novembre 2007). Par contre, à l'aide d'une méthode inverse mixte de design, l'équipe de l'EPM appliqua une correction finale aux profils optimisés afin d'enlever le gradient de pression défavorable au début de la zone à géométrie variable.

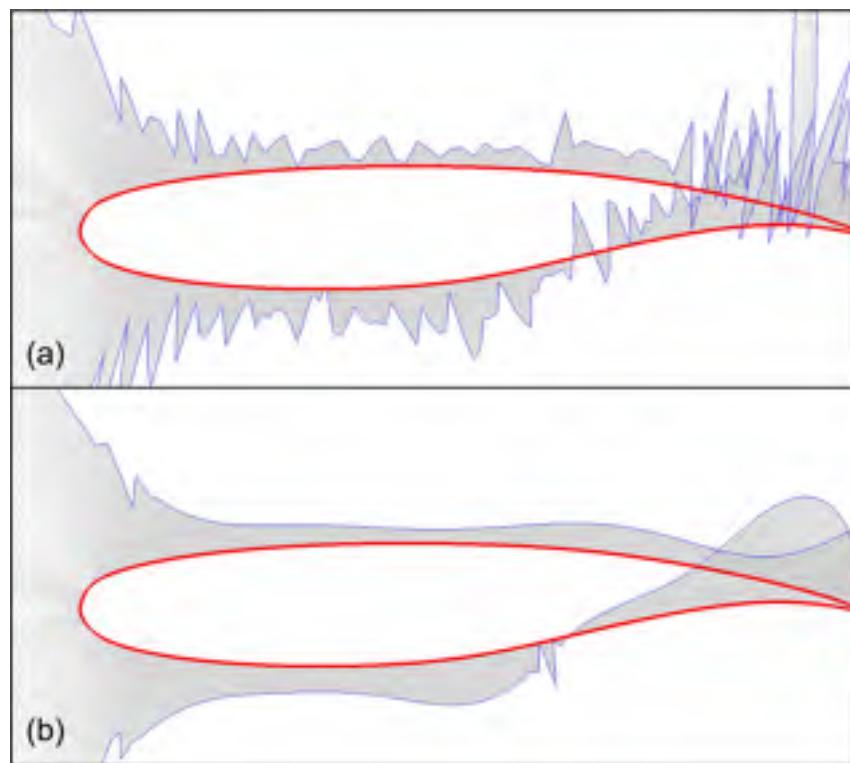


Figure 1.12 Analyse de courbure profil WTEATE1 :
(a) original, (b) avec polynôme de régression.

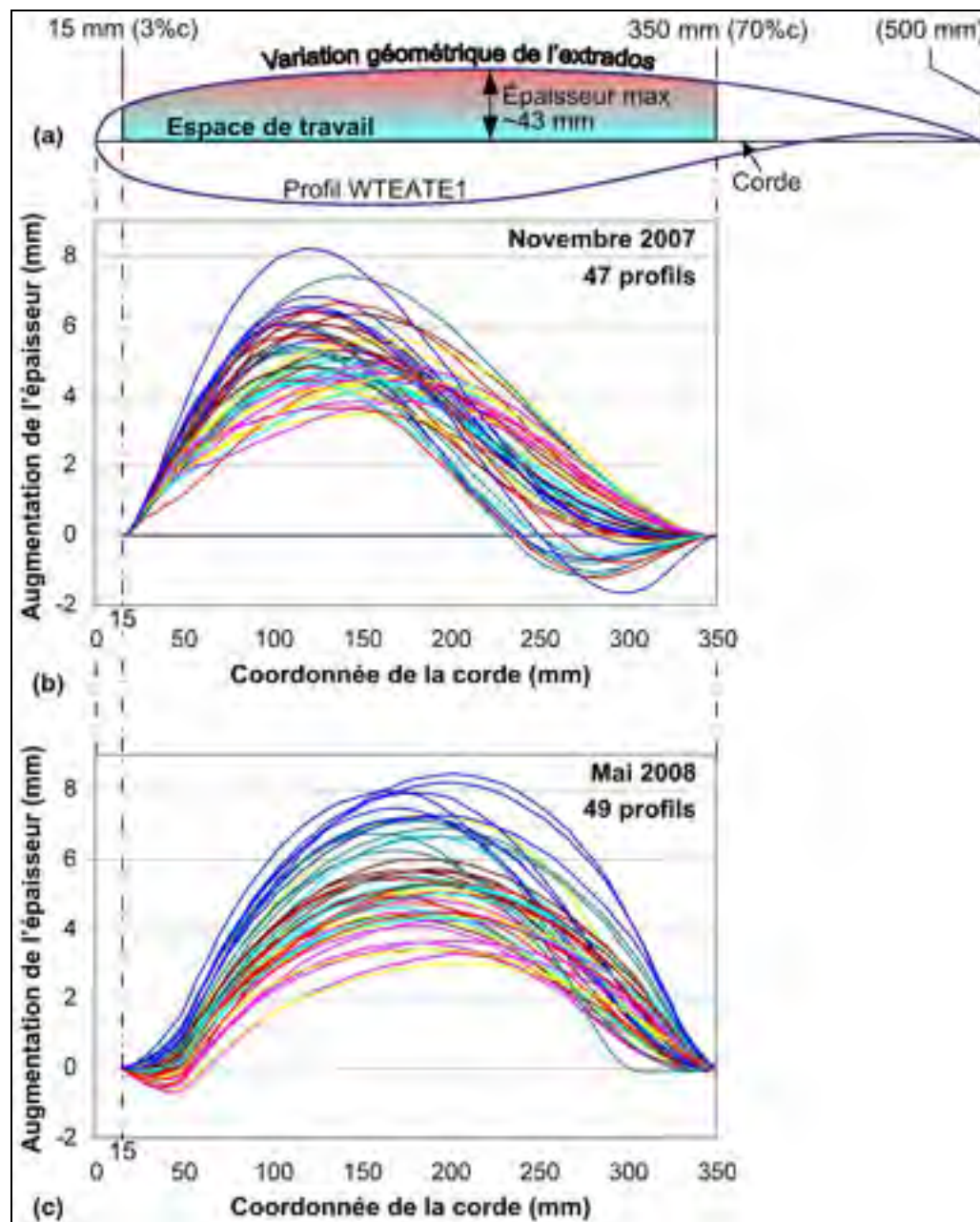


Figure 1.13 Résultats de l'équipe de l'EPM fournis au LAMSI :
 (a) espace de travail, (b) 1^{ère} série de profils optimisés (novembre 2007)
 et (c) 2^e série de profils optimisés (mai 2008).

1.2.5 Les outils de calculs numériques

Dans la réalisation du projet CRIAQ 7.1, plusieurs outils de calculs numériques ont été employés et élaborés. Concernant la préparation du cahier des charges, les travaux d'optimisation de l'équipe de l'EPM ont été réalisés à l'aide d'un algorithme génétique (GÉNIALE) et du solveur aérodynamique XFOIL 6.96. Pour plus de détails, le lecteur peut consulter l'article de Pagès, Trifu et al. (2007) présentant des travaux similaires portant sur l'optimisation de la variation géométrique de l'extrados d'un profil laminaire adaptatif, le NLF(1)-0416. En plus de sa rapidité d'exécution et de la qualité suffisamment bonne de ses prédictions, l'équipe de l'EPM a choisi le solveur XFOIL pour sa capacité à prédire la transition laminaire/turbulent. À l'aide de la méthode e^N , un critère de transition est fixé par l'utilisateur selon la valeur du facteur $N_{critique}$. Ce facteur, fixé à 7 par l'EPM, détermine la valeur du logarithme de l'amplification des ondes 2D Tollmien-Schlichting à partir de laquelle la transition se produit.

Lors de la conception de la structure active, le solveur aérodynamique XFOIL 6.96 a été utilisé avec les mêmes réglages. À la différence d'une *B-Spline*, la méthode des éléments finis fut employée pour modéliser différentes configurations de structure active. Sous le logiciel ANSYS, la modélisation inclut également les composantes de la transmission pour simuler avec plus de fidélité le comportement de l'aile laminaire adaptative. Finalement, les travaux d'optimisation se réalisèrent à l'aide du logiciel MATLAB R2008a, alors que le logiciel LabVIEW 8.6 fut employé dans l'instrumentation et le contrôle de l'aile en soufflerie.

1.2.6 La soufflerie subsonique du CNRC-IRA

Il a été jugé à propos de fournir une description sommaire de la soufflerie utilisée pour tester l'aile laminaire expérimentale à différentes conditions d'écoulement. Seulement un résumé des informations provenant du site internet du CNRC-IRA(2006) est fourni ici. L'appellation de la soufflerie de 2 m sur 3 m fait référence aux dimensions arrondies (largeur \times hauteur) de la section de sa chambre d'essai, soit 1,9 m sur 2,7 m. Cette soufflerie est localisée à Ottawa au CNRC-IRA. De nombreux organismes commerciaux, universitaires et gouvernementaux y

effectuent des travaux de recherche et développement par des essais aérodynamiques et industriels réalisés en régime subsonique. La soufflerie se caractérise par une conduite à circuit fermé qu'il est possible d'apprécier sur la photo de sa maquette fournie en Figure 1.14. En comparaison d'une soufflerie à circuit ouvert, la recirculation de l'air permet de récupérer une part de l'énergie cinétique de l'écoulement, et du même coup, d'obtenir des vitesses plus élevées pour un moteur de soufflante donné. De plus, le confinement de l'écoulement à l'intérieur de la conduite permet la réduction des niveaux de bruits. Par contre, une telle installation est souvent plus dispendieuse et nécessite beaucoup d'espace. Aussi, pour éviter toute hausse de température indésirable, elle est munie d'un système de refroidissement.

En fonctionnement, la pression statique de la chambre d'essai est maintenue près de la pression atmosphérique au moyen de trous de ventilation communiquant avec l'air ambiant. Lorsqu'un prototype est testé, les forces et les moments dans les 3 directions principales sont mesurés par des balances. C'est d'ailleurs à l'aide de la traînée brute obtenue avec la balance que l'optimisation en temps réel présentée au chapitre 5 a pu être réalisée. Les mesures brutes à la balance sont converties en coefficients aérodynamiques en utilisant les propriétés de l'écoulement et les corrections qui s'y appliquent. Le coefficient de traînée de profil (et non du prototype) s'obtient quant à lui par la mesure de l'appauvrissement de la quantité de mouvement dans la couche limite de l'écoulement. À cette fin, une traverse de Pitot est utilisée, permettant de relever la distribution de vitesse de l'écoulement dans le sillage de l'aile. Afin de visualiser le comportement de l'écoulement à la surfaces des modèles testés, la soufflerie dispose de plusieurs moyens techniques tels que : le film d'huile, la fumée ainsi que la mesure infrarouge. À ce propos, les travaux de recherche présentés aux chapitres 4 et 5 ont utilisé des mesures de transition laminaire/turbulent obtenues à l'aide d'une caméra infrarouge. Cette méthode se base sur le phénomène de convection à la surface de l'extrados, beaucoup plus importante pour un régime d'écoulement turbulent que laminaire.

Puisque l'objectif de l'aile laminaire adaptative consiste à augmenter l'écoulement laminaire, une attention particulière a été portée sur le niveau de turbulence de l'air entrant dans la

chambre d'essai. Fixé à 0,14% par le CNRC-IRA, cette perturbation initiale de l'écoulement n'a d'autre effet que de favoriser le déclenchement de la transition laminaire/turbulent. Ce niveau de turbulence, introduit dans une corrélation expérimentale, a permis à l'équipe de l'EPM de fixer le facteur $N_{critique}$ à 7, une valeur légèrement conservatrice.

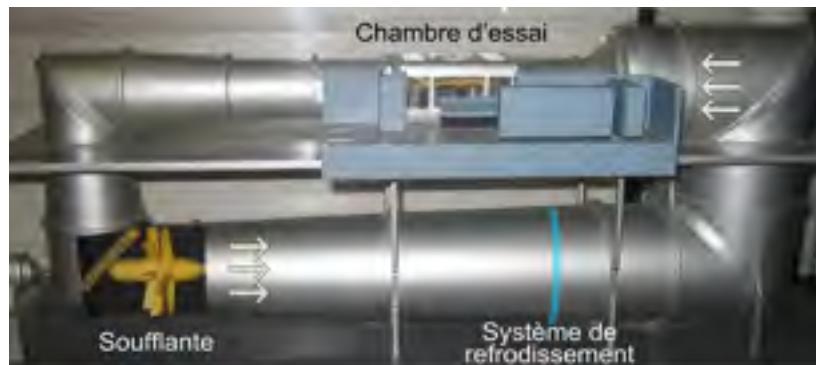


Figure 1.14 Maquette de la soufflerie de 2 m sur 3 m du CNRC-IRA utilisée pour tester l'aile laminaire adaptative.
Adaptée du CNRC-IRA (2006)

1.3 Problématique de la recherche

La conception d'une structure active soumise à un chargement aérodynamique variable est une problématique en soi. La structure doit être suffisamment flexible pour accommoder les modifications géométriques désirées sans toutefois être trop sensible aux chargements aérodynamiques. Le choix du concept, de même que la méthodologie de design utilisée, influenceront grandement le comportement de la structure active et, par conséquent, celui de l'aile adaptative.

La principale fonction de la structure active consiste à adapter le profil de l'aile laminaire en vue d'améliorer ses performances aérodynamiques sur une étendue de conditions de vol. Puisque les modifications géométriques commandées à la structure active se doivent d'être

optimales, l'exploitation de l'aile adaptative laminaire (stratégie de contrôle) est traitée comme une problématique sous-jacente aux travaux de conception.

1.4 Objectifs de la recherche

L'objectif premier poursuivi dans cette thèse est la conception de la structure active destinée à permettre l'adaptation du profil de l'aile laminaire. L'objectif sous-tendu consiste à mettre en place une méthodologie permettant la conception optimale d'une structure active destinée à œuvrer sous chargement aérodynamique.

Deuxièmement, les travaux de cette thèse visent à exploiter le plein potentiel de la structure active de l'aile laminaire dans les conditions de soufflerie. Afin d'y parvenir, la recherche s'orienta vers le développement d'une stratégie de contrôle en temps réel utilisant les outils de calculs numériques développés au stade de la conception.

1.5 Déroulement et contributions au projet

Le diagramme de la Figure 1.15 schématise le déroulement de la recherche doctorale au sein du projet CRIAQ 7.1 jalonné par trois essais en soufflerie : en octobre 2008, en février 2009 et en mai 2009. Les travaux numériques et expérimentaux ont débuté avant les essais en soufflerie afin de concevoir la structure active de l'aile laminaire adaptative. Pour y parvenir, un premier modèle numérique de structure active fut construit et validé (voir compte rendu de conférence en annexe I). Par la suite, les travaux de conception se poursuivirent avec l'utilisation du modèle numérique à l'intérieur d'une méthodologie de conception optimale spécialement développée afin de résoudre les problèmes aéro-structuraux (travaux présentés au chapitre 3). En utilisant les résultats des simulations numériques, une étude sur les bénéfices escomptés de l'aile laminaire adaptative a pu être réalisée (voir note d'ingénierie en annexe II).

Au cours des premiers essais en soufflerie, les profils adaptés selon les résultats d'optimisation utilisant le modèle B-Spline (mai 2008) ont été testés. Malheureusement, les résultats ne présentèrent aucune amélioration significative de la performance aérodynamique, tel que le démontre les points des polaires de traînée de la Figure 1.16a. Les données recueillis au cours de ces essais ont cependant été très utiles dans la poursuite des travaux de recherche portant sur l'exploitation de la structure active. En particulier, les pressions mesurées ont permis la calibration du couplage aéro-structural du modèle numérique présenté au chapitre 4. Par la suite, avec le soutien de l'étudiant à la maîtrise Corentin Sainmont de l'équipe de l'EPM, de nouveaux profils optimisés offrant des performances supérieures ont été déterminées. Le chapitre 4 de cette thèse présente les résultats de cette optimisation multidisciplinaire dont les résultats furent testés en soufflerie au mois de février 2009. Comme le témoigne les polaires de traînée de la Figure 1.16b, la capacité de l'aile expérimentale à offrir moins de traînée (C_D) pour une même portance (C_L) a pu être démontrée cette fois-ci. Les essais en soufflerie de février 2009 se sont terminés par la caractérisation du comportement aérodynamique de l'aile expérimentale pour différents états d'adaptations possibles. Ces résultats ont permis de mettre en évidence des limitations du modèle numérique. C'est pourquoi, une stratégie novatrice d'optimisation en temps réel du profil de l'aile a été développée pour être ensuite testée en mai 2009. Le chapitre 5 relate ces travaux permettant d'exploiter le plein potentiel de l'aile adaptative laminaire en soufflerie. Suivant ces résultats, une liste de recommandations en vue d'appliquer ce concept sur un avion réel a pu être formulée.



Figure 1.15 Déroulement et contributions au projet de recherche présentées dans les différentes sections de la thèse.

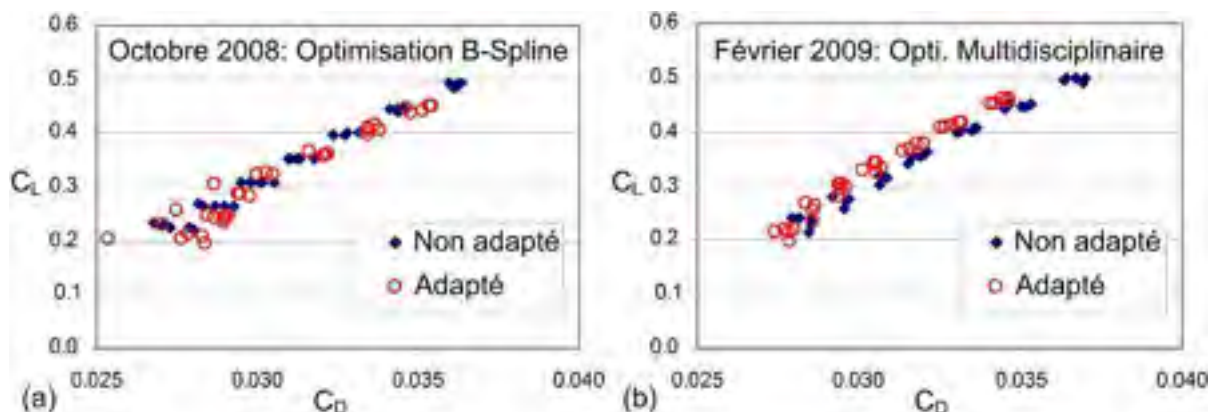


Figure 1.16 Polaire de traînée obtenue en soufflerie :
(a) octobre 2008, (b) février 2009.

D'un point de vue général, le sujet limité de cette thèse laisse dans l'ombre plusieurs activités de recherche ayant contribuées au succès du projet CRIAQ 7.1. À titre d'exemple, la modélisation numérique de la structure active et son interaction aéro-structural a permis de fournir les données nécessaires à la conception des actionneurs AMF. À cet effet, le mémoire

d'Émeric Morellon (2010) ainsi que les publications de Thomas Georges et Vladimir Brailovski énumérées dans l'avant propos de cette thèse sont à consulter pour plus de détails. Aussi, alors que la fabrication de l'aile fut assumée par des assistants de recherches attachés au LAMSI et au CNRC-IRA. L'assemblage et l'instrumentation de cette dernière ont nécessité un important travail d'équipe en collaboration avec les membres du LARCASE afin de résoudre les nombreux défis techniques rencontrés. En dernier lieu, la contribution apportée lors de la participation aux réunions multidisciplinaires de même que lors de la planification et du déroulement des essais en soufflerie est non négligeables. Réciproquement, les travaux de cette thèse n'auraient pu aboutir sans l'apport scientifique et technique des nombreux collaborateurs au projet CRIAQ 7.1. Enfin, complété au cours de l'année 2009, le projet CRIAQ 7.1 offre à présent de belles perspectives d'application à des niveaux d'avancement technologique plus élevés (TRL ~ 5-6).

CHAPITRE 2

REVUE DE LA LITTÉRATURE SUR LES AILES ADAPTATIVES

De nos jours, les avions utilisent des dispositifs hypersustentateurs permettant de modifier la cambrure du profil de l'aile et sa surface portante. Que ce soit des becs (*slats*) et/ou des volets (*flaps*) tel qu'illustrés à la Figure 2.1, ces dispositifs ont pour but d'accroître la portance de l'avion pendant les phases de décollage et d'atterrissage afin que ces manœuvres puissent se réaliser à des vitesses réduites. En régime de croisière, ces mécanismes articulés complexes sont rétractés afin de générer un minimum de traînée. D'autres surfaces articulées moins imposantes comme les ailerons sont utilisées pour diriger l'avion. Le carburant brûlé en cours de vol allège l'avion et oblige constamment le pilote à ajuster l'angle d'attaque afin de réduire conséquemment la portance. Les conditions de vols en croisière n'étant pas constantes, l'aile ne peut qu'être conçue de façon globalement optimale, offrant un compromis de performance sur l'étendue de la plage de conditions de vol. À l'égard de l'aile adaptative, il est attendu que l'utilisation de ce concept sur les avions de demain devrait améliorer leur performance aérodynamique tout en permettant des missions de vol polyvalentes.



Figure 2.1 Bec (*slat*) et volet (*flap*) de l'airbus A300.
Par Adrian Pingstone (2007) du domaine public

Maintenant que les objectifs de recherche de la thèse ont été présentés, cette section fait état des différents travaux recensés dans la littérature et jugés pertinents à l'égard des problématiques touchant la conception et l'exploitation des ailes adaptatives. À l'aide de commentaires ajoutés, ce recensement des écrits vise à situer les travaux de cette thèse dans l'état de l'art. Pour amorcer cette revue de la littérature, voyons d'abord différents concepts permettant à l'aile de s'adapter.

2.1 Les concepts

Le concept d'aile adaptative est inspiré des oiseux qui adaptent la forme de leur ailes selon leur besoins : s'envoler, atterrir, voler rapidement ou lentement. Au début du 20^e siècle, au temps des premiers avions, l'homme a utilisé ce concept pour diriger l'aéronef. Par exemple, les frères Wright contrôlaient le roulis de leur avion, illustré à la Figure 2.2, en tirant sur des câbles afin d'accentuer ou diminuer le gauchissement des ailes. Ces ailes alors flexibles ont été rigidifiées afin de permettre aux avions, comme ceux de la première guerre mondiale (1914-1918), d'atteindre des vitesses plus élevées. C'est ainsi qu'apparaissent pour la première fois les surfaces de contrôle articulées. Puis, ce n'est qu'en 1917 que le profil d'aile mince va commencer à céder sa place au profil épais. Cette possibilité avait été jusqu'alors écartée par la communauté scientifique de l'époque, convaincue que l'épaississement du profil augmenterait la traînée. Au contraire, le profil épais est toujours utilisé aujourd'hui puisqu'il permet une finesse et un coefficient de portance maximum plus élevé. De plus, l'aile au profil épais permet d'intégrer une structure en porte-à-faux éliminant la traînée produite par le câblage et les supports nécessaires à la solidité d'une aile au profil mince. Cette innovation aérodynamique réalisée au sein du camp allemand leur permettra un avantage certain lors de la mise en service du légendaire triplan Fokker Dr-1 piloté par le célèbre « Baron Rouge », Rittmeister Manfred Freiher von Richthofen. Cet avion de première guerre mondiale fut reconnu pour son taux de montée et sa manœuvrabilité exceptionnels. Finalement, d'un point de vue pratique, l'aile épaisse alloue un espace pour les réservoirs de carburant localisés autrement dans le fuselage.

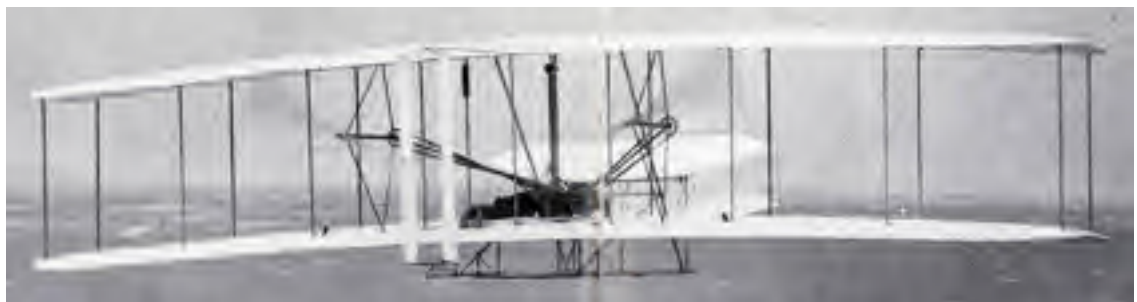


Figure 2.2 Avion des frères Wright lors du premier envol historique de 1903.

Tirée du Musée de l'air et de l'espace (1992, p.26-27)



Figure 2.3 Triplan Fokker Dr-1, premier avion de guerre à utiliser un profil épais.

Tirée de Mackworth-Praed (1990, p.218)

Concernant les avions de transport, l'innovation aérodynamique se réalisant actuellement procède par l'application et le développement des différentes méthodes permettant de maintenir le régime d'écoulement laminaire dans la couche limite sont prometteuses. Ces méthodes de contrôle de l'écoulement peuvent être **naturelles** comme dans le cas des profils NLF discutés en section 1.2.1 ou **actives** par l'utilisation de systèmes d'aspiration ou de jets synthétiques. Les deux méthodes (naturelles et actives) peut être combinées afin de donner lieu à un contrôle de type **hybride**. En parallèle, l'avancement du concept de l'aile adaptative est favorisé par la disponibilité et la capacité grandissante des logiciels de simulation numériques de même que par l'émergence des matériaux composites dans la fabrication des avions. En effet, depuis les dernières décennies, l'intérêt pour les ailes adaptatives ne cesse de croître, présage d'une nouvelle innovation aérodynamique qui marquera bientôt les avions

de demain. Les dernières décennies ont vu naître de nombreux concepts à l'essai, chacun présentant des avantages et des inconvénients. L'aile adaptative doit permettre une rigidité suffisante pour soutenir les forces aérodynamiques et la flexibilité nécessaire à l'adaptation du profil. Alors que l'adaptation peut être localisée sur le bord d'attaque, l'extrados ou l'intrados, elle peut aussi être généralisée à tout le profil dans les cas où l'aile est entièrement flexible.

2.1.1 *Belt-rib* (adaptation de la cambrure du profil)

Campanile et Sachau (2000) proposent le concept *belt-rib* permettant à une aile de varier sa cambrure tout en demeurant très rigide le long de l'envergure (voir Figure 2.4). L'idée repose sur une nervure constituée d'une grande quantité de longerons contenus à l'intérieur d'une ceinture. La disposition parallèle des longerons et leurs liaisons avec la ceinture accommodent seulement la modification géométrique de la nervure dans le plan corde-épaisseur. Cette approche n'offre pas beaucoup de degrés de liberté à l'égard des profils à générer. Par contre, son excellente rigidité au chargement aérodynamique a été démontrée expérimentalement, considérant son utilisation comme volet de bord de fuite pour l'Airbus A-340.



Figure 2.4 Design optimisé du *belt rib* concept.
Tirée de Campanile and Anders (2005)

2.1.2 Structure active (adaptation du bord d'attaque)

Chandrasekhara, Carr et al. (1997) ont utilisé le concept de la structure active installée au bord d'attaque permettant de varier son rayon. Ce système présenté à la Figure 2.5 vise à

étendre la région de faible pression sur tout l'extrados de façon à éviter le décollement de la couche limite sur la pale d'hélicoptère. La fabrication du bord d'attaque a été réalisée par procédé de moulage utilisant des plis pré-imprégnés de fibre de carbone et de verre. La conception fut réalisée par une méthode de calcul par éléments finis. Ainsi, l'épaisseur de la peau en composite a été fixée en variant le nombre de plis de façon à ce que l'évolution du profil soit satisfaisante le long de la course de l'actionneur. L'actionnement a été réalisé par l'intermédiaire d'une came et d'un bras attachés à la peau flexible. Les résultats expérimentaux ont démontré la capacité du concept à rattacher l'écoulement malgré la présence de discontinuités géométriques à la surface. Finalement, une certaine sensibilité de la structure active à l'égard du chargement aérodynamique a été observée par la variation du rayon au bord d'attaque lors d'un actionnement avec ou sans la présence de l'écoulement.

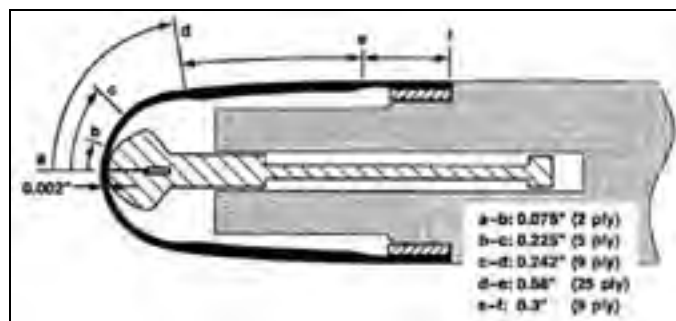


Figure 2.5 Détails de construction du modèle de profil à bord d'attaque déformable de façon dynamique.

Tirée de Chandrasekhara, Carr et al. (1997)

2.1.3 Structure compliante (adaptation du bord de fuite)

Afin de modifier la géométrie du bord de fuite de l'aile présentée en Figure 2.6, l'entreprise FlexSys Inc. utilisa le concept de la structure compliante pour créer la *Mission Adaptive Compliant Wing* (MACW) (Hetrick *et al.*, 2007). Cette aile a été spécialement conçue pour un avion de longue distance en haute altitude. Son bord de fuite ne possède aucune articulation et il est capable de fléchir de -10 à +10° avec un vrillage de 3°. La structure compliante utilisée présente une topologie géométrique optimisée pour assurer la flexion désirée dans les limites élastiques du matériau. Les résultats des essais en vol ont démontré

que le MACW présente de faibles niveaux de traînée en régime d'écoulement laminaire fortement établis sur les premier 60% de la corde de l'extrados (FlexSys_Inc., 2003).



Figure 2.6 *Mission Adaptive Compliant Wing*
Adaptée de AirForce (2007)

Le cahier des charges lié à la conception de l'aile adaptative du projet CRIAQ 7.1 demande à ce que la surface supérieure puisse permettre des changements géométriques afin de permettre l'adaptation du profil. Parmi les différents types de concepts d'aile adaptative, la structure active est favorisée puisqu'elle présente un design et une mise en forme simple en comparaison avec une structure compliante (Figure 2.6).

2.2 Les méthodologies de design

La conception d'une aile adaptative nécessite la résolution de problèmes aérodynamiques et structuraux. Le design des premières ailes adaptatives, comme celles utilisées par les frères Wright, suivait une méthodologie fondée surtout sur l'expérimentation. Aujourd'hui, cette tâche laborieuse est facilitée par l'accessibilité toujours grandissante d'outils de calculs numériques. Les problèmes aérodynamiques et structuraux peuvent être résolus **simultanément ou séquentiellement**.

2.2.1 Approche simultanée

L'approche de conception simultanée est favorable pour le design d'un concept présentant un niveau d'intégration élevé. Dans la littérature, Strelec et al. (2003) ont réalisé un couplage aéro-themo-structural afin de concevoir de façon optimale leur prototype d'aile adaptative actionné par les AMF (Figure 2.7). Afin de réduire le temps de calcul, les auteurs ont trouvé

nécessaire de simplifier le problème en réduisant leur modèle numérique structural de 3D à 2D. L'optimisation a été réalisée pour un cas d'écoulement seulement, considérant 9 variables de design associés à la localisation et au chauffage de 3 fils d'AMF. Malheureusement, lors de la fabrication du prototype, il n'a pas été possible d'installer 2 des 3 fils, obligeant de modifier la solution optimale à cause de l'espace de travail trop restreint. En somme, l'approche simultanée nécessite souvent l'évaluation d'une quantité importante de configurations puisque toutes les variables de design sont fixées en une seule optimisation. Aussi, vu la manipulation simultanée des variables structurales et aérodynamiques, le risque de solutions non réalisables physiquement est plus grand. C'est pourquoi une attention particulière doit être portée lors de la détermination des conditions frontières ainsi que des valeurs-limites des variables de design.

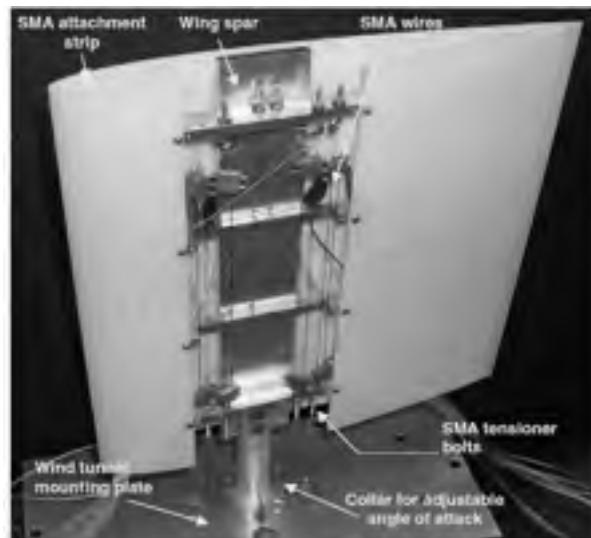


Figure 2.7 Aile adaptative utilisant des alliages à mémoire de formes.
Tirée de Strelec, Lagoudas et al. (2003)

2.2.2 Approche séquentielle

À l'égard du MACW (Figure 2.6), la conception a été réalisée en deux étapes. D'abord les formes d'aile adaptées ainsi que les chargements aérodynamiques furent définis à l'aide d'analyses aérodynamiques. Ensuite, ces résultats furent utilisés dans la conception de la

structure compliante afin que cette dernière puisse satisfaire aux modifications géométriques demandées par des conditions d'écoulement données. Il est à noter que les auteurs ont ensuite procédé à l'optimisation de la structure compliante afin de réduire les forces aux actionneurs, le poids de l'aile, le risque de flambage et les contraintes de fatigue.

Les travaux de conception de la structure active du projet CRIAQ 7.1 (chapitre 3) utilisent cette même approche de conception puisqu'elle permet d'obtenir facilement des solutions aérodynamiques et structurales raffinées. Par contre, pour surmonter l'inconvénient majeur de cette approche, soit la difficulté à assurer la compatibilité de la solution structurale avec la solution aérodynamique, un critère de performance aérodynamique a dû être introduit lors de la résolution du problème structural.

2.3 L'exploitation optimale du caractère adaptatif

Les ailes adaptatives relèvent d'un domaine relativement nouveau et les méthodes utilisées pour exploiter ces dernières en soufflerie ou en vol le sont tout autant. Après avoir parcouru la littérature à ce propos, la détermination des profils à générer à chacune des conditions d'écoulement rencontrées s'effectue à l'aide d'un plan d'expérience ou par le biais d'un algorithme d'optimisation. En outre, tel que le présente le Tableau 2.1, les méthodes trouvent également leur distinction selon le fait qu'elles se réfèrent directement au prototype d'aile adaptative (modèle physique) ou à un modèle numérique souvent moins dispendieux à utiliser. En ayant recours à un modèle numérique, les travaux d'optimisation se réalisent avant les essais expérimentaux, peu importe la technique d'optimisation employée (plan d'expérience ou algorithme). Une fois les profils optimaux déterminés par l'optimisation numérique, le contrôle du prototype d'aile adaptative s'effectue en boucle ouverte, c'est-à-dire par des commandes aux actionneurs indépendantes de la performance mesurée. Il en est également de même lorsque le prototype physique est testé selon un plan d'expérience prédéfini afin de modéliser expérimentalement la performance de l'aile adaptative. Par contre, lorsqu'un algorithme interagit directement avec le modèle physique afin de chercher le profil optimal, le contrôle est dit en boucle fermée. Afin de réaliser une optimisation en

temps réel, la performance doit être retournée à l'algorithme afin que ce dernier puisse déterminer les prochaines commandes aux actionneurs.

À l'aide d'exemples, les sections suivantes de ce chapitre fournissent de plus amples détails et explications sur chacune de ces méthodes d'exploitation.

Tableau 2.1
Méthodes d'exploitation (et de contrôle) d'une aile adaptative

Technique d'optimisation	Modèle	
	Numérique	Physique
Plan d'expérience	Optimisation numérique (contrôle en boucle ouverte)	Modélisation expérimentale (contrôle en boucle ouverte)
Algorithme		Optimisation en temps réel (contrôle en boucle fermée)

2.3.1 Optimisation numérique (boucle ouverte)

Outre pour fin de conception, la modélisation numérique peut également être employée pour la prédiction des meilleures formes de profils d'une aile adaptative à l'égard des différentes conditions de vols. Strelec et al. (2003) ont exploité leur "*Shape Memory Alloy Actuated Reconfigurable Airfoil*" à partir d'un algorithme d'optimisation génétique interrogeant le modèle numérique de leur aile expérimentale. Pour un angle d'attaque de 3°, les paramètres régissant la forme de l'aile ont pu être optimisés rapidement, permettant l'obtention d'une performance aérodynamique satisfaisante en soufflerie subsonique. Par contre, la comparaison des résultats avec les prédictions numériques ont mis en évidence certaines limitations du modèle. En effet, l'augmentation de la portance mesurée fut approximativement la moitié de celle escomptée numériquement. Ce constat suggère que d'autres formes de profils auraient possiblement permis d'obtenir une performance accrue. Toutefois, pour la finalité des travaux présentés par Strelec et al., cette marge d'erreur était

acceptable puisqu'elle permet de démontrer la capacité d'un concept d'aile adaptative utilisant des alliage à mémoire de forme.

Dans le cadre de cette recherche doctorale, la modélisation numérique a été employée afin de déterminer les formes de profils commandées en boucle de contrôle ouverte (travaux présentés au chapitre 4). L'optimisation a eu recours au plan d'expérience numérique et à l'algorithme. Alors que l'algorithme est plus rapide avec un nombre réduit d'exécution du modèle numérique, le plan d'expérience a permis de valider le bon fonctionnement de ce dernier.

2.3.2 Modélisation expérimentale (boucle ouverte)

Loin d'être obsolète, le plan d'expérience est encore très utilisé afin de modéliser le comportement d'un système physique à l'égard des variations d'un certains nombre de paramètres sélectionnés. Pour une seule variable, une corrélation expérimentale est obtenue alors que pour deux variables le comportement du système s'exprime par une surface de réponse. Peu importe le nombre de variables, cette approche est populaire en industrie pour concevoir de façon optimale un système physique trop complexe à modéliser numériquement. Dans le cas d'une aile adaptative soumise aux différentes conditions de vol, le profil doit être optimisé afin d'obtenir les meilleures performances aérodynamiques possibles.

Dans cet ordre d'idées, afin de procéder à des essais en haute altitude, le prototype du MACW fut installé sous l'avion *Scaled Composite White Knight* tel que présenté à la Figure 2.8. À cet effet, une matrice d'essais contenant 36 points a été définie afin de générer les différentes adaptations possibles de l'aile (6 incrément) à l'égard de toutes les conditions de vols rencontrés (6 angles d'attaque). Les résultats ont permis de déterminer le profil de l'aile le plus performant à l'égard de chaque condition du vol, une information essentielle pour l'exploitation future de cette technologie sur un avion réel.

Il est à noter que, lorsqu'elle est menée avec minutie, l'expérimentation a l'avantage de présenter des résultats plus fiables que toute prédition numérique, favorisant ainsi l'exploitation plus adéquate de tout système. Par contre, cette approche exige beaucoup plus de ressources pour être mise en œuvre que toute autre. D'ailleurs, la durée cumulative des essais en vol de la maquette du MACW a été de 27 h, ce qui représente une somme d'argent considérable.

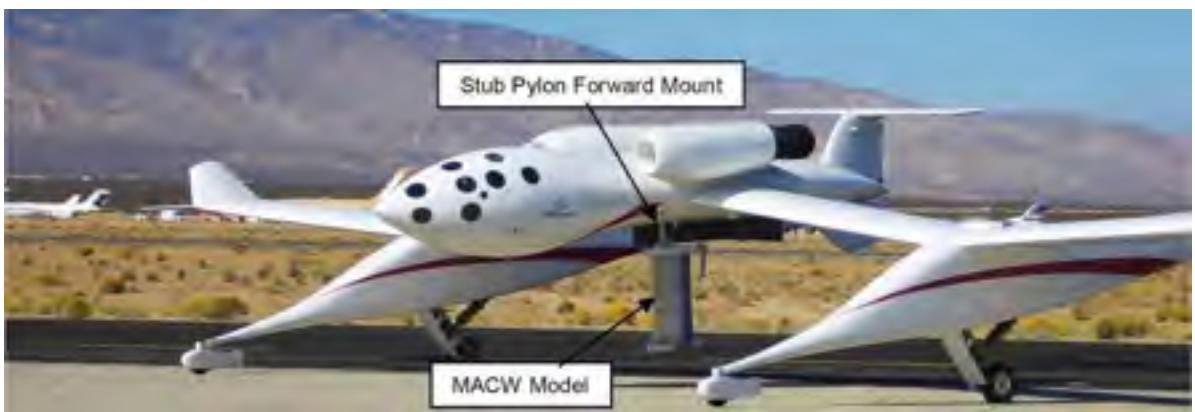


Figure 2.8 MACW prototype installé sous l'avion Scaled Composite White Knight.
Tirée de Hetrick, Osborn et al. (2007)

À l'égard de l'aile laminaire adaptative, la modélisation expérimentale a également été utilisée. Les résultats découlant de cette méthode ont permis de relever les limitations du modèle numérique (travaux présentés au chapitre 5) et de calibrer l'algorithme dédié à l'optimisation en temps réel.

2.3.3 Optimisation en temps réel (boucle fermée)

Finalement, la troisième approche d'exploitation nécessite l'utilisation d'un *Hardware In the Loop* (HIL), expression anglaise signifiant un dispositif physique permettant de fournir une rétroaction sur la performance d'un système physique. L'optimisation peut alors être réalisée en temps réel à l'aide d'une boucle de contrôle fermée. L'industrie de l'automobile, tout comme celle de la robotique, sont familiers avec les HIL qui facilite la conception ou l'exploitation optimale d'un système. Les travaux présentés par Hemker, Stelzer et Stryk

(2009) fournissent un exemple d'utilisation du HIL pour maximiser la vitesse de marche et la stabilité d'un robot humanoïde. Le robot est considéré comme le HIL puisque ses performances sont retournées en temps réel à l'algorithme de l'optimiseur qui tente d'ajuster au mieux ses paramètres de marche. Suite à un nombre réduit d'expériences, l'approche HIL identifie le meilleur mouvement de marche qui aurait été difficilement obtenu par un simple ajustement intuitif des paramètres.

Dans le domaine des ailes adaptatives recensées dans la littérature, les premiers travaux utilisant un HIL datent des années 1977-1979. Levinsky et al. (1982) utilisent cette approche pour exploiter en soufflerie transsonique une aile à géométrie reconfigurable représentative de l'avion F111 TACT présentée à la Figure 2.9. Le choix de cette approche de contrôle fut justifié par le grand nombre de paramètres régissant la forme de l'aile, soit les 12 actionneurs hydrauliques contrôlés indépendamment. Dans ce cas, la balance aérodynamique de la soufflerie agit à titre de HIL en permettant de connaître en temps réel la performance de l'aile. Ainsi, par l'entremise d'un algorithme d'optimisation, plusieurs formes d'aile ont pu être générées automatiquement, d'une itération à l'autre, jusqu'à l'obtention d'une forme jugée optimale. Cette approche a permis d'exploiter convenablement le potentiel de cette aile, permettant une réduction significative de la traînée ($\Delta C_D = -0.0026$).

Il est important de noter toutefois que ce prototype d'aile reconfigurable a souffert d'une intégration structurale défaillante lors des premiers essais en soufflerie. En effet, le design de l'aile a dû être modifié avant sa seconde entrée en soufflerie pour réduire les effets aéroélastiques indésirables. Malgré cette mesure, les auteurs prétendent que de meilleures performances aérodynamiques auraient été possibles sans le flambage et l'affaissement du joint glissant de la peau flexible au bord d'attaque. De nos jours, l'utilisation de modèles numériques permettant de prédire l'interaction entre la structure de l'aile et l'écoulement permet d'éviter, ou du moins de réduire, ce genre de problème d'intégrité structurale.



Figure 2.9 Vol de l'avion F111 TACT au dessus du désert de Mojave en Californie.
Tirée de NASA (1976).

Près de 30 ans plus tard, dans le domaine du micro véhicules aériens (MAVs), Boria et al. (2009) ont présenté un algorithme d'optimisation génétique utilisant une approche HIL pour maximiser la portance et l'efficacité de leur prototype d'aile adaptative (voir Figure 2.10) testé en soufflerie subsonique. La valeur de la fonction objective de chaque profil d'aile modifiée a été mesurée en temps réel à l'aide de la balance de la soufflerie munie de jauge de déformation. Cette approche a permis de localiser des formes d'aile optimales malgré l'hystérésis aérodynamique/électrique rencontrée à ce faible nombre de Reynolds. Cette hystérésis a affecté la répétitivité des mesures fournies par le HIL et, conséquemment, a fait augmenter le nombre de formes d'aile à évaluer. Finalement, compte tenu de la considération de seulement deux variables de design (positions des servomoteurs 1 et 2, Figure 2.10) et des problèmes inhérents à la répétitivité des essais, les auteurs concluent que l'optimisation en temps réel n'a pas permis de surpasser l'exploitation par modélisation expérimentale qui aurait été plus rapide. Par contre, pour un plus grand nombre de paramètres à fixer, l'approche HIL aurait eu définitivement sa raison d'être.



Figure 2.10 Aile adaptative d'un MAV exploitée en HIL avec deux variables de design.

Tirée de Boria, Stanford et al. (2009)

En terminant, à l'égard du projet CRIAQ 7.1, Popov et al. (2009) ont réalisé un contrôle de l'aile en boucle fermée en utilisant des capteurs de pression de Kulite installés sur l'aile pour agir de HIL. À l'aide d'un algorithme d'optimisation standard, 18 minutes ont été nécessaires avant d'obtenir la forme d'aile modifiée maximisant le régime d'écoulement laminaire sur l'extrados pour une condition découlement donnée. En comparaison avec la méthode de la modélisation expérimentale qui nécessite environ 30 minutes, il semble réaliste d'exploiter plus efficacement le caractère adaptatif de l'aile laminaire en utilisant une combinaison des différentes approches mentionnées précédemment, à savoir : une optimisation en temps réel supportée par l'optimisation numérique et calibrée en utilisant la modélisation expérimentale. Cette idée de méthodes combinées a conduit au contrôle en boucle mixte (ouverte/fermée) de l'aile adaptative laminaire présenté au chapitre 5.

CHAPITRE 3

ARTICLE#1 « OPTIMIZED DESIGN OF AN ACTIVE EXTRADOS STRUCTURE FOR AN EXPERIMENTAL MORPHING LAMINAR WING »

D. Coutu, V. Brailovski et P. Terriault,

École de technologie supérieure, 1100 rue Notre-Dame Ouest,
Montréal (PQ), Canada, H3C 1K3

Ce chapitre a été accepté pour publication au journal « Aerospace Science and Technology ».

Numéro de confirmation : AESCTE-D-09-00133.

DOI : [10.1016/j.ast.2010.01.009](https://doi.org/10.1016/j.ast.2010.01.009)

Résumé

Cet article présente le développement et l'application d'une méthodologie de design propre aux problèmes aéro-structuraux afin de concevoir de façon optimale une structure active interagissant dans l'écoulement aérodynamique. Cette structure active est la composante maîtresse de l'aile laminaire adaptative du projet CRIAQ 7.1. Constituée d'un extrados flexible sous lequel repose un système d'actionnement, elle permet la modification du profil de l'aile à l'égard de différentes conditions d'écoulement variant entre Mach 0.2 et 0.3 avec des angles d'attaque compris entre -1 et 2°. Le cahier des charges provient des collaborateurs de l'École Polytechnique de Montréal qui ont fourni les formes de profils modifiés que le prototype d'aile sera appelé à reproduire en soufflerie. Ainsi, la structure active se doit d'être suffisamment rigide pour soutenir les efforts aérodynamiques et suffisamment souple pour permettre l'adaptation du profil d'aile.

Sous ANSYS, l'utilisation de la méthode des éléments finis permit de construire un modèle structural de la structure active alors que l'évaluation de son comportement aérodynamique fut assurée par le solveur XFOIL 6.96. Dès lors, ces outils numériques furent employés pour la réalisation d'une analyse de sensibilité permettant d'identifier les variables de design les plus influentes et leurs valeurs limites : le nombre de plis du laminé de composite (variant de 3 à 8) et le nombre de lignes d'action (variant de 0 à 7). Ces 48 configurations possibles de

structure active ont été comparées au moyen d'une analyse multicritère considérant la performance aérodynamique (régime laminaire maximum) et la performance mécanique (énergie d'actionnement minimum). Les configurations instables ont été retranchées par l'utilisation d'une contrainte basée sur la variabilité de la performance aérodynamique. Parmi les configurations restantes, la structure active constituée de 4-pli et 2 lignes d'action s'est démarquée comme celle offrant le meilleur compromis entre la rigidité et la souplesse, soit celle permettant d'importantes augmentations du régime d'écoulement laminaire à un moindre coût d'énergie d'actionnement. Afin de simplifier ces travaux de conception, une hypothèse a été posée afin que l'évaluation du travail nécessaire aux actionneurs puisse être réalisée qualitativement en considérant simplement l'énergie de déformation de la structure. Aussi, afin de réduire le nombre des calculs numériques sans compromettre les résultats, il a été vérifié que l'analyse du comportement structural et aérodynamique de la structure active puisse se réaliser successivement, sans la nécessité d'un couplage aéro-structural complet.

Abstract

This paper focuses on the design of an active extrados structure for an experimental morphing laminar wing, which has been tested in a subsonic wind tunnel. Actuators localized inside the wing box apply individually controlled displacements over the flexible structure, made from laminate composite, to modify the airfoil profile in accordance with the database, which is built using XFOIL aerodynamic solver. This database contains a set of wing profiles, which maximize laminar flow under a given set of cruise flight conditions: Mach number 0.2 to 0.35 and attack angles -1 to 2°. A finite elements structural model of the active extrados has been developed with ANSYS software. Two main design parameters were identified: the number of plies in the composite laminate of the flexible extrados and the number of actuators. To balance the tradeoff between stiffness and flexibility of the active extrados structure, aerodynamic (laminar flow regime enhancement) and mechanical (low strain energy) performance criteria were considered simultaneously. Using the multi-objective optimization technique, the designer's preferences led to the selection of the 4-ply 2-actuator active extrados structure configuration.

Keywords: Optimal design; Active structure; Morphing wing; Composite material, Laminar flow improvement

3.1 Introduction

Energy conservation is a very popular subject given today's concerns for the environment and operating cost economies. Energy efficiency has become increasingly important in system design, especially in relation to transport activities. For air transport, for example, research and design advances include innovative solutions to reduce fuel consumption by decreasing airplane drag. Among these solutions, several techniques based on energizing the flow boundary layer [1,2], or using in-time modifications of the airfoil shape (morphing wing concept) have been studied [3-10]. This latter approach seems to be promising since a conventional aircraft wing profile cannot be optimally designed for an entire flight mission presenting variable flow conditions in terms of speed, altitude and angle of attack. Considering a transport aircraft for example, enhancing the laminar flow regime by using wing morphing and thereby reducing friction drag would most likely lead to fuel economy.

Recently, the feasibility of a “Morphing Laminar Wing” (MLW) concept capable of reducing friction drag by extending the laminar flow over an active wing extrados has been proven for subsonic aerodynamic conditions (Technology Readiness Level, TRL = 3-4). This project was initiated three years ago by the Consortium for Research and Innovation in Aerospace in Québec (CRIAQ), with the long-term goal to reduce aircraft fuel consumption and greenhouse gas emissions [11]. The development of the MLW prototype raised many challenges in aerodynamics [12], operating systems [13,14] and mechanics [15,16]. The MLW prototype (Figure 3.1) was manufactured and tested in the subsonic wind tunnel located at the Institute for Aerospace Research of the National Research Council Canada (IAR-NRC). For a typical cruise flight condition, Mach 0.275 and angle of attack 0.5°, the extension of the laminar flow on the wing extrados due to morphing resulted in a more than 10% lift-to-drag ratio increase, as measured on the wind tunnel balance [14]. The goal of this

paper is to present the methodology used for the experimental design of the active extrados structure for the MLW prototype.



Figure 3.1 Experimental MLW setup in the subsonic wind tunnel.

3.1.1 Morphing wing concepts and technologies

During the last decade, several morphing wing concepts have been proposed and tested [3-10] to extend the flight envelope [3,4], enhancing lift capacity [5-7], and improve laminar flow [8-10]. The common functional requirement of the morphing concept is a sufficiently flexible structure to allow morphing, while keeping enough stiffness to withstand aerodynamic forces. Campanile and Sachau [17] presented the idea of the “belt-rib concept”, which consists of balancing the reduction in wing bending stiffness by reinforcement of the

wing spars. The strength of their “belt-rib concept” allowing variable wing camber has been proven experimentally. Chandrasekhara et al. [3] designed, manufactured and tested a Dynamically Deforming Leading Edge (DDLE) airfoil, which was actuated through a mechanically-driven mandrel. To meet the functional requirements of the DDLE, the authors varied the number of layers along the airfoil surface made from laminated composite. To morph the trailing edge of an airfoil, the concept of “compliant structure” has been used recently by FlexSys [10] to create the Mission Adaptive Compliant Wing (MACW). The topology and the shape of the internal structure of the wing were designed as a unique compliant mechanism. The flight tests showed aerodynamic performance improvement when compared to a conventional wing.

The MLW concept developed in this work is based on morphing an upper wing surface, given the relative simplicity of this approach in terms of industrial implementation. As presented in Figure 3.2, the MLW consists of a flexible extrados (skin) and actuators connected together through a transmission system, and it is subjected to variable flow conditions (aerodynamic loads). The modification of the airfoil profile occurs when actuators located inside the wing box apply individually controlled displacements to the flexible extrados. The overall stiffness and integrity of the experimental wing is provided by the rigid intrados. The front and rear edges of the flexible extrados are connected to the rigid intrados in such a way that ensures profile tangency continuity, accommodates shape modifications and sustains aerodynamic forces. It results in a flush-glued joint near the leading edge and a sliding-plane link at the aft end, including a compensation spring placed between the flexible and rigid structures. The design methodology developed and applied in this paper defines the active extrados structure configuration to balance its stiffness and flexibility efficiently by proper selection of material constituents and number of components.



Figure 3.2 Conceptual design of the MLW.

Although the actuator group's design is beyond the scope of this paper, the reader may be interested to know that among the actuators suitable for wing morphing applications, active material-based actuators, such as shape memory or piezoelectric, appear to be promising candidates. They can easily be embedded into systems and provide maximum mechanical work with minimum additional weight and space requirements, as demonstrated by Pinkerton and Moses [18] in their work on altering the camber of a small airfoil using piezoelectric actuators. However, from a comparative study of different active material-based actuators, the highest energy density among all active materials belongs to shape memory alloys (SMA) [19]. For that reason and the other reasons cited above, SMA actuator technology has been adopted for the MLW [16].

3.1.2 Morphing wing design methodologies

Whatever the morphing wing concept is, the design methodology requires the solution of aerodynamic and structural problems, which can be realized simultaneously or sequentially. For example, Justin K. Strelc et al. [7] used coupled structural and aerodynamic simulations to design an SMA-driven reconfigurable airfoil with the highest maximum lift-to-drag ratio. These coupled fluid-structure simulations offered the possibility to build a highly integrated concept, but at the expense of an excessively large number of variables and therefore design configurations to evaluate. On the contrary, aerodynamic calculations for the MACW design project [20] were performed prior to structural simulations. The aerodynamic problem was solved with the definition of the reference and modified airfoil shapes, which maximize natural laminar flow over the MACW. This so-called sequential approach facilitated design refinement, but may need additional efforts to make structural solutions fully compatible with the aerodynamics.

Within the framework of this project, the sequential approach has been used to allow design refinement. The aerodynamic calculations are performed prior to structural modeling. The innovative aspect of the design methodology presented in this work resides in the elaboration of the structural solution, where aerodynamic and mechanical performance parameters have

been considered simultaneously to establish a compromise between MLW's stiffness and flexibility, while ensuring compatibility with the aerodynamic solution. To this end, the multi-objective optimization (MOO) technique has been used to select an active structure configuration according to designer preferences.

First, a finite element (FE) structural model of the flexible extrados was built, considering the properties of each component and their integration. Thereafter, for a given set of aerodynamic conditions, each CFD-optimized profile was considered as a target to be reproduced by the active structure. From sensitivity analysis results, the application of the loading conditions, including actuator displacements and aerodynamic loading, was simplified to reduce computation time. Similarly, the number of design variables for the active structure was reduced to the two principally significant ones. Using a series of working hypotheses, an objective function of the multi-criteria design problem was built with two performance criteria (aerodynamic and mechanic) linked together through a coefficient of relative importance. The structural and the aerodynamic performances of each active structure configuration were then evaluated with FE and CFD analysis over the entire flow range of interest. Finally, among the retained controllable design solutions, the MOO of the active structure performances led to the selection of an optimum design configuration based on the best stiffness/flexibility tradeoff.

3.2 CFD optimization of the MLW

3.2.1 The CRIAQ 7.1 MLW

The initiators of the CRIAQ 7.1 project have defined the geometry and the operating flow condition envelope for the experimental wing. The 2D WTEATE1 airfoil has been chosen as the base (reference) profile, with a 500 mm chord and a 990.6 mm span. The WTEATE1 airfoil has a maximum thickness/chord ratio of 16% (80mm/500mm) and is similar to a family of natural laminar flow-capable supercritical airfoils [21]. Although the cruise flight regime of commercial aircraft is transonic, this profile with extrados morphing capabilities was intended to be tested for two-dimensional laminar flow enhancement under subsonic

wind tunnel conditions ($M = 0.2$ to 0.35). This simplification was taken to facilitate MLW aerodynamic analysis from the numerical and experimental points of view. The angle of attack envelope ($\alpha = -1$ to 2°) was selected to correspond to cruise flight conditions. To reduce the friction drag and therefore fuel consumption of an aircraft, the MLW should exhibit a controlled extension of the laminar flow over the extrados, through modification of its geometry. Since the wing morphing influences not only drag but also lift forces, the angle of attack should be corrected to ensure constant lift conditions, and thereby allow the reliable comparison of the aerodynamic performance of different airfoil geometries.

3.2.2 Aerodynamic solver

For the purpose of this design study related to a bi-dimensional laminar airfoil, XFOIL 6.96, the well-known free-licensed aerodynamic analysis code written by Mark Drela in 1986 [22,23] was chosen. It uses a high-resolution panel method with a Karman-Tsien compressibility correction to obtain an inviscid solution. This solution is incorporated into the viscous equations and solved by the full-Newton method. After testing the code for subsonic airfoil analysis/design, H. A. Madsen and A. Filippone [24] concluded that for the cruise flight angles of attack (beyond the C_{Lmax} point), XFOIL gives acceptable aerodynamic coefficients compared to the experimental data. This accuracy in lift and drag is a strong indication of the good transition prediction capability of the software, thanks to the e^N method used for the boundary layer and wake formulations. (In the framework of the MLW project, the critical amplification factor N_{crit} was set to 7, a value representative of the wind tunnel turbulence intensity, $T = 0.14\%$.).

Compared to other CFD solvers, XFOIL is faster and has been used, therefore, in a series of works on morphing airfoils [25, 26]. Also, XFOIL can provide a lift-specified solution; a modality which facilitates the same constant-lift design approach as that used in this work. Finally, although XFOIL prediction accuracy may not match the wind tunnel results perfectly because of three-dimensional flow effects (which it cannot describe), it appears to be a

perfectly adequate tool for comparative numerical aerodynamic testing of different active structure configurations.

3.2.3 CFD-optimized wing shape database

After several theoretical studies, CRIAQ 7.1 aerodynamic specialist Dr O. Trifu delimited the flexible portion of the upper surface between 3% (15 mm) and 70% (350 mm) of the chord. A constant-lift CFD extrados optimization [27] was performed with the transition point location over the extrados (x_{tr}/c) as the indicator of airfoil aerodynamic performance [11]. The results were then compiled in a 2D optimum wing profile database covering the flow condition range encompassing 7 Mach numbers ($M = 0.2$ to 0.35 incremented by 0.025) and 7 angles of attack ($\alpha = -1^\circ$ to 2° incremented by 0.5°). As shown in Table 1, the studied flow cases were numbered from C1 to C49 with two ignored (C1 and C8), because for these two cases, laminar flow was already extended beyond the flexible zone of the extrados.

Thus, in the present work, 47 flow cases and their corresponding optimized wing profiles define the target morphing envelope for the active structure. This shape modification envelope is superposed on the reference WTEATE1 profile in Figure 3.3a along with the optimized profile for the C25 flow case, shown here as an example. It can be observed that all the shape modifications, except the extrados portion located between 230 mm (46%c) and 350 mm (70%c) of the chord length, have a positive sign (convex shape). Figure 3.3b compares the laminar/turbulent transition point locations and the corresponding drag coefficients of the WTEATE1 and CFD-optimized profiles over all the studied flight conditions. The laminar flow extension and the consequent drag reduction provided by such an MLW concept are indeed noticeable.

Tableau 3.1
Optimization flow cases

Mach number	Angle of Attack, deg.						
	-1.0	-0.5	0.0	0.5	1.0	1.5	2.0
0.200	C1	C2	C3	C4	C5	C6	C7
0.225	C8	C9	C10	C11	C12	C13	C14
0.250	C15	C16	C17	C18	C19	C20	C21
0.275	C22	C23	C24	C25	C26	C27	C28
0.300	C29	C30	C31	C32	C33	C34	C35
0.325	C36	C37	C38	C39	C40	C41	C42
0.350	C43	C44	C45	C46	C47	C48	C49

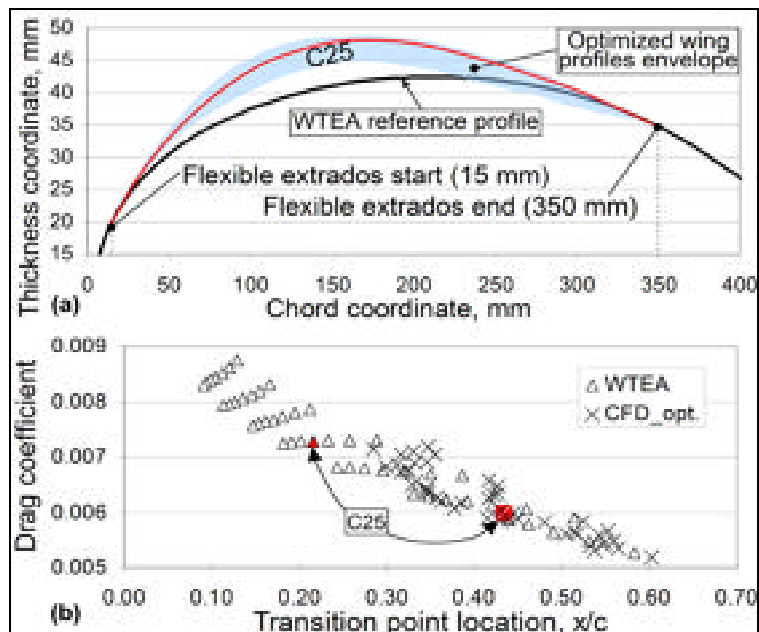


Figure 3.3 CFD-optimized profiles of the MLW: (a) shape modification envelope; (b) drag coefficient as a function of the extrados transition point location for the CFD-optimized and the WTEATE1 reference profiles. (C25 flow case is taken as an example.)

3.3 Active structure modeling

3.3.1 Flexible extrados constituents and properties

To fulfill the functions of the flexible extrados, the use of a laminated composite is justified by the important polyvalence such a material offers to the designer in terms of stacking sequence, number, nature and extent of plies. The laminated composite structure used in the present study is manufactured from the Huntsman 8602 Reinfusion low-viscosity (175 cP) epoxy resin system and two types of plies, shown in Figure 3.4: low-modulus unidirectional Carbon (9 oz./square yard) and 2 x 2 twill woven **Hybrid** carbon/Kevlar (5.1 oz./square yard). During vacuum-assisted resin transfer molding, the laminate is formed to the reference shape of the WTEATE1 upper profile using a machined aluminum mould. To minimize the laminate weight, all the plies are oriented so as to optimize their flexural properties in respect to the 2D wing profile modifications. Thus, their higher elastic moduli are aligned with the wing chord, being the reference direction, leading to a typical $[0^H/0^C/\dots]_S$ laminate stacking sequence. To increase the stiffness and to ensure shape modification uniformity in the span direction, without affecting flexural behavior in the chord plane, steel stiffeners are fixed to the inner surface of the laminate, precisely where the actuators will be connected to the structure (Figure 3.4).

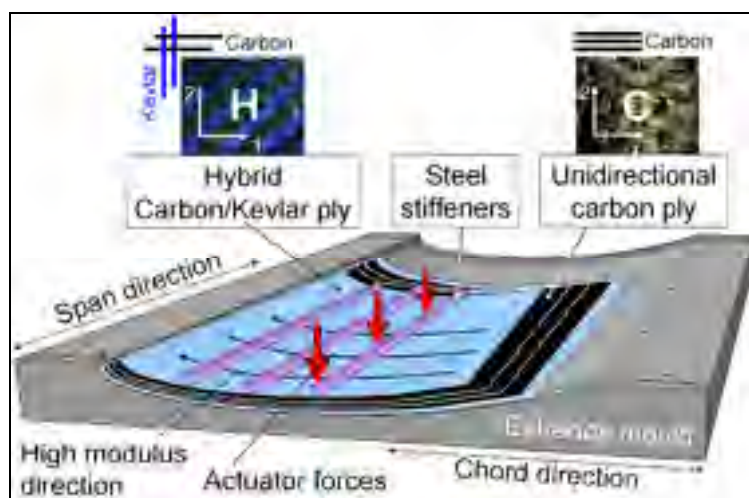


Figure 3.4 Flexible extrados with steel stiffeners (manufacturing setup).

The Poisson ratio (ν_{12}), tensile (E_1, E_2) and shear (G_{12}) moduli of the Hybrid carbon/Kevlar and unidirectional carbon plies have been measured according to the ASTM D3039 and ASTM D3518 test methods. For the purpose of numerical analysis, other elastic constants were approximated and they are summarized in Table 2. In-plan directions 1 and 2 (see Figure 3.4) are along and perpendicular to the carbon fibers' orientation and direction 3 is perpendicular to the 1-2 plane.

Tableau 3.2
Elastic constants from testing and approximation

Plies	ASTM D3039			ASTM D3518		Approximation	
	E_1 GPa	E_2 GPa	ν_{12}	G_{12} GPa	E_3 GPa	$G_{23}=G_{13}$ GPa	$\nu_{23}=\nu_{13}$
Hybrid carbon/Kevlar	32.9	17.1	0.12	2.1	$E_2^{(Carbon)}$	$G_{12}^{(C/K)}$	0.01
Unidirectional carbon	99.9	5.5	0.25	3.2	$E_2^{(Carbon)}$	$G_{12}^{(Carbon)}$	0.01

3.3.2 Structural FE modeling

The finite element model of the active structure is built in ANSYS software using SHELL99 elements for the flexible structure and SHELL63 for the compensation leaf spring, as presented in Figure 3.5. The front end (3%c) of the flexible extrados is fixed and the aft end (70%c) coupled with the compensation spring, with locked rotation around the “z” axis, to ensure slope profile continuity. The 2D-aspect of shape modification implies uniform shape changes in the span direction. Thus, actuation is realized by imposing uniform displacements along span-wise oriented actuation lines, as if the stiffeners shown in Figure 3.4 were used. After mesh convergence analysis, a mapped mesh using 13.5 mm (2.7%c) maximum size elements is generated. Because no edge effect at either span end is expected, applying periodic symmetry conditions allows the entire span of 990.6 mm to be reduced to a 20 mm (4%c) span section (corresponding to 64 finite elements) offering the same calculation

accuracy with lower computational time. During post-processing, numerical results depending on the wing span length are scaled to a unit meter span using the 1000/20 ratio.

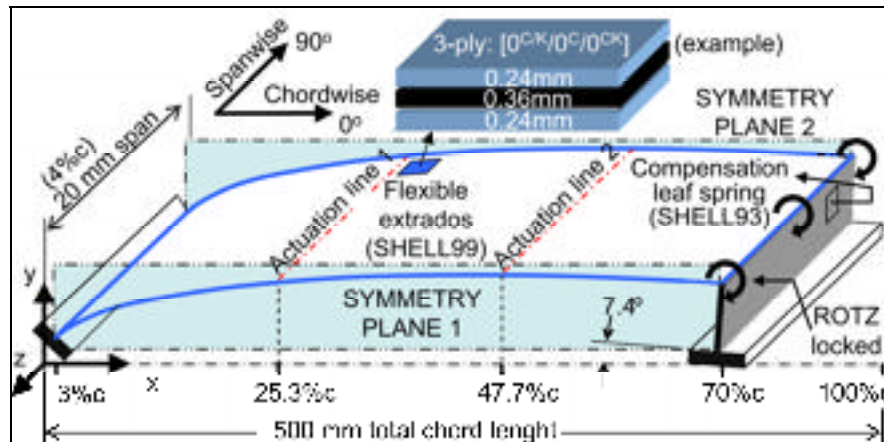


Figure 3.5 Numerical model of the active structure using ANSYS software ($N_a = 2$ and $N_p = 3$).

This structural finite element model has been experimentally validated by the authors as to its ability to predict the flexural behavior of a flexible structure subjected to displacement-controlled actuation [15]. In respect to the specific extrados structure shown in Figure 3.5, the loading conditions applied to it under given flow conditions combine: (1) displacement on each actuation line, and (2) 2D distribution of pressure and friction drag forces over the extrados. From the CFD optimization results (section 2.3), these loading conditions can readily be determined for each flow case: angle of attack and Mach number.

3.4 Sensitivity analysis

3.4.1 Simplification of the loading conditions

Assumptions have been put forward to simplify the application of loading conditions (displacements, pressure distributions and friction drag forces) to the FE model without compromising the validity of the numerical results.

Displacements

Displacements on actuation lines can be obtained by comparing a given CFD-optimized profile to the reference WTEATE1 profile. These displacements are imposed on the flexible structure in the vertical direction only, with no restraining chord-wise shifts due to shape accommodation. For an active structure with 3 plies and 4 actuators, targeting the C25 CFD-optimized profile for instance, the vertical displacements (U_y) to be provided by each of 4 actuators are evaluated respectively at 4.83, 6.61, 4.48 and 1.25 mm (Figure 3.6). But, since a chord-wise shift occurs during shape modification, the resulting position of the actuation points will not lie on the targeted profile. They will be shifted in chord-wise direction towards the leading edge. Let us take two of the four actuation points as an example. Vertical corrections of -0.24 (5% U_y) and 0.14 mm (11% U_y) should be applied to actuation points #1 ($x = 82$ mm) and #4 ($x = 283$ mm) to keep them on the targeted profile because of their respective 1.23 and 1.61 mm chord-wise shifts. Since the variation of the laminar flow portion of the chord corresponding to these corrections remains small (an increase of 1.2 % c for the present example), the authors simplify calculations by neglecting any chord-wise shifts due to shape accommodation of the flexible extrados. This analysis has been repeated for other active structure configurations, and the transition point locations also presented similar negligible variations over the flow range of interest.

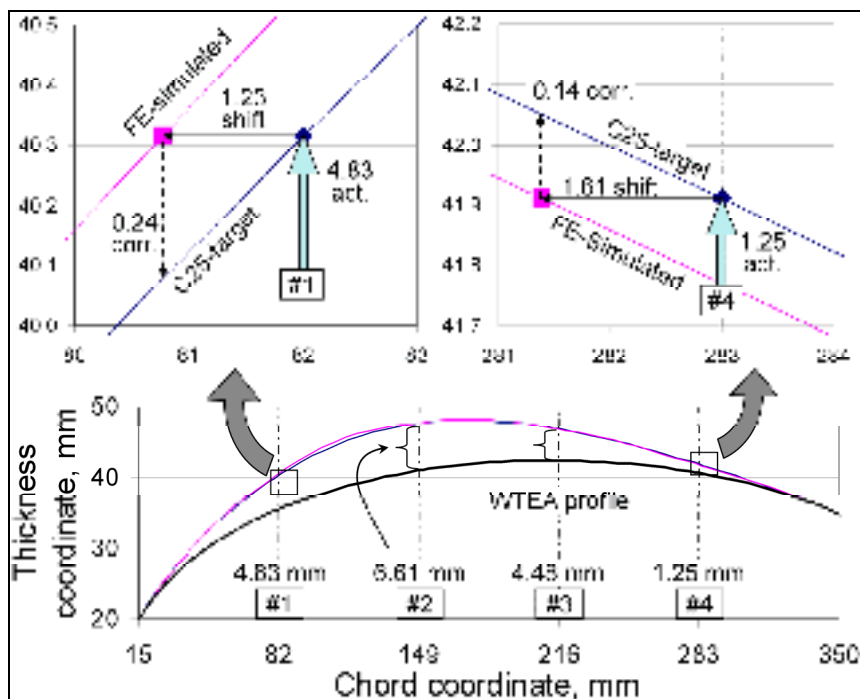


Figure 3.6 Chord-wise shifts of the actuation lines during morphing of the “3-ply and 4 actuators” active structure according to the C25 optimized profile.

Pressure distribution and friction drag forces

The pressure distribution Δp calculated with Eq. (3.1) corresponds to the pressure acting on the extrados as a result of the difference between the inside and the outside pressures.

$$\Delta p = p_{ext} - p_{int} = q_\infty (C_p - 1) \quad (3.1)$$

This relation is obtained by assuming that the pressure inside the wing box, p_{int} , is considered to be the total flow pressure, giving a conservative pressure evaluation. Outside the wing box, the external static pressure distribution p_{ext} is determined from the pressure coefficients provided by CFD-calculations. In fact, this pressure distribution will differ from that produced by the FE-modeled active structure, and only coupled aero-structural iterative calculations could solve this problem. In this work, however, aero-structural coupling is neglected to decrease calculation time without compromising results’ validity.

To illustrate this point, Figure 3.7 presents the evolution of structural and aerodynamic parameters as a function of the number of iterations for a low-stiffness (high aerodynamic sensitivity) 3-ply_2-act structure. Note that whereas the maximum absolute shape thickness deviation converges after 4 iterations (Figure 3.7a), the transition point location oscillates with a tendency to converge towards a certain value after approximately 15 iterations (Figure 3.7b). For the C49 case (highest aerodynamic loading), the iterative calculations result in a laminarity difference of only 0.6% c (0.181 towards 0.187 x/c , Figure 3.7b). Similar and even smaller aerodynamic performance variations were observed for all the active structure configurations studied.

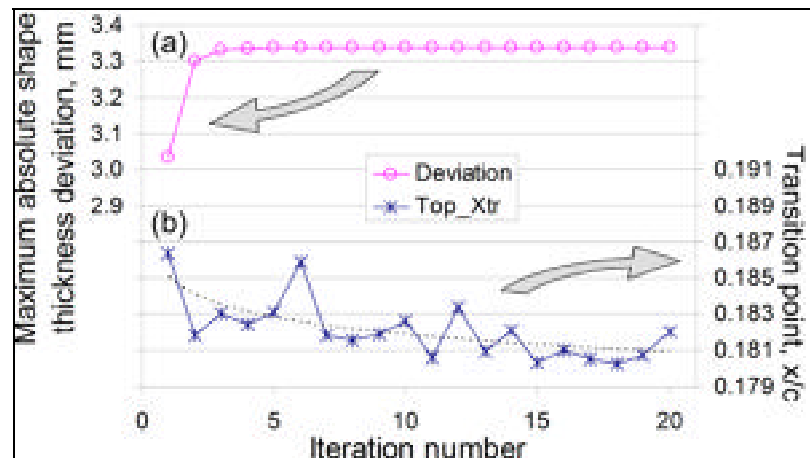


Figure 3.7 Evolution of aero-structural parameters for each coupled iteration for the 3-ply and 2-actuator active structure under the C49 flow condition case.

Finally, the friction drag forces over the skin are not taken into account in the structural FE analysis. For the 3-ply_2-act configuration under the extreme C49 flow case the friction drag shear τ can be integrated along the chord direction over the flexible part of the extrados. It results in a force component R_{tx} , which does not exceed 12 N per one meter of span. Considering that the compensation spring reactions at the aft end of the extrados is much larger (766 N), the friction drag forces over the extrados are neglected. This simplification can be made for all the FE analyses, since the friction force must be lower for all the flow cases other than C49.

In sum, considering the sensitivity analysis results in respect to loading conditions, the following simplifications are made:

- small deviations from the targeted shape -- due to the flexible extrados chord-wise shifts occurring during actuation -- are neglected;
- the pressure distribution applying over any modified wing profile is assumed to be equal to that of the target CFD-optimized profile;
- the friction drag forces over the flexible extrados are neglected in structural calculations.

It is worth noting that for the closed-loop control of the MLW [14], the authors have performed fully-coupled aero-structural modeling of the MLW prototype, which was manufactured using the results of this study, to allow direct comparison of the numerical and experimental (wind-tunnel) results.

3.4.2 Design parameters of the active structure

The flexural behavior of the active structure depends on the design parameters of the laminate (number of plies, stacking sequence), actuators (location and number) and on the linkage mechanism (compensation spring stiffness). Therefore, once the FE model is built and validated, a sensitivity analysis is performed to identify the design parameters that are the most influential, and that need to be considered in the optimization work. The results presented in Figure 3.8 show that the number of actuators (Na) and the number of plies (Np) are two major design parameters affecting the morphed airfoil shape. In fact, when reproducing CFD-targeted vertical displacements for C25 flow conditions with active structures having different Na (Figure 3.8a) and Np (Figure 3.8b), we observe that the morphed shapes do not correspond exactly to the CFD-optimized shapes. Note that this mismatch between the morphed and targeted geometries noticeably affects the laminar flow. For the C25 flow case (Figure 3.8b), $Na = 4$ and $Np = 8$ correspond to the worse set of design parameters since the transition point location over the morphed shape is reduced from 43.3 to 39.5 %c as compared to the CFD-optimized profile. On the other hand, for the C25 flow

case, $Na = 2$ and $Np = 5$ correspond to the best design parameters, since the transition point location over the morphed shape is reduced only from 43.3 to 41.3% c as compared to the CFD-optimized profile. In the C49 case, $Na = 7$ and $Np = 5$ correspond to the worst set of design parameters (performance drops from 30 to 20.3% c), whereas $Na = 2$ and $Np = 5$ correspond to the best set (no performance drop is calculated). These results confirm that the design configuration with smaller geometrical mismatch does not necessarily correspond to higher aerodynamic performance (see Figure 3.8b), because the latter does not only depend on the profile position, but also on the slope and curvature.

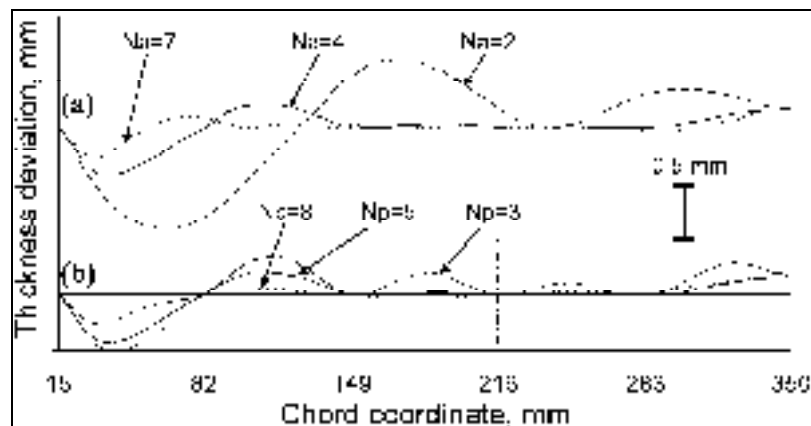


Figure 3.8 Shape deviation of the FE-modeled in respect to the CFD-optimized C25 profile (horizontal solid line):
 a) 5-ply with 2, 4 and 7 actuators;
 b) 4 actuators with 3, 5 and 8 plies.

In this work, assembly constraints and designer judgment define the limits between which the Np and Na design parameters can be varied. Hence, the actuator number varies between 0 and 7, the latter being the maximum number of actuators that can reasonably be contained inside the wing box, while the former is used for reference purposes, representing so-called “semi-active” aeroelastic airfoils [28]. These actuators are uniformly distributed under the flexible part of the extrados as illustrated in Figure 3.9 for cases with 1, 4 and 7 actuators.

For any ply number, the laminate is symmetric and equilibrated to avoid undesirable torsion/flexural coupling. For any ply configuration, the two Hybrid carbon/Kevlar plies

remains stacked exterior to the laminate and only the number of interior unidirectional carbon plies varies, as shown in Figure 3.9 for 3, 5 and 8-ply laminate. When the number of plies is fewer than 3 or greater than 8, either the aerodynamic stability is compromised, or excessively high actuation forces are required. Finally, combining all the proposed design cases: $Na = 0$ to 7 and $Np = 3$ to 8, 48 active structure configurations are generated. The compensation spring stiffness is fixed because its influence on the shape changes remains negligible, as shown by preliminary numerical analysis.

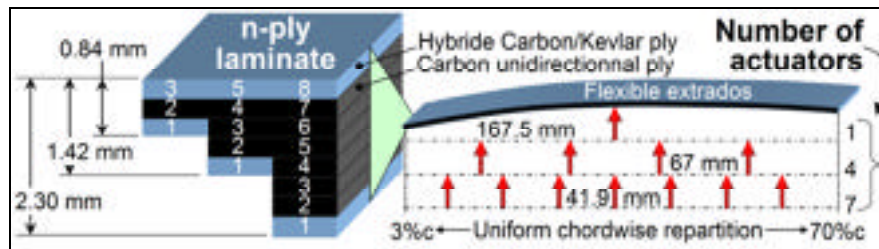


Figure 3.9 Variable design parameters of the flexible extrados: number of actuators (Na) and plies (Nb).

The sensitivity analysis not only allowed identification of the design variables but also assisted in formulation of the design optimization objectives. As expected, it was shown that high stiffness active structures require more actuation work, but demonstrate higher capacity to reach target profiles. On the other hand, better profile conformity does not warrant better aerodynamic performances. This means that different design configurations should be compared directly in respect to their aerodynamic performances, as shown in the next section.

3.5 Multi-objective optimization

The Multi-Objective Optimization (MOO) presented in this paper uses a simple additive weighting method [29] to formulate the objective function. All the possible design configurations are evaluated and compared graphically using a Pareto frontier to allow comprehensive evaluation of the optimization problem. Selection of the final active structure configuration is justified in accordance with the designer's preference.

3.5.1 Formulation of the objective function

From sensitivity analysis, although the proximity of the active extrados with the targeted CFD-optimized profile may be desirable, aerodynamic performance parameters are to be used to ensure a structural design that is compatible with the MLW's aerodynamic objectives. As the main goal of the MLW is to extend the laminar flow regime over the extrados, a net gain in laminar flow extension (G_{lam}) due to wing morphing can be expressed by comparing the transition point location over the extrados' of the modified and of the reference WTEATE1 profiles:

$$G_{lam} = x_{tr} / c - (x_{tr} / c)_{WTEATE1} \quad (3.2)$$

On the other hand, higher mechanical performance credentials can be attributed to an active structure which requires less mechanical work to be provided from actuators, leading to the use of less-powerful actuation systems. The minimization of this parameter is a common objective of aircraft designers aiming at minimizing size and weight of all embarked systems, which are assumed here to be proportional to power requirements. Strain energy (E_{strain}) stored inside the active structure, which is deformed to reach a target shape, contains two contributions: mechanical work provided by actuators (E_{act}), and air stream energy (E_{air}):

$$E_{strain} = E_{act} + E_{air} \quad (3.3)$$

Generally, aerodynamic suction assists the movement of the flexible extrados in the direction of the required shape modification, in respect to the reference profile, while opposing any return of the modified profile to its reference position. The mechanical work requested from the actuators depends on the design of a given active structure and its aerodynamic sensitivity. In contrast, the air stream energy is design-independent and is only a function of the flow conditions and wing profile. It can therefore be postulated that the lower the strain

energy stored in the active structure deformed under given flow conditions, the lower the mechanical work that is needed from the actuators to impose target displacements.

In order to compare different active structure designs under variable flow conditions, the mean gain in transition point location $\overline{G_{lam}}$ and the mean strain energy $\overline{E_{strain}}$ are selected as two global performance parameters, where performances of different designs are averaged with equal importance attributed to each flow case considered. The optimum active structure design will therefore be the one that will maximize the first performance parameter, while minimizing the second:

$$\overline{G_{lam}} = \frac{1}{47} \sum_{M=0.2}^{M=0.35} \sum_{\alpha=-1^\circ}^{\alpha=2^\circ} G_{lam} \quad (3.4)$$

$$\overline{E_{strain}} = \frac{1}{47} \sum_{M=0.2}^{M=0.35} \sum_{\alpha=-1^\circ}^{\alpha=2^\circ} E_{strain} \quad (3.5)$$

These mean values allow formulation of the objective function f to minimize:

$$f = w_{Aero} \frac{\overline{G_{lam}}|_{\max}}{\overline{G_{lam}}|_i} + (1 - w_{Aero}) \frac{\overline{E_{strain}}|_i}{\overline{E_{strain}}|_{\min}} \quad (3.6)$$

where the maximum laminar gain $\overline{G_{lam}}|_{\max}$ and the minimum strain energy $\overline{E_{strain}}|_{\min}$, respectively, are used to normalize the performance ratios. In order to combine the designer's tradeoffs against each performance criterion, a relative importance coefficient of aerodynamic performance (w_{Aero}) is used, which varies between 0 (only mechanical energy performance is considered) and 1 (only aerodynamic performance is considered).

3.5.2 Configuration evaluation

To select an optimum design of the active structure, each of the 48 FE-modeled configurations is analyzed for its ability to reproduce the corresponding CFD-optimized profiles over the 47 flow cases. Inside the nested loops, Figure 3.10 presents the performance evaluation process applied to a given active structure subjected to specific flow conditions. The loading conditions are applied to the ANSYS FE structural model to simulate shape modifications. The resulting strain energy serves as an evaluation of the active structure mechanical performance (Eq. (3.6)), and the coordinates of the modified profile are transmitted to Xfoil. The latter is used for evaluation of the active structure aerodynamic performances (Eq. (3.5)) via calculations of the transition point location under constant-lift aerodynamic conditions.

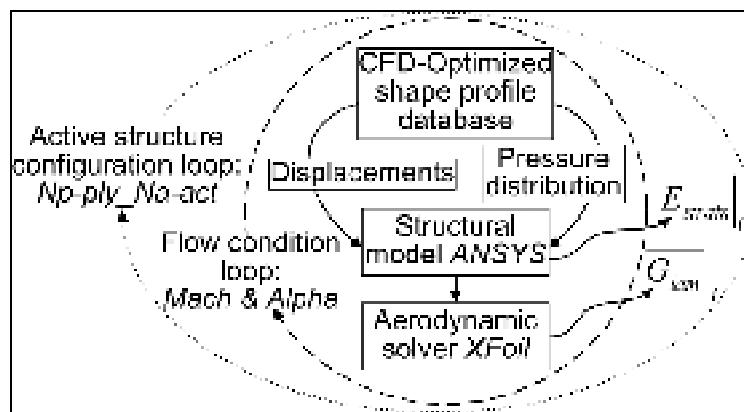


Figure 3.10 Nested loops for all active structure performance evaluation

Since the similitude in mean laminar gain values between the FE-modeled and the CFD-optimized profiles does not guarantee a similar aerodynamic behavior at each of the 47 flow cases, a supplementary state variable is introduced to constrain the design space. For each given active structure configuration, the root mean square deviation (RMSD) of the x_{tr}/c value is evaluated for all the flow conditions:

$$RMSD\left(\frac{x_{tr}}{c}\right) = \sqrt{\frac{1}{47} \sum_{M=0.2}^{M=0.35} \sum_{\alpha=-1^\circ}^{\alpha=2^\circ} \left(\frac{x_{tr}}{c} - \left(\frac{x_{tr}}{c} \right)_{CFD-Opt} \right)^2} \quad (3.7)$$

3.5.3 Configuration selection

The formulated optimization problem can be defined as discrete (incremental variables: N_p and N_a), multi-objective (two performance criteria: aerodynamic from Eq. (3.5) and mechanical from Eq. (3.6)) and a constrained (Eq. (3.8)). Analyzing the RMSD values (Figure 3.11) allows 34 feasible active structure configurations to be identified. The rejected configurations cannot be actively controlled because their profile modifications are dominated by aerodynamic fluctuations. In Figure 3.11, the semi-active aeroelastic airfoils (zero-actuators) present the mean transition point locations that are superior to those of the CFD-optimized profiles, but this is obtained at the cost of a deficient shape conformity between the target and the FE-modeled profiles. Furthermore, other low-stiffness active structures: one-actuator configuration with any number of plies and 3-ply configuration with two or three actuators, manifest equally significant aerodynamic instability. Finally, FE calculations of three low-stiffness active structures (0-act_3 and 4-ply, 1-act_3ply configurations) were unable to converge, thus indicating their incapacity to sustain the applied aerodynamic loads.

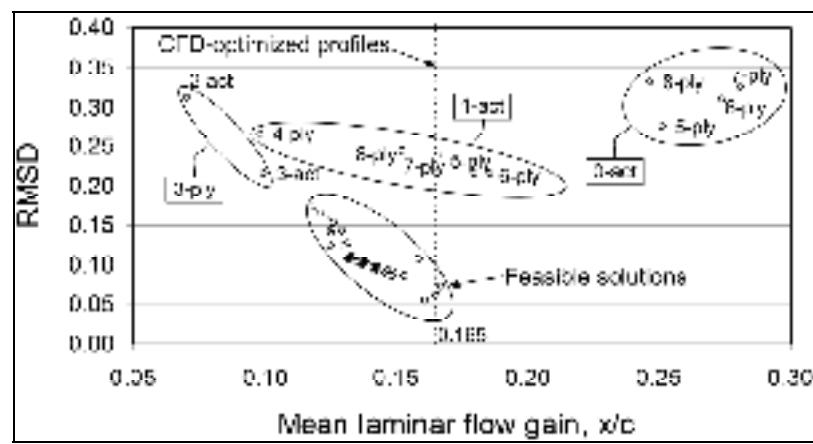


Figure 3.11 Laminar gain deviation (RMSD) and mean laminar flow gain for all FE-modeled active structure configurations.

The remaining design configurations are presented in the objective space of Figure 3.12, using the aerodynamic and mechanical performance parameters as abscissa and ordinate, respectively. According to the MOO technique [30], a Pareto frontier is built, highlighting the three best configurations for a subsequent decision analysis: “3-ply_5act”, “4-ply_2act” and “5-ply_2act”.

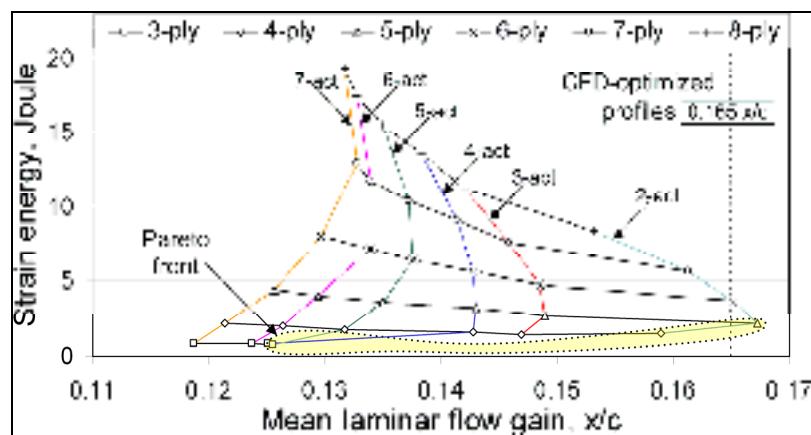


Figure 3.12 Objective plot for all active structure configurations
(the three best configurations are encircled by a dotted line).

For a given relative importance coefficient from 0 to 1, the objective function (Eq. (3.6)) is plotted to determine which of the three Pareto frontier solutions best fits the designer’s preferences (Figure 3.13).

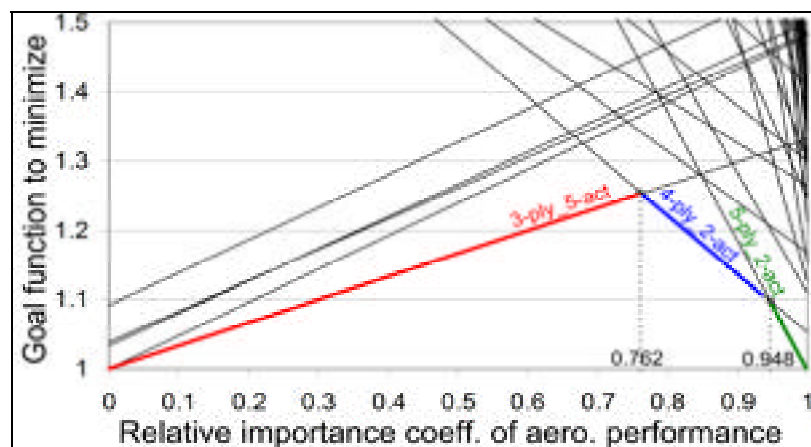


Figure 3.13 Evaluation of Pareto solutions over a range of tradeoffs.

First, the “5-ply_2-act” configuration is rejected, as it appears to be optimal only for the highest and narrowest range of the relative importance coefficient of aerodynamic performance ($w_{Aero} = 0.95$ to 1.0). Between the two remaining solutions (“4-ply_2-act” and “3-ply_5-act”), system simplicity should be taken into consideration because the fewer parts a mechanical system contains, the more dependable it is. Thus, the “4-ply_2-act” active structure configuration is chosen. From its tradeoff range, this solution offers an excellent aerodynamic performance conformity with the CFD-optimized profiles ($w_{Aero} = 0.948$), combined with a relatively low actuator work requirement ($w_{Aero} = 0.762$). Although the mean laminar flow gain of the selected configuration ($0.159 \text{ } x/c$) is slightly below that of the CFD-optimized profiles ($0.165 \text{ } x/c$) (see Figure 3.12), this aerodynamic performance is considered quite satisfactory.

3.6 Conclusion

An approach to the optimal design of an active structure for an experimental MLW has been developed and applied. A finite element structural model of the active structure has been developed and an aerodynamic solver was used for the active structure performance evaluation. The sensitivity analysis simplified the loading conditions and limited the design parameters of the active structure to the number of plies and the number of actuators. The MOO technique guides a designer to the selection of a 4-ply, 2-actuator active structure configuration using aerodynamic and mechanical performance parameters simultaneously. Further work will update the FEM according to the manufactured prototype characteristic to be used to determine the best optimized shapes for each flow condition of interest. To this end, the FEM will be coupled to the aerodynamic solver XFOIL, with the results verified in subsequent wind tunnel tests.

3.7 Acknowledgments

The authors would like to thank CRIAQ, NSERC, Bombardier Aerospace and Thalès Canada for their financial support which made this research possible. Also, the authors thank Dr O.

Trifu from Ecole Polytechnique de Montréal for his collaboration in this work. Finally, the authors acknowledge G.-H. Simon from Thalès as the project initiator.

3.8 References

1. Melton, L. P., Schaeffler, N. W., Yao, C.-S., and Seifert, A., Active control of flow separation from supercritical airfoil leading-edge flap shoulder, *Journal of Aircraft* 42 (5) (2005) 1142-1149.
2. Masad, J. A., and Abid, R, Effect of laminar flow control by suction on separation, *Journal of Fluids Engineering* 118 (2) (1996) 410-412.
3. Chandrasekhara, M. S., Carr, L. W., Wilder, M. C., Paulson, M. C., and Sticht, C. D., Design and development of a dynamically deforming leading edge airfoil for unsteady flow control, *Proceedings of the 17th IEEE International Congress on Instrumentation in Aerospace Simulation Facilities*, 29 Sep. - 2 Oct. 1997, pp. 132-140.
4. Perkins, D. A., Reed Jr., J. L., and Havens, E., Morphing wing structures for loitering air vehicles, *45th AIAA/ASME/ASCE/AHS/ASC Structures*, Vol 5, Palm Springs, CA, United States, 19-22 Apr. 2004, pp. 4006-4015.
5. Baron A., B. Benedict, Branchaw N., Ostry B., Pearsall J., Perlman G. and Selstrom J., Morphing Wing (MoW), Department of Aerospace Engineering, Rept. ASEN 4018, University of Colorado at Boulder, Dec. 2003.
6. Yang, S.-M. Han and J.-H. Lee, I., Characteristics of smart composite wing with SMA actuators and optical fiber sensors, *The International Journal of Applied Electromagnetics and Mechanics* 23 (3-4) (2006) 177-186.
7. Strelec, J. K., Lagoudas, D. C., Khan, M. A., and Yen, J., Design and implementation of a shape memory alloy actuated reconfigurable airfoil, *Journal of Intelligent Material Systems and Structures* 14 (4-5) (2003) 257-273.
8. Munday, D., and Jacob, J., Active control of separation on a wing with conformal camber, *39th AIAA aerospace sciences meeting and exhibit*, 8-11 Jan. 2001, Reno, Nevada, AIAA-2001-0293.
9. Martins, A. L. and Catalano, F.M., Aerodynamic optimization study of a mission adaptive wing for transport aircraft, *15th AIAA Applied Aerodynamics Conference*, Atlanta, GA, 23-25 June 1997, pp. 471-480.

10. Hetrick, J. A., R. F. Osborn, et al., Flight testing of Mission Adaptive Compliant Wing, Waikiki, HI, United states, American Institute of Aeronautics and Astronautics Inc (2007).
11. Botez, R.M., Molaret, P. and Laurendeau, E., Laminar flow control on a research wing project presentation covering a three year period, 2007 AERO Conference and 54th Annual General Meeting, 2007 CASI Annual General Meeting, Toronto, Ont., Canada, 25-26 April 2007.
12. Pagès, L., Trifu, O. and Paraschivoiu, I., Optimized laminar flow control on an airfoil using the adaptable wall technique, 2007 AERO Conference and 54th Annual General Meeting, Toronto, Ont., Canada, 25-26 April 2007.
13. Popov, A.V., Botez, R.M. and Labib, M., Transition point detection from the surface pressure distribution for controller design, *Journal of Aircraft* 45 (1) (2008) 23-28.
14. Coutu, D., Brailovski, V., Terriault, P., Mamou, M., Laurendeau, E., Real-Time Optimization of a Research Morphing Laminar Wing in a Wind Tunnel, ASME Conference on Smart Material, Adaptive Structures and Intelligent Systems, Oxnard, USA, 2009.
15. Coutu, D., Brailovski, V., Terriault, P., and Fischer, C., Experimental validation of the 3D numerical model for an adaptive laminar wing with flexible extrados, Proceedings of 18th International Conference on Adaptive Structures and Technologies, Ottawa, Canada, 3-5 Oct. 2007.
16. Georges, T., Brailovski, V., Coutu, D., Terriault, P., Design diagram for linear SMA actuators integrated in a morphing wing structure, SMST'07, Tsukuba, Japon.
17. Campanile, L. F. and D. Sachau, The belt-rib concept: a structronic approach to variable camber, *Journal of Intelligent Material Systems and Structures* 11(3) (2000) 215-24.
18. Pinkerton, T. L. and R. W. Moses, A Feasibility Study to Control Airfoil Shape Using THUNDER, 1997.
19. Waram, T.. Actuator applications, in: V. Brailovski, S. Prokoshkin, P. Terriault & F. Trochu (Eds.), *Shape Memory Alloys: Fundamentals, Modeling and Applications*, Ecole de technologie superieure, Montreal, Quebec, Canada, pp. 732-754
20. Youngren, H., Multi-Point Design and Optimization of a Natural Laminar Flow Airfoil for a Mission Adaptive Compliant Wing, 46th AIAA Aerospace Sciences Meeting and Exhibit, Reno, NV, USA, AIAA Paper 2008-293.
21. Eggleston B., Poole R.J.D, Jones,D.J. and Khalid M., Thick superficial airfoil with low drag and natural laminar flow, *Journal of Aircraft* 24 (6) (1987) 405-411.

22. Drela, M. and Giles, M.B., Viscous-Inviscid Analysis of Transonic and Low Reynolds Number Airfoils, AIAA Journal 25 (10) (1987) 1347-1355.
23. Mark Drela, XFOIL 6.9 User Guide, MIT Aero & Astro, Harold Youngren, Aerocraft, Inc., 11 Jan 2001
24. Madsen, H. A. and A. Filippone, Implementation and Test of the XFOIL Code for Airfoil Analysis and Design, Risø National Laboratory, Roskilde, Denmark, 1995, 59p.
25. Jepson, J. K., Gopalarathnam, A., Inverse Design of Adaptive Airfoils with Aircraft Performance Considerations, Journal of Aircraft 42 (6) (2005) 1622-1630.
26. Namgoong, H., Crossley, W. A., Lyrinthzis, A. S., Aerodynamic Optimization of a Morphing Airfoil Using Energy as an Objective, AIAA Journal 45 (9) (2007) 2113-2124.
27. Trifu, O., Pagès, L., Sainmont, C. and Paraschivoiu, I., Optimization of the reference airfoil and completion of the CFD database, Task 1.6/7 report, Project CRDPJ 331810 - 05, Ecole Polytechnique de Montreal, Nov. 2007.
28. Campanile, L. F., Lightweight Shape-Adaptable Airfoils: A New Challenge for an Old Dream, in: Adaptative structures: Engineering Application, I. B. David Wagg, Paul Weaver, Micheal Friswell Chichester, (Eds.), John Wiley and Sons Ltd ,West Sussex, UK, 2007, pp. 89-136.
29. Hwang C. L. and Yoon K., Multiple attribute decision making, methods and applications, Edit. Springer Verlag, 1981, 259p.
30. Azarm S., Optimization, in: Edward Magrab, Shapour Azarm, B. Balachandran, J. Duncan, H.D. James, Keith E. Herold, Gregory C. Walsh (Eds.), An Engineer's Guide to MATLAB with Applications from Mechanical, Aerospace, Electrical, and Civil Engineering, second ed., Pearson Education Inc., Upper Saddle River, NJ, 2005, pp. 603–652.

CHAPITRE 4

ARTICLE#2 « AERO-STRUCTURAL MODEL FOR MORPHING LAMINAR WING OPTIMIZATION IN A WIND-TUNNEL »

D. Coutu¹, V. Brailovski¹, P. Terriault¹, M. Mamou², Y. Mebarki²

¹École de technologie supérieure, 1100 rue Notre-Dame Ouest,
Montréal (PQ), Canada, H3C 1K3

²Conseil National de Recherche du Canada - Institut de Recherche en Aérospatiale,
Ottawa, Ontario, Canada, K1A 0R6

Ce chapitre est la version révisée de l'article soumis à « *Journal of Aircraft* ».

Numéro de confirmation : 2009-12-C000232.

Résumé

À l'aide de la modélisation numérique, l'article soumis dans le « *Journal of Aircraft* » vise à utiliser de façon optimale le caractère adaptatif de l'aile expérimental du projet CRIAQ 7.1. Les travaux de cet article suivent la fabrication du prototype et se rapporte aux deux premières entrées en soufflerie (octobre 2008 et février 2009). Alors que les résultats des premiers essais en soufflerie servent à améliorer et valider les prédictions du modèle numérique, au cours de la seconde série d'essais se réalise l'exploitation optimale de l'aile adaptative laminaire.

Pour y parvenir, le modèle structural d'éléments finis initialement utilisé lors de la phase de conception fut revu et calibré pour représenter avec plus de fidélité le comportement adapté du prototype fabriqué. Pour ce faire, des essais d'actionnement en force et déplacement, de même que de mesures de coordonnées du profil, ont été réalisés. Par la suite, le solveur aérodynamique XFOIL fut couplé au modèle structural avec des corrélations expérimentales décrivant l'évolution des pressions de l'écoulement selon le nombre de Mach.

Finalement, les courses optimisées des actionneurs ont été déterminées en faisant intervenir successivement des algorithmes d'optimisation globaux et locaux interrogeant le modèle

aéro-structural. En soufflerie, ces courses optimisées pour 8 cas d'écoulement variant entre Mach 0.2 et 0.3 avec un angle d'attaque entre -1 to 2° ont donné lieu à une augmentation du comportement laminaire de la couche limite sur une distance moyenne de 25% de la corde. Conséquemment, une réduction moyenne de 18.5% de la traînée de profil a été mesurée par une traverse de Pitot. Ces résultats ont été à la hauteur des prédictions du modèle numérique, bien que ce dernier ne puisse prendre en charge les effets d'écoulement tridimensionnel (3D) en soufflerie.

Abstract

An aero-structural numerical model of a two-dimensional morphing laminar wing prototype is built and validated for different flight conditions: Mach numbers ranging from 0.2 to 0.3, and angle of attack ranging from -1° to 2°. The active structure of the wing is modeled using the commercial finite element software ANSYS. The aero-structural interaction is achieved by coupling the free-license aerodynamic solver XFOIL to ANSYS. This model is used to minimize the drag force under constant-lift conditions during wing tunnel testing using a two step optimization algorithm (global and local search). The wake pressure wind-tunnel measurements show that the extrados morphing results in an average 18.5% drag reduction for 8 flow cases covering the flow condition range of interest. Simultaneously, the infrared thermography measurements record an average laminar flow extension of 25% the wing chord over the upper wing surface. The experimental and numerical results are in good agreement, thus validating the use of an aero-structural model to efficiently manage the shape of a morphing laminar wing.

4.1 Nomenclature

b	=	airfoil span (mm)
c	=	airfoil chord (mm)
ΔC_d	=	drag coefficient reduction during wing morphing
Cl	=	lift coefficient
C_p	=	pressure coefficient: $(p-p_\infty)/q_\infty$
M	=	Mach number
p	=	static pressure (Pa)
p_∞	=	freestream pressure (Pa)

q_∞	=	freestream dynamic pressure = $0.5 \cdot \rho_\infty \cdot V_\infty^2$ (Pa)
S	=	wing surface area (m ²)
x	=	chord-wise distance from airfoil leading edge (mm)
x_{tr}	=	transition point location from airfoil leading edge (mm)
α	=	angle of attack (degree)
δ	=	vertical displacement imposed by the actuator (mm)
ρ_∞	=	freestream air density (kg/m ³)

4.2 Introduction

Environmental concerns have led to calls for cleaner and quieter aircraft and for diminishing the aviation industry's dependence on petroleum. Based on the study performed by the International Council on Clean Transportation (ICCT) [1], average fuel consumption (on both a seat-km and a ton-km basis) of commercial jet aircraft was reduced by 51% from 1960 to 2008. It is claimed that the introduction of widebody aircraft and of high bypass ratio turbofans are the two major breakthrough technologies that have contribute to the doubling of the average efficiency of aircraft in the past 50 years.

The International Air Transport Association (IATA) [2] predicts that "morphing wings" will be one of the next breakthrough technologies thanks to the availability of higher fidelity numerical models and the increasing use of composite materials. Even now, an increasing number of morphing wing concepts such as the FlexSys Mission Adaptive Compliant Wing (MAC-Wing), the NextGen's Batwing morphing concept and the NASA morphing aircraft are appearing in the literature [3]. Four years ago, the Consortium for Research and Innovation in Aerospace in Quebec (CRIAQ) initiated a research project to demonstrate the feasibility of the morphing wing technology to extend the laminar flow on the wing upper surface of under subsonic cruise flight conditions (CRIAQ7.1) [4]. This project was completed in 2009 with the results [5-12] offering new perspectives for the development of such a morphing technology at higher Technology Readiness Levels (5<TLR<6)..

4.3 Overview of the CRIAQ7.1 morphing laminar wing project

In the framework of the CRIAQ7.1 project, an experimental Morphing Laminar Wing (MLW) with a 500 mm chord length and a 990.6 mm span length was designed, manufactured and tested in a subsonic wind tunnel. The concept is shown in Figure 4.1 and it consists of a supercritical airfoil with a flexible extrados capable of adapting its shape to the variable flow conditions in order to increase the natural laminar flow over the wing upper surface. The flow conditions of interest ranged from Mach numbers 0.2 to 0.3 (in 0.025 increments), and the angles of attack varied between -1 and 2° (in 0.5° increments), for a total of 35 cases. The flexible extrados was made from a 4-ply composite laminate shell attached to the leading edge and to a compensation spring at the aft end to ensure profile tangency. Two linear Shape Memory Alloy (SMA) actuators were used to morph the two-dimensional wing profile. The number of actuators and the number of plies were two independent design variables chosen to offer the best trade-off between the aerodynamic performance of the morphing wing and the mechanical work provided by the actuation system to morph the extrados. This multi-criterion optimization task was performed using the finite element software ANSYS and the aerodynamic flow solver XFOIL [5]. The experimental MLW was assembled and tested in the subsonic wind tunnel located at the Institute for Aerospace Research of the National Research Council Canada (IAR-NRC) [13]. This closed-circuit wind tunnel has a 2×3 m test section operating under atmospheric conditions with speed uniformity of +/-0.07% and 0.14% turbulence intensity.

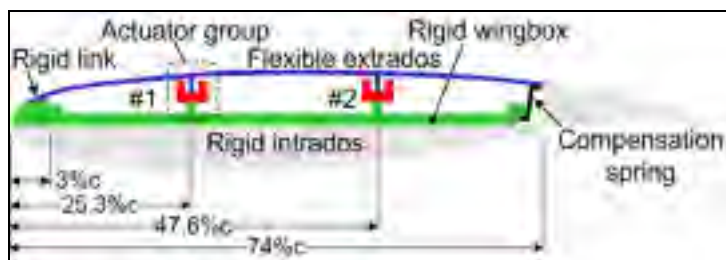


Figure 4.1 MLW concept with active extrados [6].

4.3.1 Morphing wing control approaches

When a morphing wing prototype is tested in a wind tunnel or in flight, the wing shape may be controlled using either open-loop or closed-loop approaches. Generally, an open-loop control approach is used to characterize structural integrity (Lockheed Martin morphing aircraft [14]) or aeroelastic behavior (NextGen Morphing Aircraft Structure [15]) of a developed morphing wing concept. In both of the above-mentioned cases, the morphing wing prototypes were successfully tested in the NASA-Langley Transonic Dynamics Tunnel for several morphing configurations using open-loop controllers.

To control the shape of a morphing wing prototype in-flight, both types of controllers can also be used. For example, two open-loop control techniques have been proposed to optimize the shape of a morphing wing. The first technique relies on a Design-of-Experiment (DOE) approach. To find the best trailing edge morphing flap deflection that minimizes the lift-to-drag ratio, the MAC-Wing of Hetrick et al [18] was tested during 27 hours of flight. The open-loop controller repetitively commanded a significant set of morphing configurations over the range of flight conditions of interest. From the results, the authors pretend that MAC-Wing can achieve a 15% increase in aircraft endurance by continuously optimizing the lift-to-drag ratio. The major drawback of such a procedure is that a large amount of time is required to pass through the test matrix. The DOE approach was not compatible with the CRIAQ7.1 budget available for wind tunnel testing with its 35 flow conditions to be studied and was therefore rejected.

The second open-loop optimization technique relies on the predictions of a numerical model. Strelec et al. [19] used an aero-thermomechanical model to optimize the design variables of their Shape Memory Alloy Actuated Reconfigurable Airfoil in order to maximize the lift-to-drag ratio for 3° angle of attack subsonic flow conditions. Tested in a low speed wind tunnel, the wing was actuated to the single deformed configuration using an open-loop controller. Unfortunately, the measured aerodynamic performance was less than expected due to prototype manufacturing issues.

However, to optimize the shape of a morphing wing prototype in-flight, the closed-loop control approach appears to be more beneficial because it uses hardware-in-the-loop to continuously measure the wing performance. One of the first relevant examples of this approach is the wind tunnel test of a computer-controlled Self-Optimizing Flexible Technology wing model. This work, realized by Levinsky et al. in 1979 [16], used the wind-tunnel balance to close the loop and an iterative algorithm to optimize the stroke of six actuators that control the wing shape. A nearly 10% drag reduction was achieved in the transonic wind tunnel at constant lift conditions. In the field of micro-air vehicles, Boria et al. [17] also used this approach to maximize the lift-to-drag ratio of the morphing Zimmerman planform wing. However, despite the positive results obtained, the authors concluded that given the inherent complexity of the hardware-in-the-loop, an open-loop approach could have led to similar results.

This work is limited, to an open-loop morphing wing control approach as a first step in the development of a MLW control strategy. A closed-loop MLW control approach was tested by the authors and the results obtained are submitted for publication elsewhere [11,12]. In the following sections, a structural finite-element model (ANSYS) and an aerodynamic two-dimensional panel method code with integral boundary layer theory (XFOIL) are presented separately and then in a coupled formulation. First, an overview of the ANSYS model and its validation under wind-off conditions is given. Then, to evaluate the effect of the FEM discrepancies on the aerodynamic performance predictions, the aerodynamic solver XFOIL 6.96 is used. The aero-structural interaction uses wind-tunnel empirical correlation data to apply true aerodynamic loads over the flexible extrados. A convergence study of the aero-structural model is performed, and the results obtained are validated by the wind-tunnel measured aerodynamic pressure distributions over the prototype extrados. To find the actuator strokes that maximize the aerodynamic performance of the MLW prototype, a two-step optimization procedure using the aero-structural model is discussed. The first step is based on a generalized pattern search using a MATLAB-supported algorithm, and the second step uses a local search algorithm specifically developed for this application. Furthermore, wind-tunnel measured balance forces, wake pressures and infrared thermography data are

compared with the numerically predicted results. Finally, recommendations are drawn and extrapolated to real aircraft applications.

4.4 Overview of the CRIAQ7.1 morphing laminar wing project

The finite element model (FEM) of the flexible structure, built in ANSYS software, includes span-wise stiffeners and several transmission components, such as pivot axes and cranks (see Figure 4.2).

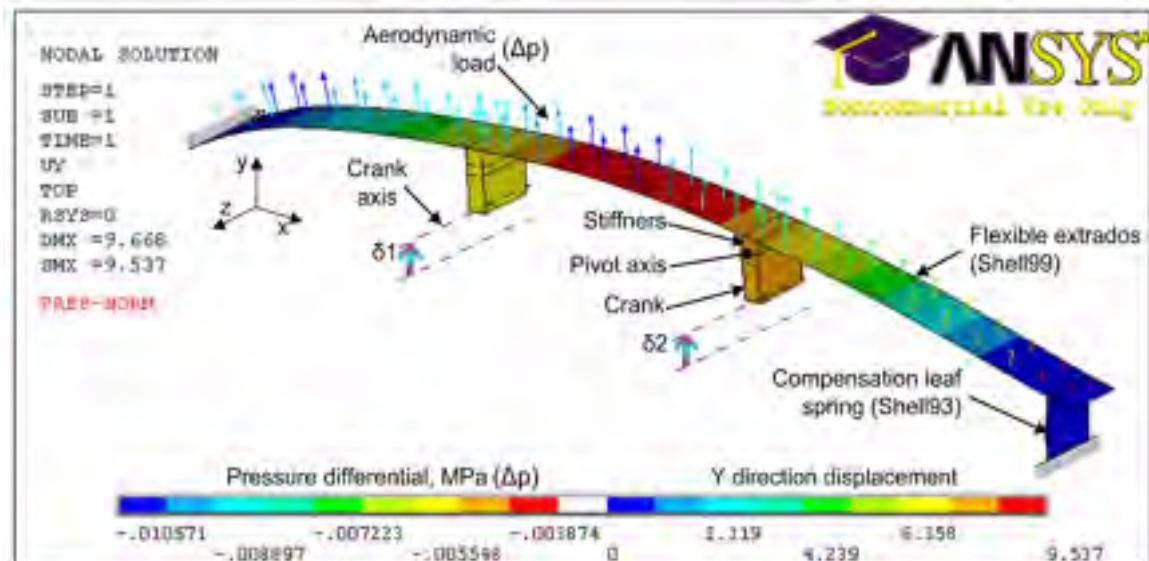


Figure 4.2 Structural FEM

4.4.1 Validation of the reference prototype geometry

The unmorphed geometry of the manufactured prototype was measured using a Mitutoyo BRT Strato 7106 coordinate measuring machine (Figure 4.3a), and then compared with the targeted geometry (see Figure 4.3b) to implement the measured deviations into the structural FEM solver.

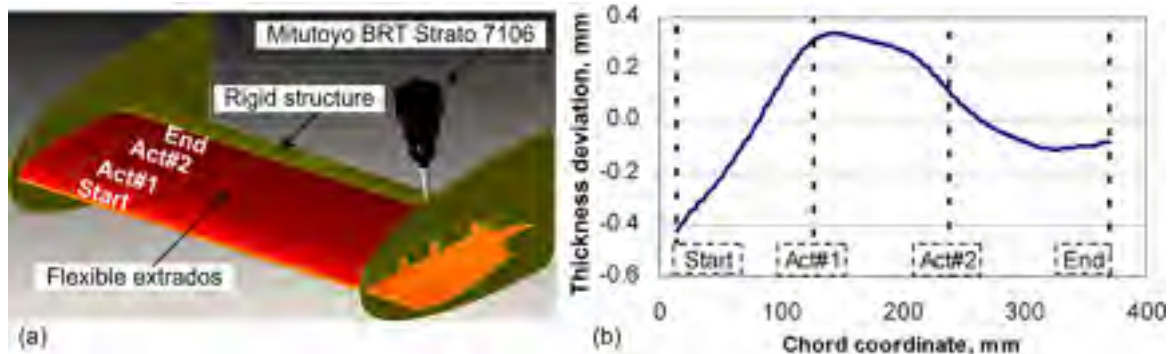


Figure 4.3 Unmorphed profile characterization: (a) coordinate measuring machine setup and (b) deviation of the manufactured from the designed (targeted) reference profile

4.4.2 Force-displacement actuator diagrams

To ensure that the flexible-structure FEM is accurate in terms of its structural response, its force-displacement behavior was verified experimentally. Figure 4.5 presents a schematic illustration of the test bench containing the flexible structure with four anchor points: the rigid link (1), two actuator lines (2-3) and a compensation spring (4). Displacements of the flexible structure were measured using a linear potentiometer (6). The SMA actuation system was replaced by a manual screw driving system (7) containing a load cell (5) to measure the actuation force.

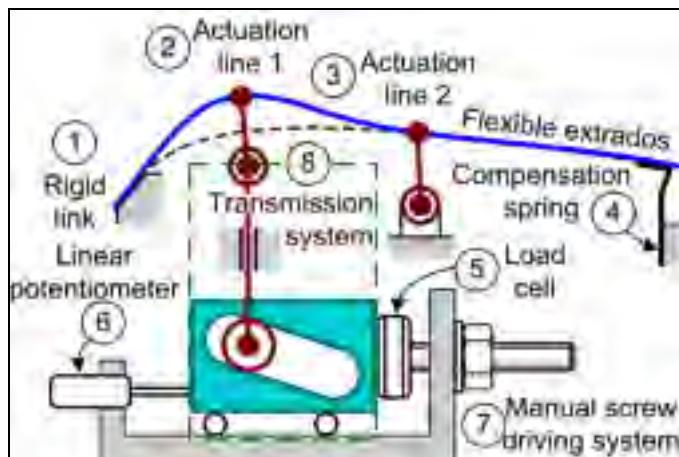


Figure 4.4 Force-displacement test bench for the active structure.

The force-displacement curves presented in Figure 4.5a,b were obtained by driving one actuation line between its displacement limits while restraining another actuation line. The force-displacement response of the active structure (EXP_act1&2) was compared to the numerical predictions (FE_act1&2). It can be observed that the model adequately predicts the overall behavior of the flexible extrados, except for the hysteresis caused by friction in the power transmission system. Consequently, the load-free position of each actuation line at the end of the loading-unloading cycle does not correspond to zero, and a negative force of nearly 100 N must be applied to return the extrados to its reference position. Considering that the SMA actuation system is displacement-controlled in using a linear potentiometer feedback signal, the SMA wires' heating and cooling temperatures are automatically regulated to compensate for the mechanical hysteresis [10].

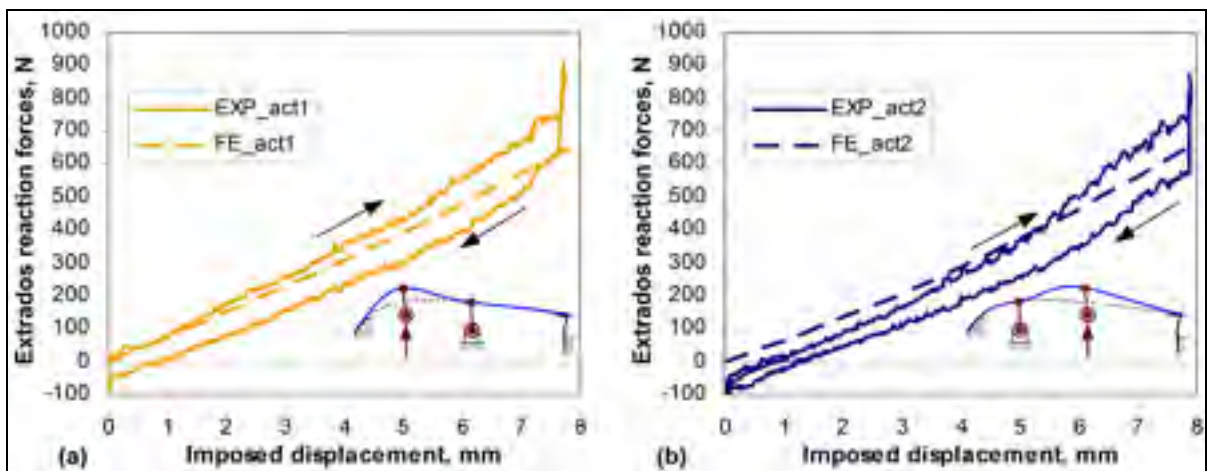


Figure 4.5 Force-displacement diagrams comparison: (a) first and (b) second actuation lines; EXP –experimental, FE – calculated data.

4.4.3 Validation of the FEM shape modification response under actuation

To validate the numerical model in terms of its ability to predict the shape modifications of the active structure, a custom-designed laser profilometer was built (see Figure 4.6a). The coordinates of the extrados profile were collected using two measuring devices: an optical shaft encoder (Sumtak #LBL-015-1000) and a mobile LASER displacement sensor (Wenglor

#CP35MHT80), aligned along the chord ('X') and the thickness ('Z') axes of the wing, respectively. Thickness modifications under actuation were measured experimentally and calculated numerically by subtracting the unmorphed profile coordinates from the morphed profile coordinates (see the two upper curves in Figure 4.6b). The deviations (see the two lower curves Figure 4.6b) were obtained by subtracting the experimental thickness modifications from those predicted numerically. Two sets of actuator displacements were used for this validation. First, the Shape Memory Alloy (SMA) actuators deformed the extrados close to the full stroke of 8 mm (1^{st} set: $\delta_1=6.37$, $\delta_2=7.68$). The displacements were then adjusted to approximately one-half of the previous values (2^{nd} set: $\delta_1=3.94$, $\delta_2=3.83$). As can be observed in Figure 4.6b, the geometrical deviations vary between -0.12 and +0.14 mm for the first 250 mm of the chord length and reach +0.59 mm closer to the aft end of the flexible extrados. For each portion of the chord delimited by the flexible extrados attachment points, the minimum or maximum numerical thickness deviations are given as a percentile of the applied strokes δ_1 , $(\delta_1+\delta_2)/2$ or δ_2 .

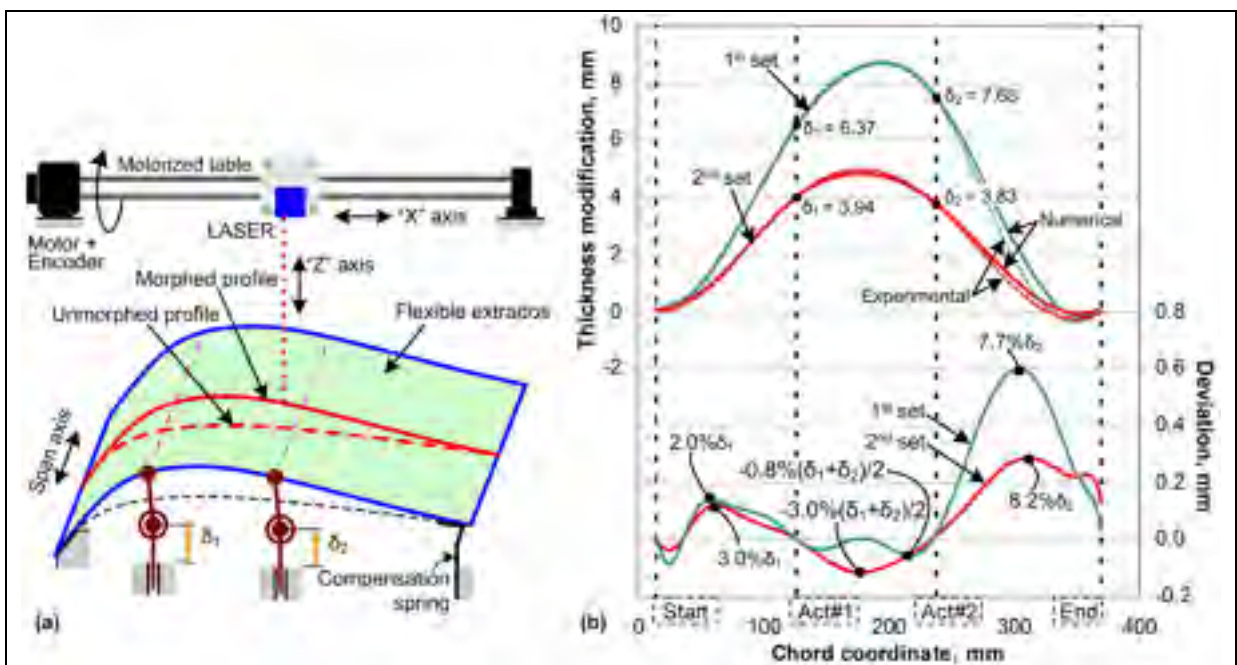


Figure 4.6 Validation of the shape modification for two sets of actuators' displacements: (a) bench test setup and (b) comparison of the numerical and experimental thickness modifications..

4.5 Aerodynamic effects of the deviations between FEM predictions and experiments

To quantify the effect of deviations between structural model predictions and experiments on the aerodynamic performance of the wing prototype, CFD analyses were carried out using XFOIL 6.96 [20]. This code, written by Mark Drela in 1986, uses a high-resolution panel method with a Karman–Tsien compressibility correction. The resulting inviscid solution is incorporated into the viscous equations and solved by the full-Newton method. For low angles of attack or lift coefficients ($Cl < Cl_{max}$), the solver provides reasonably accurate drag and Cp distribution for Mach numbers below 1.05, which works well for this study (Mach number of 0.3). Moreover, from the viscous solution, the laminar-to-turbulent transition is predicted using a simplified e^N method with the N_{crit} factor fixed to 7, a value representative of the turbulence level of the NRC wind tunnel incoming flow [21].

Figure 4.7 shows the XFOIL-calculated polar curves for the experimentally measured and calculated profiles for the 1st and 2nd sets of actuator displacements for angles of attack varying from -1 to 20 with 0.50 increments, and the highest Mach number of 0.3 (see Fig 6b). Generally speaking, the effects of the modeling errors on the aerodynamic performance calculations decreased as the drag coefficient decreased. The largest difference in terms of drag coefficient (a 9.0% shift) was observed for the 2nd set of actuator displacements, and it corresponds to the highest Mach number and angle of attack (Mach 0.3 and $\alpha = 2^\circ$). This result could be expected since the 2nd set of displacements corresponds to the greatest thickness deviations between the flexible extrados attachment points: (+3.0% δ_1 , 3.0%($\delta_1+\delta_2$)/2 and +8.2% δ_2). The differences in terms of lift coefficient are less significant, and the largest value shows a 1.9% shift for the 1st set of displacements at Mach 0.3 and $\alpha = 1^\circ$.

Although the modeling errors affected the predictions of the morphing wing aerodynamic performance, the structural FEM model appears to be suitable for the optimal strokes calculations. Indeed, Figure 4.7 shows that, for both sets of actuator displacements, the angles of attack that minimize the drag for Mach number 0.3 are the same ($\alpha_1 = 0$ for the 1st

set and $\alpha_2 = -0.5^\circ$ for the 2nd set) whether the profile deviations are considered or not. Therefore, the structural model can be considered ready to be coupled to an aerodynamic solver to assess the aero-structural interaction.

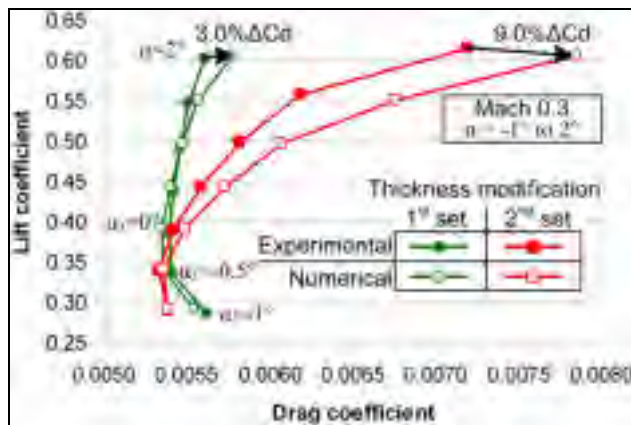


Figure 4.7 The effects of modeling error on the predicted aerodynamic performance for the 1st and 2nd sets of actuator displacements (see also Figure 4.6b).

4.6 The aero-structural model and its wind tunnel validation

4.6.1 Preliminary works

Since the extrados morphing affects aerodynamic pressure distribution over the MLW, and the aerodynamic pressure distribution affects the extrados geometry, the aero-structural interaction must be modeled. XFOIL software is well-suited to be coupled to the ANSYS structural model due to its short execution time and its capability to be launched from an external command line. Note that at the very beginning of the CRIAQ7.1 project, XFOIL was already being used by our collaborators from the Ecole Polytechnique de Montreal to generate a series of optimized airfoil profiles and to establish the technical requirements for the MLW [24].

4.6.2 Aero-structural interaction

The aero-structural coupling between the structural FEM and the aerodynamic solver XFOIL was achieved with an iterative algorithm coded in ANSYS parametric design language. As sketched in Figure 4.8, for a given set of actuator strokes and flow conditions, the coupled model solves a steady-state problem to calculate the aerodynamic performance and actuation forces (the latter were used for SMA actuator design, see Georges et al.[9]). Actuators' strokes are applied as vertical displacements of the transmission crank axis, whereas a linear interpolation table is used for the aerodynamic load. To accelerate the convergence, the initial pressure distribution corresponds to that calculated by XFOIL for each optimized profile, without considering any aero-structural interaction [24]. Subsequently, the nonlinear structural problem is solved with ANSYS and the aerodynamic performance of the resulting modified shape is evaluated by XFOIL. To favor an accurate viscous solution, XFOIL re-panels the airfoil using splines generated from the FEM's nodes' coordinates. During subsequent iterations, the ANSYS routine uses the previously calculated XFOIL pressure distribution to update the pressure load interpolation table.

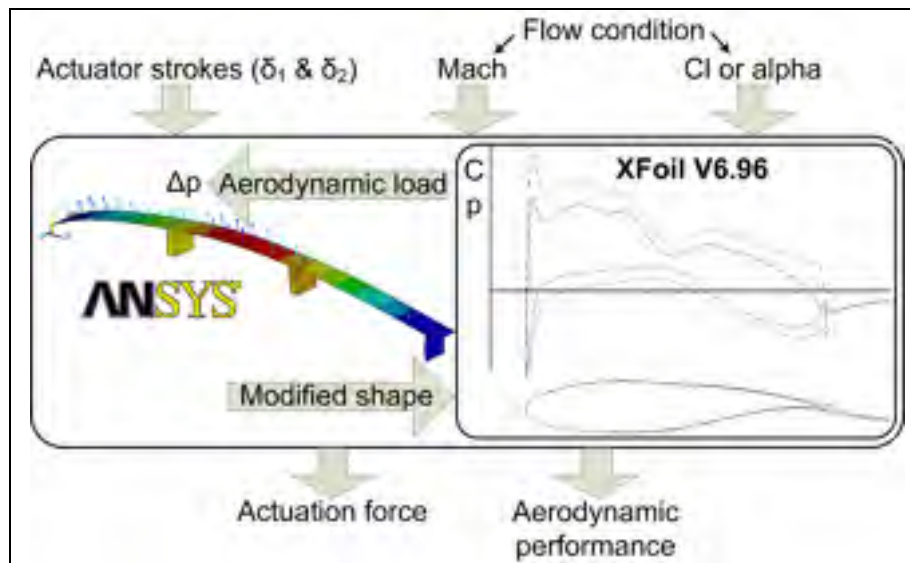


Figure 4.8 Aero-structural interaction of the coupled model..

4.6.3 Empirical correlation for pressure loading

The pressure load (Δp) is defined by Eq. (1) as a difference between the external (p_{ext}) and internal (p_{int}) pressures applied to the active structure. Given that the external pressure is directly related to the pressure distribution (C_p), a new load formulation can be derived from the dynamic (q_∞) and the total (p_{tot}) pressure data (see Eq. (2) and Eq. (3)). Preliminary wind-tunnel runs showed a significant pressure evolution as the Mach number increases. Given that the closed-circuit wind tunnel was vented to the atmospheric pressure, the higher the Mach (M) number, the higher the total pressure, while the lower the pressure inside the MLW prototype (see plots $f_1(M)$ and $f_2(M)$ in Figure 4.9). Empirical correlations were derived for the total (p_{tot_gauge}) and the internal (p_{int_gauge}) pressure gauges as shown in Eq. (4). Finally, the pressure load applied on the flexible extrados can be evaluated by Eq. (5) using both the $f_1(M)$ and the $f_2(M)$ correlation functions.

$$\Delta p = p_{ext} - p_{int} \quad (1)$$

$$p_{ext} = q_\infty \cdot (C_p - 1) + p_{tot} \quad (2)$$

$$\Delta p = q_\infty \cdot (C_p - 1) + p_{tot} - p_{int} \quad (3)$$

$$p_{tot} - p_{int} = p_{tot_gauge} - p_{int_gauge} = f_1(M) - f_2(M) \quad (4)$$

$$\Delta p = q_\infty \cdot (C_p - 1) + f_1(M) - f_2(M) \quad (5)$$

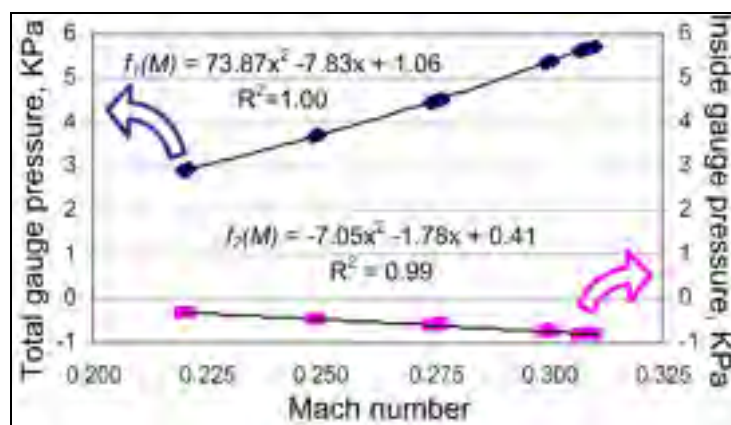


Figure 4.9 Wind tunnel pressure variations and empirical correlation.

4.6.4 Empirical correlation for pressure loading

A convergence study was performed to determine the reasonable number of iterations required to achieve adequate aero-structural coupling. For this purpose, the highest pressure loading flow case was considered (Mach 0.3; $Cl = 0.602$) with actuators' displacements close to the maximum ($\delta_1=6.70$ mm; $\delta_2=7.95$ mm). Figure 4.10a presents the maximum variations of the pressure load and shape modifications as percentiles of the values obtained in previous iterations without regard to its sign, for the first 20 iterations. Separate convergence criteria were established for both parameters: pressure load convergence of 1% was reached at the 3rd iteration, while shape modification convergence of 0.001% was reached at the 5th iteration. Therefore, the minimum number of iterations to ensure an adequate convergence of the coupled aero-structural model was set to five.

For verification, the absolute values of the variation (given as a percentile of the value of the previous iteration) of the drag coefficient and of the laminar/turbulent transition over the morphing extrados are presented in Figure 4.10b for the first 20 iterations. After the 3rd iteration, the drag prediction remains constant, whereas the transition point location varies between 46.4 and 46.5% of the chord length. These results are considered satisfactory, as the maximum variation of the transition prediction remains under 0.2% after the 3rd iteration,. Therefore, five iterations appear to be sufficient to ensure reliable aero-structural interaction.

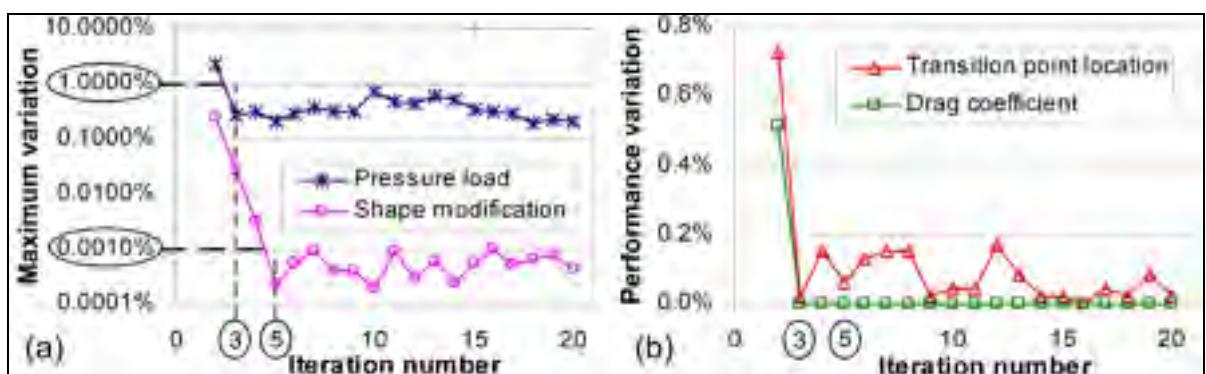


Figure 4.10 Aero-structural convergence study: (a) maximum absolute variation of the pressure load and shape modifications and (b) absolute variation of the drag coefficient and location of the laminar/turbulent transition.

When comparing two curves of Figure 4.10a, the maximum pressure load variation ($\sim 1\%$) is about one thousand times greater than the maximum shape modification variation ($\sim 0.001\%$). This observation is coherent with the active structure design intent, wherein the numbers of plies and actuators were determined with the objective of ensuring sufficient stiffness in the flexible structure, thus limiting the sensitivity of the morphing structure to pressure load variations. Finally, small continuous variations (noise) in the aero-structural model response can be explained by the use of numerical interpolation methods and the limited number of significant digits used for data exchange between XFOIL (6 digits) and ANSYS (8 digits).

4.6.5 Validation of the coupled model in terms of pressure distribution calculations

To validate the aero-structural model, the pressure distribution over the active structure extrados was experimentally measured and compared with the numerical predictions in Figure 4.11. A pressure sensors array over the morphing extrados and a pressure port inside the model were used for this purpose. Unfortunately, during the installation, two reference pressure tubes near the leading edge were pinched accidentally. Consequently, the sharp pressure peak close to the leading edge could not be measured. Also, in the area before the first actuator line, where the flow suddenly accelerates and decelerates, numerical calculations overestimated the measured aerodynamic loads. Fortunately, on the remaining part of the morphing extrados, the numerical predictions were satisfactory. In sum, the pressure load prediction appears to be sufficiently reliable to allow the use of the aero-structural model for MLW shape optimization.

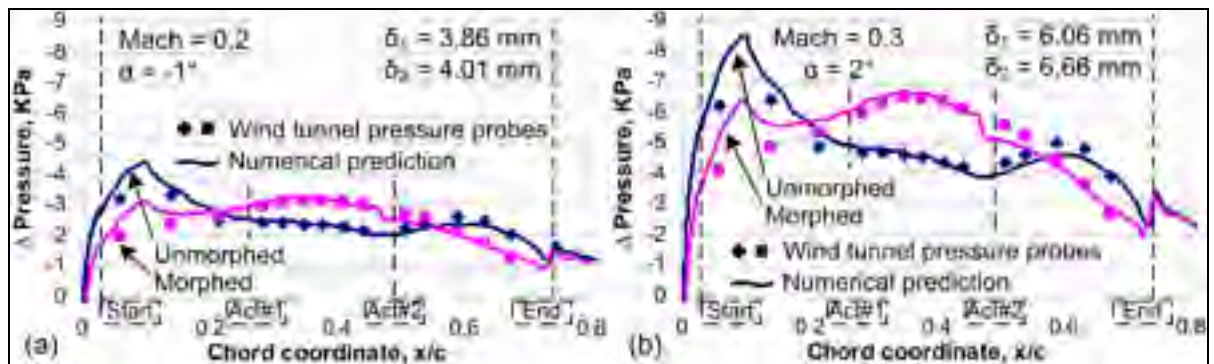


Figure 4.11 Numerical and experimental pressure differentials over the flexible extrados for two aerodynamic cases: (a) Mach 0.2 and Alpha -1° and (b) Mach 0.3 and Alpha 2° .

4.7 Actuator strokes' optimization

4.7.1 Optimization problem:

To find the best wing profile for each of the 35 flow cases, the actuators' strokes were optimized using the aero-structural coupled model presented earlier. The profile drag under constant lift conditions was selected as an objective function to minimize. Since shape morphing affects the profile lift, an appropriate adjustment of the angle of attack to keep the lift constant allows an objective comparison of the morphed and unmorphed profiles. Note that for subsonic flow, friction drag, which is the main component of the profile drag, decreases when the boundary layer is laminar instead of turbulent [23]. Therefore, an important laminar flow regime enhancement is expected from optimal wing morphing.

In this work, the design range for each actuator stroke lay between 0 and 8 mm, the physical limits of the prototype. To devise an appropriate optimization method, the objective function was first calculated over the entire design range using 0.2 mm actuator stroke increments, for a total of 1681 points. Each point corresponded to a given set of two actuator strokes and required approximately 30 seconds of computation time (dual-core 2.0 GHz desktop). For two particular flow cases ($M=0.25 \alpha=-1^\circ$ and $M=0.25 \alpha=0.5^\circ$), the results of this full design search scan were plotted as response surfaces with their respective contour levels, as shown

in Figure 4.12. For both flow cases, the objective function presents several local minima that represent different optimal actuator strokes. Since the response surfaces calculation is a very costly task if it needs to be repeated for every possible flow condition (see Table 4.1), a two-step optimization procedure has been proposed [25]. The first step, called global or “rough” optimization, uses standard optimization algorithms to find a preliminary target point near the optimum zone, and the second step, called local optimization or “fine tuning”, uses a custom routine to determine the final optimum actuation stroke.

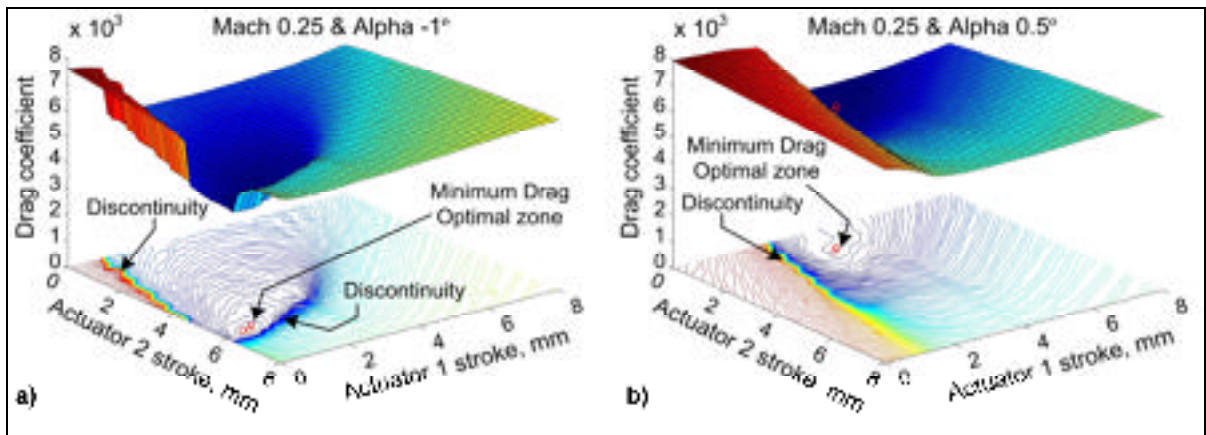


Figure 4.12 Numerical drag coefficient response for: (a) Mach 0.25 & Alpha -1° and (b) Mach 0.25 & Alpha 0.5°.

4.7.2 Global optimization

The presence of discontinuities in the objective function (see Figure 4.12) suggests that traditional search methods, using the surface gradients, are not well-suited. Thus, a direct search algorithm, the “Generalized Pattern Search positive basis 2N”, available in MATLAB [26], was selected and is presented as an example in Figure 4.13. Using a client-defined pattern, this simple method searches among a set of points; thereby forming a mesh around a given point. The point that minimizes the objective function becomes the current point for the next iteration. The pattern search was executed in MATLAB with additional instructions such as the actuation limits (0-8 mm) and the initial searching point, corresponding to half of the maximum actuator stroke ($\delta_1 = \delta_2 = 4\text{mm}$).

Stopping criteria were adjusted so that the algorithm would stop when the distance between two consecutive points becomes smaller than 0.024 mm, or when the number of iterations reaches 100. Each evaluation was kept in memory by the algorithm to avoid re-computing points located within 0.01 mm of their neighbors. For both flow cases tested and presented in Figure 4.13, searches converged successfully (the design variable fell below 0.024 mm tolerance) to reach the target zone, requiring about 94 function evaluations for each case (see Table 4.1 for the number of objective function evaluations).

4.7.3 Local optimization

The local optimization algorithm used a specially developed routine which calls on the aero-structural model to evaluate all the points surrounding the best point found during global optimization until the optimum actuation zone is completely delimited. All the points in this optimum zone had an objective function value equal to or smaller than the current optimum plus an average tolerance of 0.2% C_d . A stroke increment of 0.2 mm was used to sufficiently localize the optimum zone while minimizing the number of evaluations (computation time). The optimal zones and their centers are presented in Figure 4.13 for both flow cases. The local optimization method proved to be effective and robust, requiring about 33 objective function evaluations for each case (see Table 4.1).

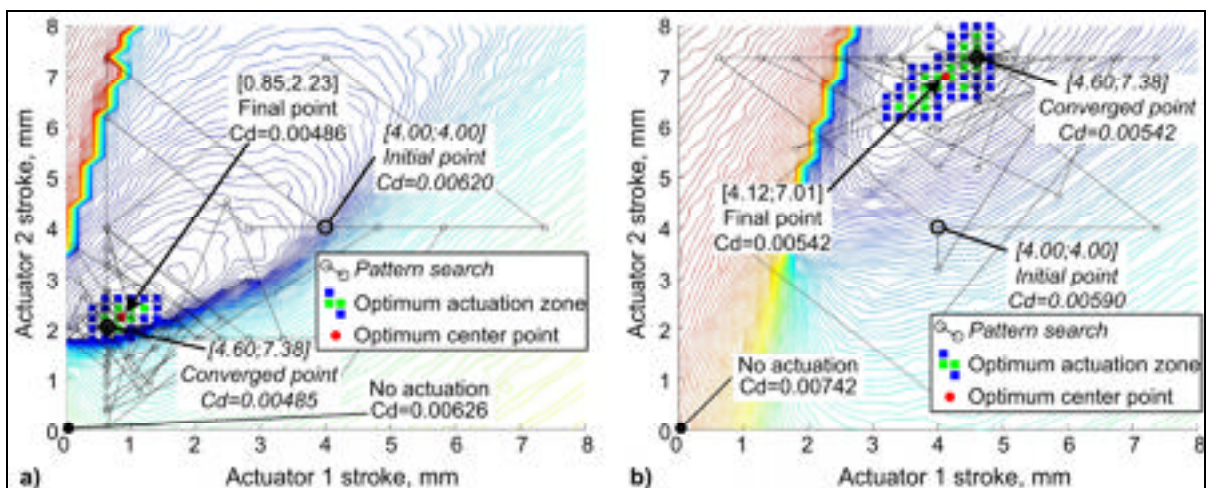


Figure 4.13 Two-step optimization method for: (a) Mach 0.25 & Alpha -1° and (b) Mach 0.25 & Alpha 0.5°.

4.7.4 Optimization results

For the 35 flow cases, the two-step optimization procedure required 13-times less computation time than the full design search scan. The resulting optimum strokes of two actuators were linearly interrelated up to the second actuator 8 mm stroke limit (Figure 4.14). Note that for both actuators, the higher the Mach number and the angle of attack, the higher the optimum strokes. Finally, an 8 mm maximum stroke is reached for 15 of the 35 aerodynamic flow cases, which indicates that the full benefits of morphing cannot be exploited using current prototype configuration (see the surfaces representation of Figure 4.15).

Table 4.1
Computation time for optimization

Otimization methods	1 case	35 cases
• Numerical surface calculus	13h	455h estimated
• 2 steps optimization	1h11	44h12
o Global optimization	0h50	25h09
o Local optimization	0h21	19h03

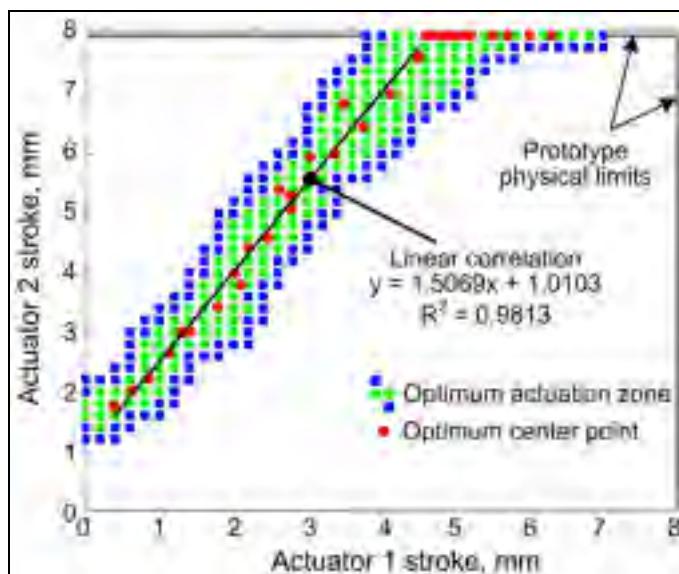


Figure 4.14 Optimum strokes for actuator 1 and 2 resulting from the centers of the optimal zones.

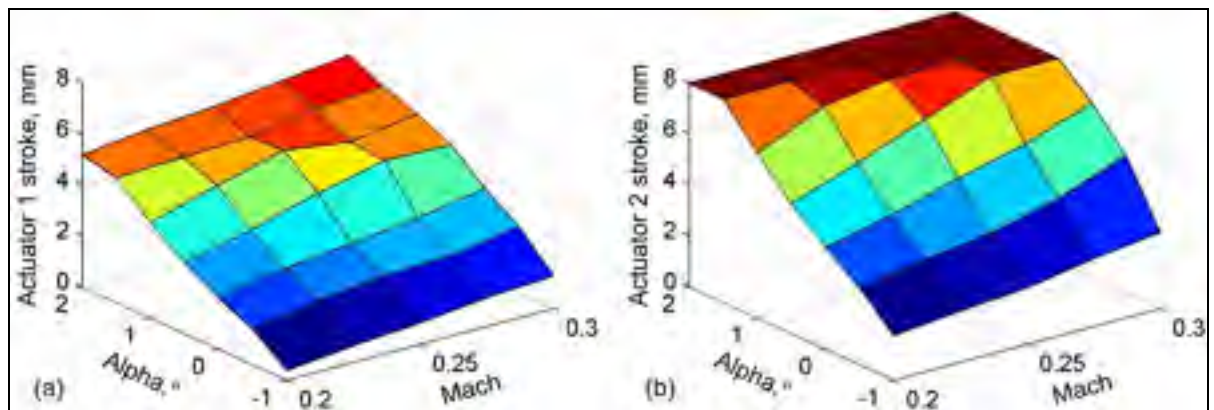


Figure 4.15 Optimization results as a function of the Mach number and the angle of attack.

4.8 Wind-tunnel validation

4.8.1 Experimental set-up

The results of numerical optimization were validated on the MLW prototype mounted vertically in the NRC 2 x 3m wind tunnel (Figure 4.16a). The wall interference was cancelled through proper correction of the experimental data. Two aerodynamic fences were installed on the prototype's ends to promote a two-dimensional flow over the wing. However, despite these precautions, wind-tunnel balance measured drag appeared to be about four times greater than that calculated numerically, due to the presence of rigid wing ends and aerodynamic fences. Thus, a traversing wake-rake containing 41 total and four static pressure probes was added to measure the drag coefficient more accurately using the momentum method. Two proportional, derivative and integral controllers were used to command the actuators' strokes using linear potentiometer feedback [10]. For the 35 flow conditions generated in the wind tunnel, open-loop MLW control was performed by applying 35 numerically optimized stroke combinations compiled inside a database (Figure 4.16b).

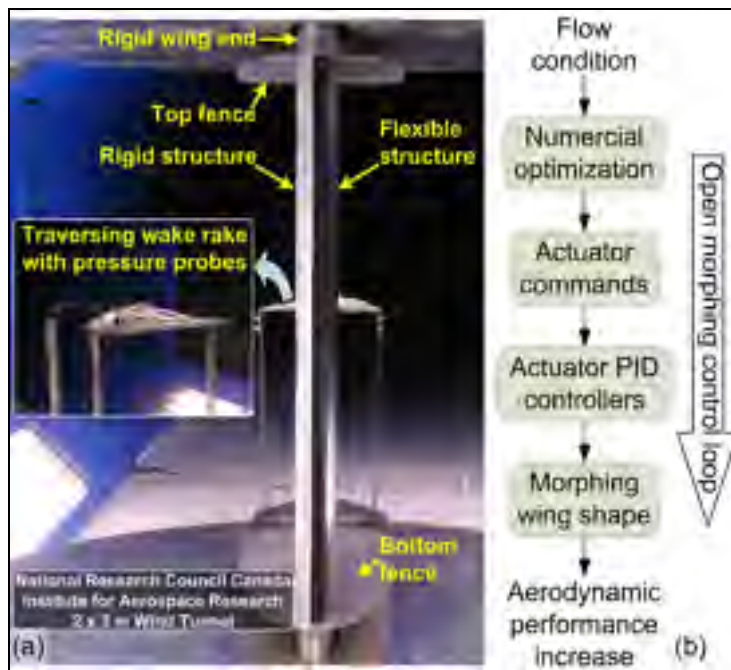
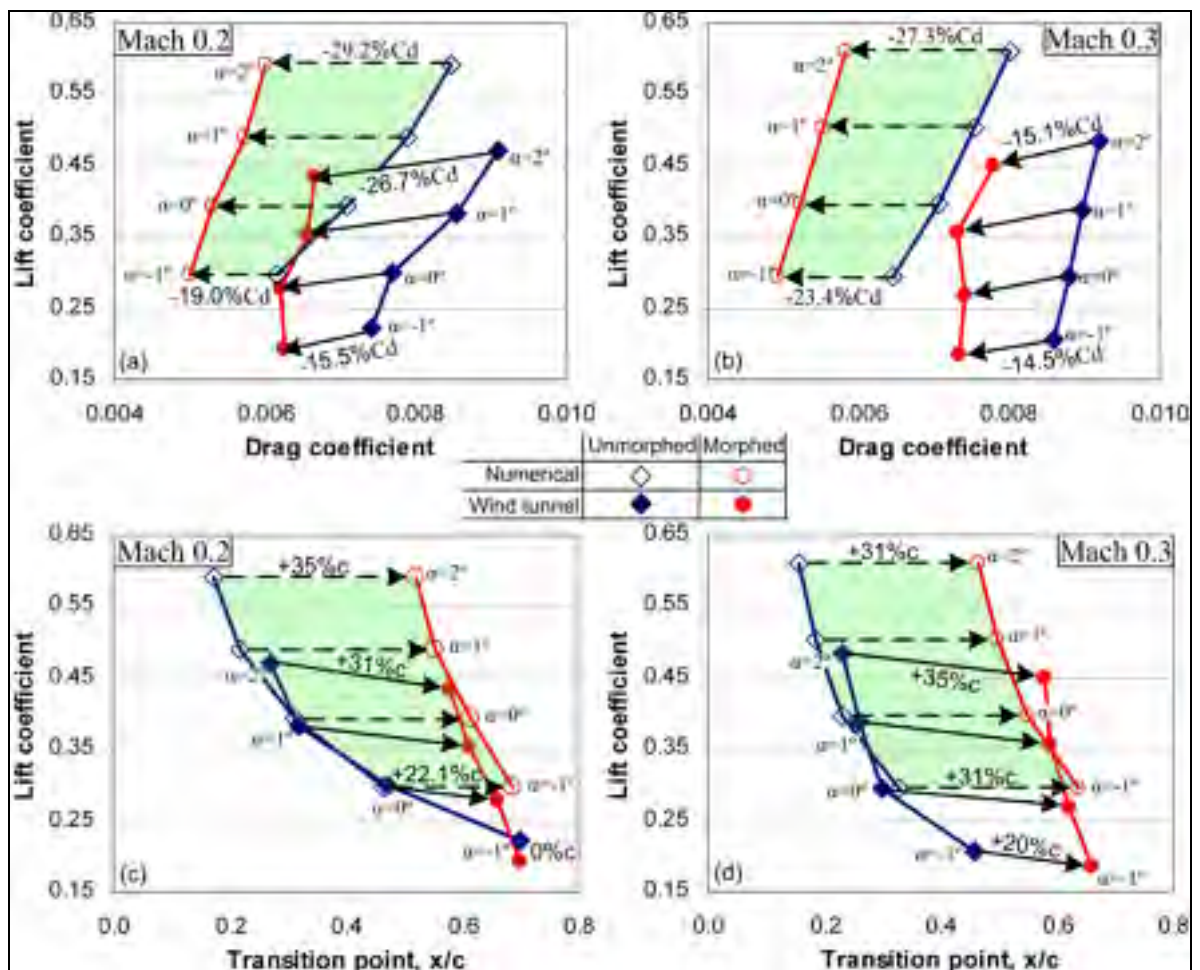


Figure 4.16 (a) Experimental MLW in the wind tunnel, (b) open-loop control.

4.8.2 Morphing wing performance

Wing morphing resulted in a reduced drag under quasi-constant lift conditions. Using balance lift and wake pressure measurements, Figure 4.17 presents the morphing test results for eight flow cases covering the flow condition range of interest: Mach 0.2 and 0.3, with angle of attack varying from -1 to 2°, incremented by 1°. As presented in Figure 4.17(a, b), the measured drag reduction varies between 14.5 and 26.7% with an average value of 18.5%. Unfortunately, the measured lift forces were found to slightly decrease during morphing (average value of 9%), suggesting that the angle of attack adjustments (reduction) required to compensate for the lift increase caused by morphing were overestimated. However, the considerable shift in the polar curve due to wing morphing proves the effectiveness of open-loop control. In other words, the shape optimization realized with the aero-structural model allows the MLW drag reduction potential to be experimentally validated.



**Figure 4.17 Numerical and experimental morphing effect over the aerodynamic lift vs drag coefficients (a, b) and over the laminar flow transition (c, d) for flow conditions ranging from alpha -1 to 2° (1° increments) at given Mach number:
(a, c) Mach 0.2; (b, d) Mach 0.3.**

In addition, the InfraRed thermography (IR) technique shows that the boundary layer laminar/turbulent transition location (x_{tr}) over the upper surface of the wing is extended toward the trailing edge when the shape is morphed (Figure 4.17(c-d)). This effect results in a laminar flow extension from 0 to 35% c , with an average value of 25% c for the eight flow conditions. Figure 4.18 presents a 31% c laminar flow regime extension for the Mach 0.2 and alpha 2° flow case, based on the temperature picture comparison of the unmorphed profile ($x_{tr} = 27\%c$) with the morphed profile ($x_{tr} = 58\%c$). These IR results, together with the balance and wake-rake pressure measurements, prove the feasibility of a significant drag reduction (reduction of aircraft fuel consumption and greenhouse gas emission) through the

enhancement of the laminar flow regime over the upper surface of an experimental MLW equipped with an active extrados.

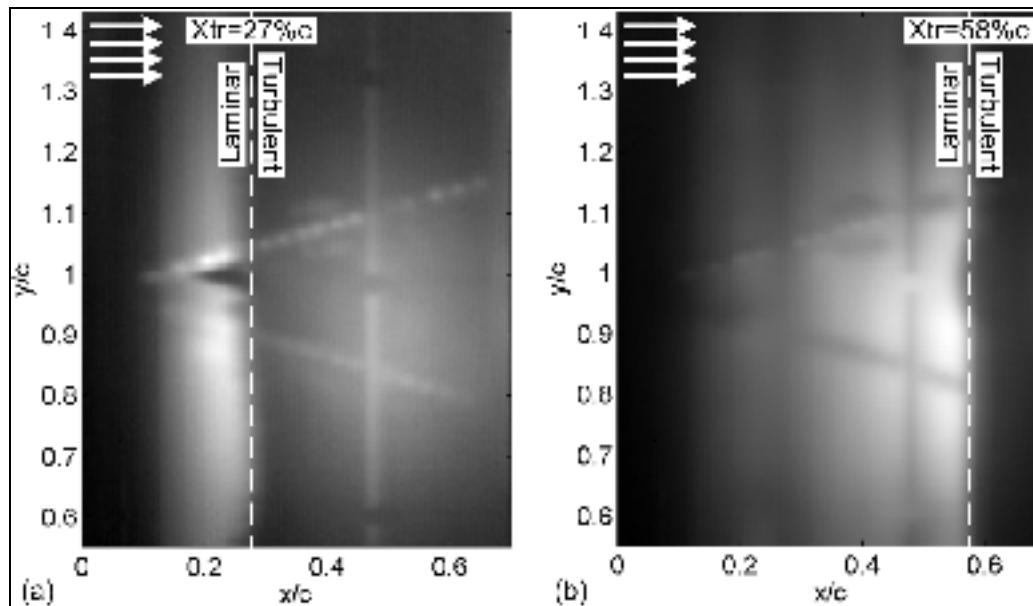


Figure 4.18 Laminar/turbulent flow transition over the active structure using infrared thermography visualization for Mach 0.2 and Alpha 2°:
(a) unmorphed profile; (b) morphed profile.

4.9 Discussion of the comparison of the experimental and numerical results

The drag reduction obtained during morphing as well as the laminar flow regime enhancement was consistent with the numerical predictions, as presented in Figure 4.17. However, the numerical aerodynamic coefficients (lift and drag) and the transition point were almost uniformly shifted over the entire test space. For example, the drag measured by the wake-rake was greater than that predicted, which can have two possible explanations. It could be explained by the interference of the pressure sensors on the wing surfaces, diminishing the flow velocity measured by the wake rake. Or, it could be due because the two-dimensional aerodynamic solver XFOIL does not describe any three-dimensional effects, which reduces the effective angle of attack: the lower the angle of attack, the greater the laminar flow extent over the extrados and the smaller the drag.

XFOIL generally gives an optimistic prediction of the laminar flow regime development (L. Pagès [21]), whereas the calculated laminar flow over the extrados is closer to the leading edge than that experimentally measured by the IR camera. One explanation could be an overestimation of the wind tunnel turbulence intensity due to the underestimation of the N factor. However, in such a case, the calculated drag and lift forces would have been, respectively, higher and lower than the experimental data, which is not the case. Finally, despite the noticeable differences between the experimental and numerical results, the consistent drag reduction and laminar flow improvement obtained in the wind tunnel prove the reliability of the aero-structural model and its utility for MLW shape optimization.

4.9.1 Beyond the prototype's physical limitations

Having determined that a significant improvement of the aerodynamic performance of a morphing wing can be obtained, the following question can now be raised: to what extent do the actuators' stroke limitations (maximum stroke of 8 mm) affect a wing's optimal aerodynamic performance? To answer this question, the stroke optimization study was repeated without considering the prototype's physical limitations, and the results are presented in Figure 4.19 and Figure 4.20.

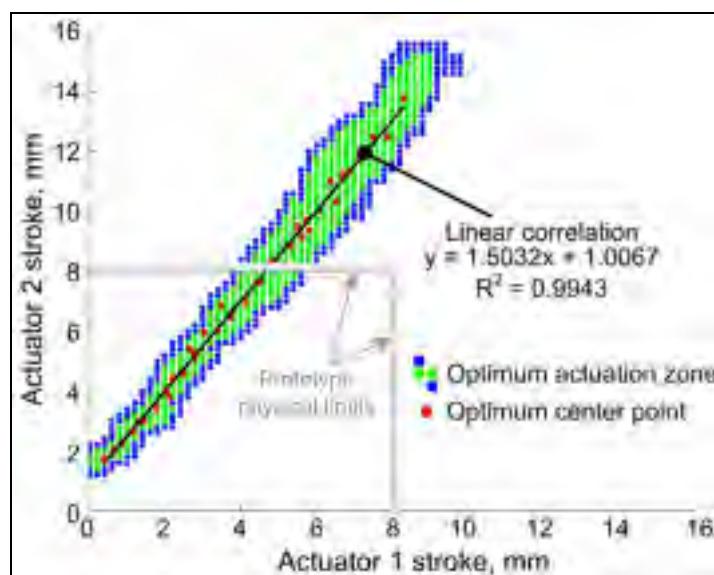


Figure 4.19 Optimum strokes for actuator 1 and 2 with no physical limitations of the actuation strokes (to be compared with Figure 4.14).

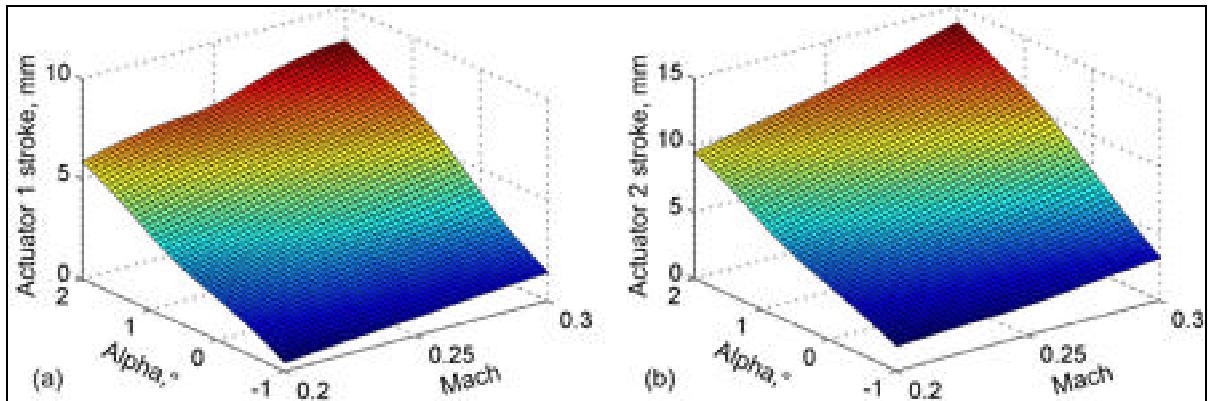


Figure 4.20 Optimization results as a function of the Mach number and the angle of attack without consideration of the prototype's physical limits

If the unmorphed profile is considered as the reference, the unlimited optimization offers better performance than the limited optimization, especially for high Mach numbers (Figure 4.21a) and high angles of attack (Figure 4.21b) because these conditions are indeed less favorable to maintain a laminar flow regime [23]. However, the gain in drag reduction is relatively small: -30.2 instead of -27.3% for the conditions least favorable to laminar flow: Mach 0.3 and Alpha 2°. For the 15 flow cases where actuation strokes exceed 8 mm, the mean relative drag reduction is only improved by less than 1%, a value that might not justify the efforts and complexity related to such a significant extension of the maximum actuator strokes (from 8 to 13.8 mm).

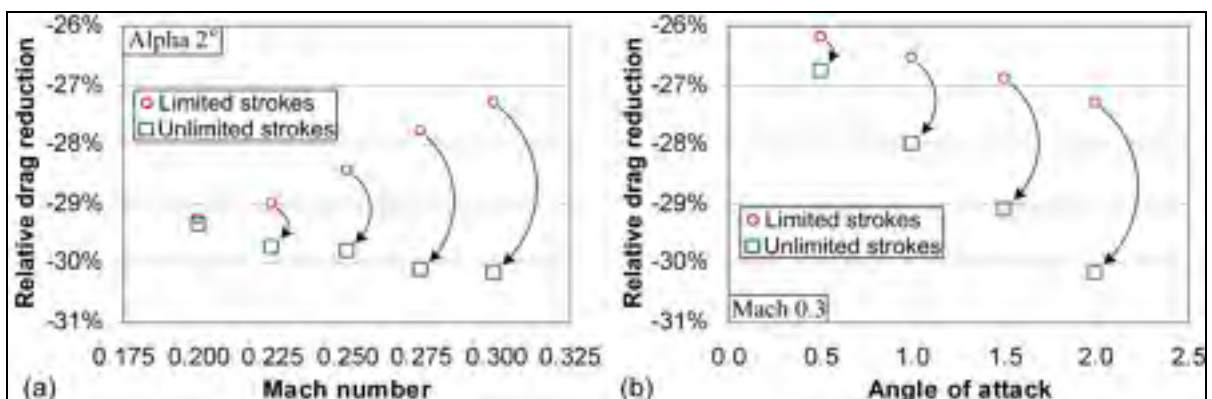


Figure 4.21 Relative drag reduction upon morphing from the unmorphed profile for limited and unlimited actuator strokes: (a) Mach number variation at 2° angle of attack (b) Angle of attack variation at Mach number 0.3

4.10 Conclusion and recommendations

The wind tunnel optimization of the MLW profile was successfully realized using a coupled aero-structural numerical model. An ANSYS structural finite-element model of the MLW was first validated under wind-off conditions using experimentally measured actuator force-displacement characteristics and wing profile modifications. The structural model was then coupled with the aerodynamic solver Xfoil and the aero-structural model was calibrated and validated using experimental wind-tunnel pressure data. Finally, the MLW optimization problem was solved using a two-step search algorithm to determine the optimum actuator strokes to be applied, using an open-loop control approach. The experimental results provided by a wind-tunnel balance, a wake rake, and an infrared camera showed a significant aerodynamic performance enhancement in terms of drag reduction and laminar boundary layer improvement due to wing morphing. A successful comparison of the experimental and numerical results validated the utility of the aero-structural model for an open-loop control of the MLW, despite its inherent limitations to describe miscellaneous three-dimensional aerodynamic effects.

To reduce the difference between the numerical and the experimental results, and thus promote the search for better MLW morphing shapes, the use of a higher fidelity numerical method is recommended. To come closer to applying the MLW concept to a real aircraft, serious consideration of the linear relationship between both actuator strokes presented in Figure 4.14 is warranted. In this case, only one actuator connected to a multi-segment transmission mechanism could power two or more actuation lines. Also, it was found that actuator strokes vary continuously in respect to the Mach number and angle of attack evolution (see the surface of Figure 4.15). This particularity allows the use of simple interpolation to feed an open-loop controller within a given range of flow conditions. The next step of this project is to develop a closed-loop morphing control strategy using real-time aerodynamic performance feedback signals, such as balance coefficients or infrared data, to fully benefit from the potential offered by a MLW. Through this study presented by Coutu et

al. [11-12], the aero-structural model serves as an estimator, accelerating the real-time optimizer convergence towards an optimum morphed shape.

4.11 Acknowledgments

The authors acknowledge the contributions of C. Fischer, S. Bérubé and J.-S. Ratelle to the design and manufacture of the experimental MLW prototype used in this study, and those of T. Georges and E. Morellon for their role in experimental testing. The authors would like to thank the Consortium for Research and Innovation in Aerospace in Quebec (CRIAQ), the Natural Sciences and Engineering Research Council of Canada (NSERC), Bombardier Aerospace, and Thales Canada for their financial support. Also, the authors thank Dr O. Trifu (currently at CAE) and C. Sainmont from Ecole Polytechnique de Montréal for their collaboration in this work. Finally, the authors acknowledge G.-H. Simon from Thales as the project initiator.

4.12 References

1. Rutherford, D. and Zeinali, M., “Efficiency Trends for New Commercial Jet Aircraft, 1960 to 2008,” [online], 2009, http://pre2010.theicct.org/documents/ICCT_Aircraft_Efficiency_final.pdf [retrieved 10 March 2010].
2. IATA, “The IATA Technology Roadmap Report, 3rd Edition,” [online], 2009, 50 p., http://www.iata.org/SiteCollectionDocuments/Documents/Technology_Roadmap_May2009.pdf [retrieved 10 March 2010].
3. Thill, C., Etches, J., Bond, I., Potter, K., and Weaver, P., “Morphing skins,” The Aeronautical Journal, Vol. 112, No. 1129, 2008, pp. 117-139.
4. Botez, R. M., Molaret, P. and Laurendeau, E., “Laminar flow control on a research wing project presentation covering a three year period,” 2007 Canadian Aeronautics and Space Institute Annual General Meeting [CD-ROM], Toronto, Ont., Canada, 25-26 April 2007.
5. Coutu, D., Brailovski, V., Terriault, P., “Optimized design of an active extrados structure for an experimental morphing laminar wing”, accepted for publication in Aerospace Science and Technology, published online January 2010. doi:10.1016/j.ast.2010.01.009

6. Coutu, D., Brailovski,V., Terriault, P., "Promising benefits of an active-extrados morphing laminar wing," *Journal of Aircraft*, published online, Vol. 46, No. 2, March–April 2009, pp. 730, 731. doi:10.2514/1.40657
7. Sainmont, C., Paraschivou, I., and Coutu, D., "Multidisciplinary approach for the optimization of a laminar airfoil equipped with a morphing upper surface," *NATO AVT-168 Symposium on "Morphing Vehicles"*, Evora, Portugal, 2009.
8. Popov, A. V., Grigorie, L. T., Botez, R. M., Mebarki, Y., Mamou, M., "Modeling and testing of a morphing wing in open-loop architecture," *Journal of Aircraft* (Submitted for publication 26 July 2009).
9. Georges, T., Brailovski, V., Morellon, E., Coutu, D., Terriault, P., "Design of shape memory alloy actuators for morphing laminar wing with flexible extrados," *Journal of Mechanical Design*, published online, Vol. 131, No. 9, 2009, 091006-pp 1-9. doi:10.1115/1.3160310
10. Georges, T., Brailovski, V., Morellon, E., Coutu, D., Terriault, P., "Wind-tunnel testing of shape memory alloys actuators as morphing wing driving systems," *ASME Conference on Smart Material, Adaptive Structures and Intelligent Systems [CD-ROM]*, Oxnard, USA, Sept. 2009.
11. Coutu, D., Brailovski, V., Terriault, P., Mamou, M., Laurendeau, E., "Real-Time Optimization of a Research Morphing Laminar Wing in a Wind Tunnel," *ASME Conference on Smart Material, Adaptive Structures and Intelligent Systems [CD-ROM]*, Oxnard, USA, Sept. 2009.
12. Coutu, D., Brailovski, V., Terriault, P., Mamou, M., Mebarki, Y., Laurendeau, É., "Real-Time Optimization of a Morphing Laminar Wing in a Wind Tunnel," *Journal of Intelligent Material Systems and Structures* (Submitted for publication April 2009).
13. CNRC-IRA., "2 m x 3 m Wind Tunnel: Technical Specifications," National Research Council Canada web site. [on line], <http://www.nrc-cnrc.gc.ca/eng/facilities/iar/2x3/technical.html>, [retrieved 10 may 2010].
14. Love, M. H., Zink, P. S., Stroud, R.L., Bye, D.R., Rizk, S., and White, D., "Demonstration of morphing technology through ground and wind tunnel tests," *Collection of Technical Papers - 48th AIAA/ASME/ASCE/AHS/ASC Structures, Structural Dynamics and Materials Conference*, Waikiki, HI, United States, 23-26 April 2007, pp. 337-348.
15. Andersen, G. R., Cowan, D. L., Piatak, D. J., "Aeroelastic modeling, analysis and testing of a morphing wing structure," *Collection of Technical Papers - 48th AIAA/ASME/ASCE/AHS/ASC Structures, Structural Dynamics and Materials Conference*, Waikiki, HI, United States, 23-26 April 2007, pp. 359-373.

16. Levinsky, E. S., and Palko, R. L., "Tests of an Improved, Computer-Controlled, Self-Optimizing, Variable-Geometry Wing," AIAA Paper 1982-599, 1982.
17. Boria, F., Stanford, B., and Ifju, P., "Evolutionary Optimization of a Morphing Wing with Wind-Tunnel Hardware in the Loop," AIAA Journal, Vol. 47, No. 2, February 2009, pp. 399-409.
18. Hetrick, J. A., Osborn, R. F., Kota, S., Flick, P. M., and Paul, D. B., "Flight testing of Mission Adaptive Compliant Wing," Collection of Technical Papers - 48th AIAA/ASME/ASCE/AHS/ASC Structures, Structural Dynamics and Materials Conference, Waikiki, HI, United States, pp. 92-109.
19. Strelec, J. K., Lagoudas, D. C., Khan, M. A, and Yen, J., "Design and implementation of a shape memory alloy actuated reconfigurable airfoil," Journal of Intelligent Material Systems and Structures, published online, Vol. 14, No. 4-5, April-May 2003, p. 257-273. doi:10.1177/1045389X03034687
20. Drela, M., "XFOIL: An analysis and design system for low Reynolds number airfoils," Lecture Notes in Engineering, Vol. 54, 1989, pp. 1-12.
21. Pagès, L., "Maximisation de la laminarité d'un profil d'aile par optimisation de la forme de l'extrados," Master Dissertation, Mechanical Dep., Ecole Polytechnique de Montreal, Montreal, Quebec, Canada, 2007.
22. Pagès, L., Trifu, O. and Paraschivoiu, I., "Optimized laminar flow control on an airfoil using the adaptable wall technique," 2007 Canadian Aeronautics and Space Institute Annual General Meeting [CD-ROM], Toronto, Ont., Canada, 25-26 April 2007.
23. Anderson, J. D., "Introduction to the fundamental principles and equations of viscous flow", Fundamentals of aerodynamics, 3rd ed., McGraw-Hill, New York, 2001, pp. 713-744.
24. Trifu, O., Pagès, L., Sainmont, C. and Paraschivoiu, I., "Optimization of the reference airfoil and completion of the CFD database," Task 1.6/7 report, Project CRDPJ 331810 - 05, Ecole Polytechnique de Montreal, Montreal, Quebec, Canada, Nov. 2007
25. Falk, A., Barthold, F. J., Stein, E., "A hierarchical design concept for shape optimization based on the interaction of CAGD and FEM," Structural and Multidisciplinary Optimization, Vol. 18, No. 1, Aug. 1999, p 12-23. doi:10.1007/BF01210687
26. MATLAB, "Genetic Algorithm and Direct Search Toolbox™," Ver. 7.6.0.324 (R2008a), The MathWorks, Inc, 1984-2008.

CHAPITRE 5

ARTICLE#3 « LIFT-TO-DRAG RATIO MORPHING LAMINAR WING CONTROL USING WIND-TUNNEL BALANCE AS HARDWARE-IN-THE-LOOP »

D. Coutu¹, V. Brailovski¹, P. Terriault¹, M. Mamou², Y. Mebarki², Éric Laurendeau³

¹École de technologie supérieure, 1100 rue Notre-Dame Ouest,
Montréal, Québec, Canada, H3C 1K3

²Conseil National de Recherche du Canada - Institut de Recherche en Aérospatiale,
Ottawa, Ontario, Canada, K1A 0R6

³Bombardier Aéronautique, 400 Ch. Côte Vertu Ouest, Dorval, QC, Canada, H4S 1Y9

Ce chapitre est la version révisée d'un article soumis au « Journal of Intelligent Material Systems and Structures ». Numéro de confirmation : JIM-10-046.

Résumé

L'article contenu dans ce chapitre a été soumis au « Journal of Intelligent Material Systems and Structures » et présente une seconde approche d'exploitation (contrôle en boucle fermée) permettant à l'aile expérimentale du projet CRIAQ 7.1 de soutirer le plein potentiel de son caractère adaptatif. Malgré l'exploitation satisfaisante de l'aile lors de sa deuxième entrée en soufflerie (février 2009), des points de mesures supplémentaires prélevées à la fin des essais ont mis en évidence les limitations de la modélisation numérique. Ce constat justifia la poursuite de travaux permettant à l'aile de manifester des performances aérodynamiques supérieures lors de sa troisième et dernière entrée en soufflerie (mai 2009).

Pour y parvenir, il a été choisi de résoudre le problème d'optimisation du profil de l'aile directement en soufflerie. Ainsi, la balance mesurant les forces aérodynamiques fut employée à titre de *hardware-in-the-loop* afin de fournir en temps réel la valeur du ratio L/D. Un algorithme d'optimisation a été conçu et calibré pour cette application à l'aide de surfaces de réponse décrivant le comportement expérimental de l'aile. Ces surfaces proviennent des points de mesure supplémentaires effectués à la fin de la seconde série d'essais en soufflerie. D'autre part, afin de réduire au minimum le temps de convergence, le modèle aéro-structural

développé précédemment (voir en chapitre 4) fut utilisé comme estimateur. En d'autres mots, l'approche en boucle ouverte est utilisée pour initier l'optimisation en temps réel afin de fournir une première modification de profil susceptible d'être optimale. Ensuite, en moins de 4 minutes supplémentaires, l'optimisation en temps réel convergea vers un profil offrant des performances aérodynamiques équivalentes ou supérieures. En comparaison au profil non activé, l'amélioration du ratio L/D de l'aile s'est située entre 10.6 et 15 %, soit environ 1.2% de plus que ce que le permet l'approche en boucle ouverte utilisant les prédictions du modèle aéro-structural. En parallèle, une caméra infrarouge a mesuré une extension moyenne du régime d'écoulement laminaire de 30 à 60 % de la corde d'aile. La robustesse du contrôleur a également été vérifiée dans la soufflerie. Finalement, une analyse critique des résultats obtenus a permis la formulation d'une série de recommandations en vue d'une application de la technologie de l'aile laminaire adaptative sur un avion réel.

Abstract

This paper presents the development and the results of the wind-tunnel performance optimization of a two-dimensional morphing laminar wing model under cruise flight flow conditions (Mach number ranging from 0.2 to 0.3 and the angle of attack, from -1° to 0.5°). To take advantage of the complete morphing wing potential, wind tunnel balance was used as a hardware-in-the-loop to give the instantaneous lift-to-drag ratio. A novel optimization algorithm was developed and calibrated using experimentally-obtained response surfaces of the morphing wing. To reduce the convergence time, an ANSYS-XFoil coupled aero-structural numerical model was used to give an initial morphed shape. During wind-tunnel testing, the closed loop control approach allowed a lift-to-drag ratio enhancement of between 10.6 and 15% as compared to the unactuated profile. Simultaneously, infrared camera measured an average laminar flow extension of from 30 to 60% the wing chord. The closed-loop morphing wing control strategy resulted in the similar or slightly superior morphing wing aerodynamic performance (lift-to-drag ratio) as compared to the open-loop control approach. Controller robustness was also verified in the wind tunnel. Finally, a critical analysis of the obtained results allowed formulation of recommendations for the use of the developed morphing wing technology in real aircraft applications.

Keywords: Wind tunnel, morphing laminar wing, optimization algorithm, hardware-in-the-loop, closed-loop controller.

5.1 Introduction

Interest in morphing wings to enhance aerodynamic performance has increased considerably over the last decade. Environmental preoccupations juxtaposed with oil cost increases both call for cleaner and more economical aircraft. In Europe, the Aeronautics Joint Technology Initiative “Clean Sky” program aims at reducing the noise and CO₂ emission related to aeronautic activities by half from 2000 to 2020 and was officially started in 2008. In the U.S., from 2009 to 2014, the Continuous Lower Energy, Emissions and Noise Technology or CLEEN program is being executed under the Federal Aviation Administration (FAA) with the help of NASA. One of the objectives of this program is to develop and demonstrate certifiable aircraft technology that reduces fuel burn by 33% compared to current technology. Morphing wings and laminar flow control are two technologies that present a high potential for environmentally friendly aircraft. Compared to conventional wings, which are optimized for a given set of flow conditions, morphing wings ideally allow maximizing the aerodynamic performance under any operating conditions. For the 787 aircraft which will soon enter in service, Boeing has planned to test and develop a Trailing Edge Variable Camber (TEVC) system to reduce cruise drag and realize significant fuel-burn saving (between 340 and 450 kg in weight) (Flightglobal, 2006), which seems to be the first practical application of a morphing wing on a commercial jet.

It is well known that a laminar boundary layer minimizes viscous drag better than a turbulent boundary layer. There are several active flow control techniques to preserve the laminar flow regime over wings, such as the suction of a small amount of the boundary layer (Braslow, 1999). The laminar flow regime can also be favored passively with the so-called Natural Laminar Flow (NLF) airfoil. In Europe, the Smart High Lift Devices for Next Generation Wings (SADE) project aims at developing morphing wing devices to preserve natural laminar flow, enhancing cruise flight performance and increasing lift. From 2008 to 2012,

after evaluating several concepts, a realistic full-scale section of a morphing wing with a smart leading edge and a smart single slotted flap is to be manufactured and wind-tunnel tested.

In Canada, the CRIAQ7.1 “Laminar flow improvement on an aeroelastic research wing” project was initiated four years ago to prove the feasibility of reducing aircraft fuel consumption and greenhouse gas emission through enhancement of the laminar flow regime over an active wing body (Botez et al., 2007). This feasibility study represents one of the initial steps in the morphing wing technology development for commercial aircraft (TRL=3). Subsequently, an experimental Morphing Laminar Wing (MLW) was designed (Georges et al. 2009; Coutu et al., 2010), manufactured and wind-tunnel tested (Coutu et al., 2009; Sainmont et al., 2009; Popov et al., 2009). Simplifications were abstracted to facilitate MLW aerodynamic analysis from the numerical and experimental viewpoints. Although the cruise flight regime of commercial aircraft is transonic, the morphing wing prototype developed in this program was tested for two-dimensional laminar flow enhancement at the subsonic wind tunnel of the Institute for Aerospace Research at the National Research Council Canada (IAR-NRC). The inner and outer views of the experimental wing installed in the wind tunnel are presented in Figure 5.1 along with the equipment used to measure the lift-to-drag ratio (balance) and the laminar to turbulent flow transition of the MLW (infrared camera and Kulite pressure transducers). Moreover, a wake rake was used to measure the profile drag coefficient and to validate the two-dimensional numerical model of the MLW (Coutu et al., 2009).

This paper presents a hardware-in-the-loop optimization of the lift-to-drag ratio of the MLW in the wind-tunnel environment. Only two angles of attack corresponding to cruise flight conditions were considered ($\alpha = -1$ and $\alpha = 0.5^\circ$). However, from the results obtained, it was possible to demonstrate the capacity of the proposed closed-loop control approach for real-time morphing control and to forecast the next steps for the project.

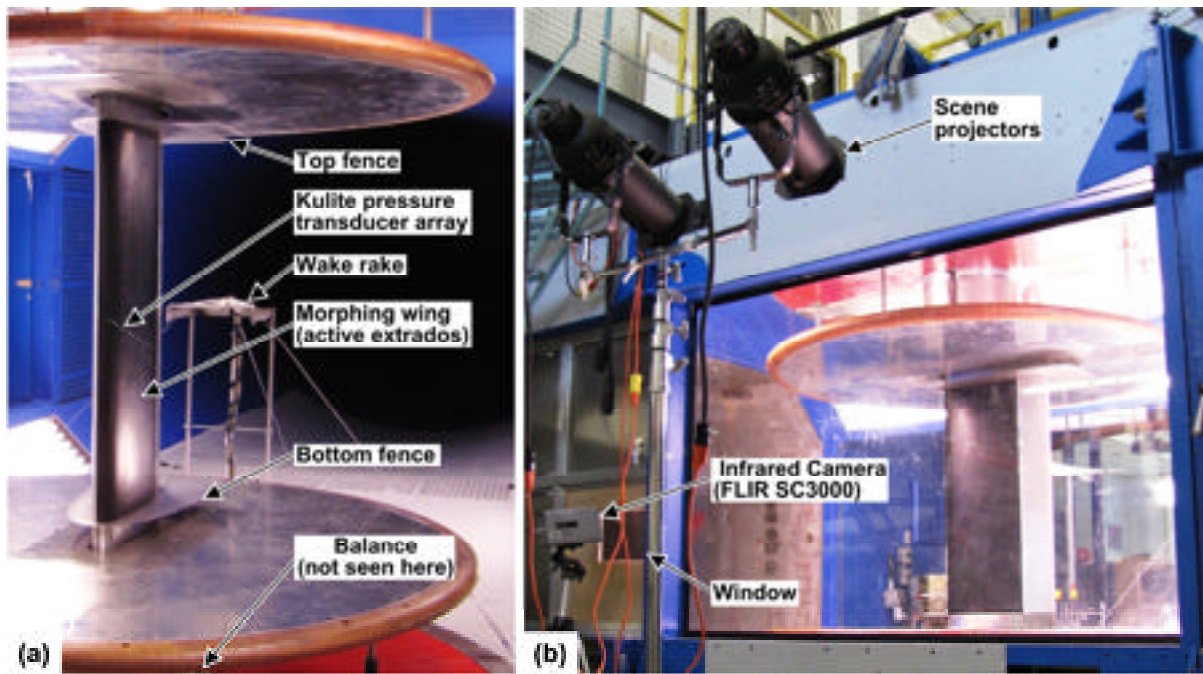


Figure 5.1 MLW setup in the 2 x 3 m IAR-NRC wind tunnel:
(a) inside and (b) outside view.

5.1.1 Morphing wing shape optimization

Although numerous morphing wing-related R&D activities are reported in the literature, few have crossed the experimental validation step, either wind tunnel or in-flight testing. Managing the shape of a morphing wing in respect to flow conditions raises additional technical challenges to overcome, such as the wing shape optimization and the morphing wing control. From the literature, two common approaches are used to determine the best morphed wing shape prior to its exploitation: (1) Numerical modeling and (2) Experimentation.

-Numerical modeling

Strelc et al. (2003) used a genetic optimization algorithm to interrogate a numerical model of their “Shape Memory Alloy Actuated Reconfigurable Airfoil” to optimize its shape parameters. For a 3° angle of attack under subsonic flow conditions, the experimental prototype rapidly reached a satisfactory morphing response. Even though the measured lift

increase was approximately half of that predicted numerically, the experimental data followed the expected trend, showing the capacity of the SMA-actuated reconfigurable wing concept. The same approach was successfully tested by the authors of this work in the framework of the CRIAQ7.1 “Laminar flow improvement on an aeroelastic research wing” project (Coutu et al., 2009a). Nevertheless, optimal morphed shape uncertainty is a commonly encountered issue for those who rely upon numerical modeling predictions to exploit this technology in real flow stream conditions.

-Experimentation

To identify the best flap deflections for several flight conditions, Hetrick et al. (2007) used the Design-Of-Experiment (DOE) approach, which allows characterization of the experimental morphing behavior of the Mission Adaptive Compliant Wing (MACW). Despite the extensive amount of time needed to pass through the test matrix (27 hours of flight testing), the results were convincing enough to conclude that the MACW technology has the potential to increase aircraft endurance by 15% or more. The DOE results were also useful as a means to validate the two-dimensional CFD analysis of the MACW.

5.1.2 Morphing wing control

The control of the morphing wing in a wind tunnel or in flight can be performed using either open- or closed-loop architectures. When the aerodynamic conditions (speed and angle of attack) of the mission are known, an open-loop controller can convey to the wing a shape contained in the wing-profile database, built prior to the mission, using either numerical or experimental optimization techniques. On the other hand, a closed-loop controller offers additional shape optimization capabilities with the use of hardware-in-the-loop that gives instantaneous feedback of the wing’s aerodynamic performance data. Some examples of this controlling technique are presented next, along with its advantages and drawbacks.

In 1977-1979, Levinsky et al. (1982) tested a Self-Optimizing Flexible Technology (SOFT) wing model in a transonic wind tunnel using closed-loop control architecture. The adjustment

of the wing shape under several flow conditions was carried out automatically via an optimizer (gradient projection optimization) that directly commanded the SOFT-wing in the wind tunnel. At each iteration, aerodynamic coefficients were obtained from the wind-tunnel balance used as a hardware-in-the-loop. This led to a significant experimental drag reduction ($\Delta C_D = -0.0026$) for constant lift and moment conditions ($C_L = 0.25$; $C_M = 0$), even though some structural integrity problems were encountered during testing.

To reduce the drag of a transport aircraft in-flight by adaptation of the configuration of the control surfaces, Glenn B. Gilyard et al. (1999) optimized flap deflections with an algorithm that uses the flight data system as a hardware-in-the-loop to evaluate the drag change. The optimization of the symmetric outboard aileron position reduced the drag of the L-1011 test bed aircraft by 2–3 drag counts (approximately 1 percent). Jacobsen et al. (2009) also used a hardware-in-the-loop approach to optimize 16 flap deflections of a wing in order to minimize the drag under a wide range of constant lift conditions in wind tunnel testing.

In the field of micro air vehicles (MAVs), Boria et al. (2009) presented a genetic optimization algorithm using a hardware-in-the-loop approach to maximize the lift and the efficiency of their experimental morphing wing prototype, tested in a wind tunnel. The objective function of each iterative morphed shape was measured using a wind-tunnel strain-gauge sting balance, which allowed prototype optimization. However, aerodynamic/electrical hysteresis encountered at low Reynolds numbers caused problems with the objective function evaluation. Consequently, the time needed for the algorithm convergence was greater than that required by the DOE optimization procedure.

In respect to the MLW prototype presented in this work, Popov et al. (2009) applied a closed-loop control strategy using a Kulite pressure-transducers array located on the wing upper surface as hardware-in-the-loop. However, their use of a mixed optimization method based on conventional algorithms required significant time for convergence, and the limited number of pressure transducers resulted in a discrete representation of the objective function, thus impeding adequate functioning of the developed controller.

5.1.3 Proposed control approach for the MLW performance optimization

This work is focused on the development and testing of an efficient and robust controller intended to fully exploit the MLW's potential in light of the CRIAQ7.1 project objectives. The originality of the controller presented in Figure 5.2 is that it combines the advantages of the different morphing control strategies. The experimental morphing shape optimization is conducted using the wind-tunnel balance (A) or the infrared camera measurement (B) as a **hardware-in-the-loop**. Although the use of such devices in real flight is not realistic, the last-generation inertial navigation systems and airdata systems provide similar feedback opportunities. For example, Glenn B. Gilyard et al. (1999) used a flight data system and a steady-state engine model as a function of the engine pressure ratio measurement to evaluate the performance improvement of the wing to a drag count unit ($\Delta D=0.0001$).

To account for the particularity of the customized SMA actuation system, an original optimization algorithm was especially designed for the application. This algorithm was validated using partial results of the **design-of-experiment** approach with a reduced test matrix to minimize wind-tunnel time occupancy. Finally, the proposed control approach relies on the **numerical model** of the MLW to give a first estimation of the initial morphed shape (contained in the optimized wing shape database), thus accelerating the morphing shape optimization convergence.

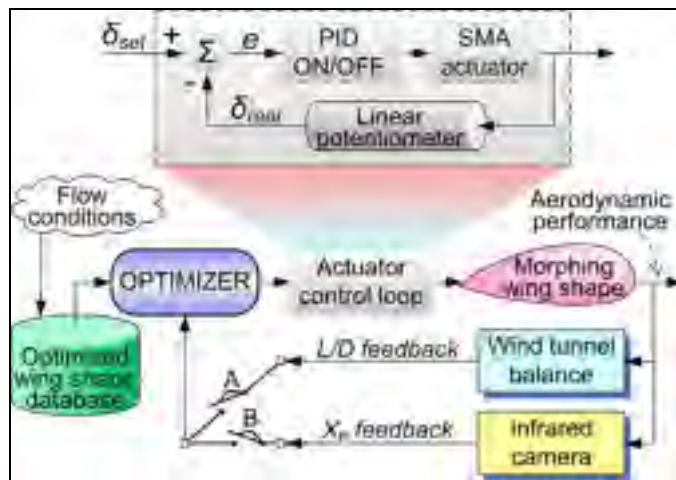


Figure 5.2 Closed-loop controller for morphing shape optimization of the MLW in a wind tunnel.

The first section of this paper gives a general description of the MLW and of the controller, and the results are presented and discussed in the last sections. The numerical model of the aero-structural interaction is first presented and compared with the wind-tunnel DOE results (response surfaces). Thereafter, the optimization algorithm is presented and its parameters are calibrated. The MLW controller setup in the wind tunnel is then discussed along with a description of the hardware used. Next, after presentation of the wind-tunnel results, the behavior of the MLW controller is analyzed in terms of the search pattern's shape, feedback signals and convergence times. For this purpose, the expected behavior of the MLW controller is simulated using the DOE response surfaces and compared with the experiment. Furthermore, open- and closed-loop shape optimization strategies are compared in terms of the controller performance and robustness. The consequent laminar flow improvement resulting from the maximization of the L/D ratio is also evaluated using an infrared (IR) camera to measure the laminar flow extension. Using an inverse approach, the measurement of the laminar flow extension is considered as an alternative feedback signal to verify the consequent L/D ratio improvement. These exercises allow the wind-tunnel balance and the IR camera to be compared as two different hardware-in-the-loop setups. Finally, recommendations envisioning a real aircraft application of the MLW concept are presented on the basis of the results obtained in this work.

5.2 Presentation of the MLW

5.2.1 The MLW concept

The MLW active structure consists of a flexible extrados (skin) and actuators connected together by a transmission system, subjected to variable flow conditions (aerodynamic loads). As presented in Figure 5.3, modification of the airfoil profile occurs when Shape Memory Alloy (SMA) actuators located inside the wing box apply independently-controlled displacements (δ_1 and δ_2) of between 0 and 8 mm (1.6% c) to the flexible extrados (for more detail, see Georges et al., 2009). A calibrated PID controller ensures the stability of the SMA actuator's response with a ± 0.02 mm precision using linear potentiometer (LP804-02 series, ± 0.15 mm accuracy) feedback on the full 8 mm stroke (see Figure 5.3). The overall stiffness and integrity of the experimental wing is provided by the rigid intrados. A numerical finite-element structure model of the flexible extrados was built and experimentally validated for 48 active structure configurations corresponding to six flexible extrados thicknesses (3- to 8-ply composite laminate) and eight actuator arrangements (0 to 7 equally span-wise distributed actuator lines). Using the multi-objective optimization approach, the “4-ply & 2 actuators” configuration was retained, as it maximized the aerodynamic performance of the MLW while minimizing the mechanical work required for morphing (Coutu et al., 2010).

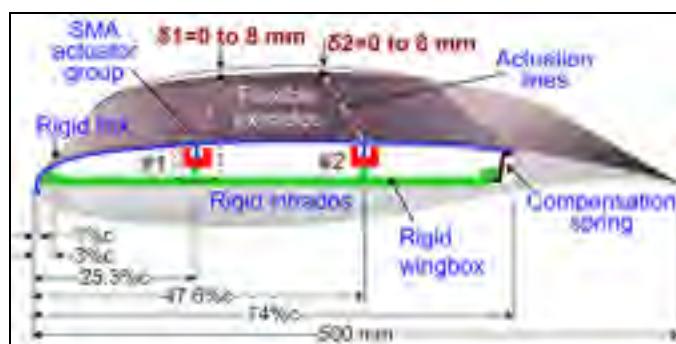


Figure 5.3 MLW wing concept using an active extrados structure.
Adapted from Coutu et al. (2009a).

5.2.2 MLW aerodynamic performance

The aerodynamic performance of a conventional wing profile can be expressed by several parameters, such as maximum lift coefficient, zero-lift drag coefficient, polar curve, stalling angle of attack, laminar/turbulent flow transition and maximum lift-to-drag ratio. All of these state-of-the-art wing performance characteristics can also be applied to a morphing wing operating under given flow conditions. Under cruise flight conditions, the CRIAQ7.1 project aims to reduce aircraft fuel consumption, which is directly related to the engine thrust, through laminar flow improvement over the MLW. Using steady flight assumptions, where the lift (L) and the drag (D) forces are equal to the aircraft weight (W) and engine thrust (T), respectively, the objective implies maximization of the MLW lift-to-drag ratio (L/D) as presented by equation (1).

$$T_{\min} = W/(L/D)_{\max} \quad (1)$$

To maintain a given flight altitude during cruise flight, an aircraft using a morphing wing, as with a conventional aircraft, has to adjust the angle of attack continuously to compensate for weight reduction caused by fuel consumption. Continuous maximization of the lift-to-drag ratio of the wing through its morphing will undoubtedly lead to the best possible fuel economy over the entire cruise flight regime. Overall aircraft performance in terms of cruise speed, range and endurance will thus be enhanced. In this experimental context, the choice of a force ratio (L/D is an example) is advantageous because it is less sensitive to miscellaneous flow perturbations.

5.3 MLW controller development for shape optimization

5.3.1 The numerical optimized wing shape database

The aero-structural model of the MLW presented in Figure 5.4 has been used to establish the optimized MLW shape database in respect to the wind-tunnel flow conditions of interest. This database contains the initial actuator displacements which are commanded using open-

loop architecture shown in Figure 5.2 (with open connectors A and B). More details on the development and the validation of the coupled model are presented in Coutu et al. (2009).

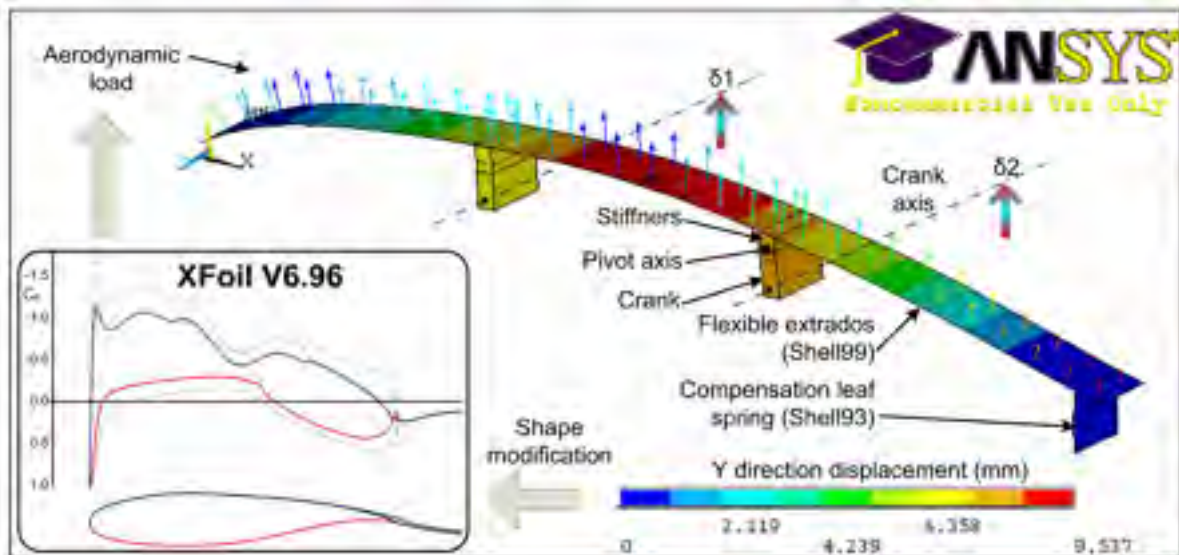


Figure 5.4 Aero-structural coupled model of the MLW active structure.

5.3.2 Design-of-Experiment (DOE)

In this work, the DOE approach was used to build the MLW response surfaces (9 flow conditions) necessary to calibrate the optimization algorithm and to validate the aero-structural model of the MLW in respect to its aerodynamic response. To build these response surfaces, the actuators' strokes were varied from 0 to 8 mm with 2 mm increments (5^2 points), and the aerodynamic response of the MLW was measured: a task requiring at least 30 min for each set of flow conditions. Figure 5.5a,b shows the contour plots of the lift-to-drag (L/D) response surfaces using actuator 1 stroke as the abscissa and actuator 2 stroke as the ordinate for Mach=0.2, Alpha=-1° and Mach=0.3, Alpha=2° cases. (These flow conditions represent minimum and maximum upper surface aerodynamic loads.) The data were smoothed using the MATLAB Spline Toolbox function “spap2” to allow cubic-order interpolation between the points. On one hand, the comparisons of the DOE results with the aero-structural model prediction (Figure 5.5c,d) were found to be generally consistent. On

the other hand, discrepancies observed between the localization of the experimental and numerical optimum zones confirm the inherent limitations of the numerical model, which is incapable of accounting for miscellaneous three-dimensional flow effects that influence the MLW performances during testing. These observations justify the need to optimize the MLW's aerodynamic performance in a closed-loop control approach. It can be observed from the DOE results that, for the angle of attack -1° , the maximum L/D ratio is contained within the actuation envelope (Figure 5.5a), whereas it tends to extend beyond the envelope for the 2° attack angle (Figure 5.5b). Given that the maximum actuator displacement of 8 mm cannot be exceeded because of the MLW design restrictions, the maximum positive angle of attack in the subsequent study will be limited to 0.5° .

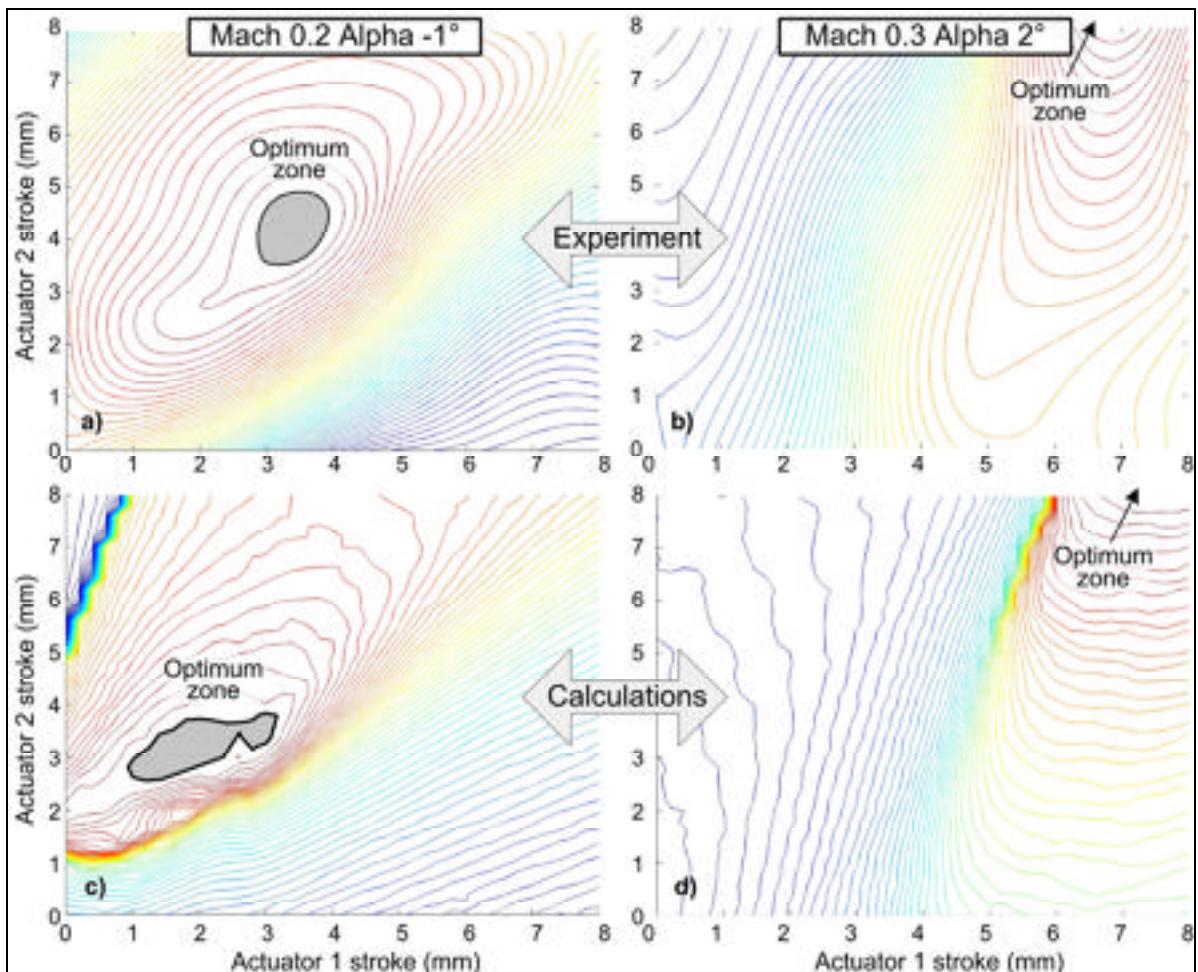


Figure 5.5 Lift-to-drag ratio response surfaces for $\text{Mach}=0.2$, $\text{Alpha}=-1^\circ$ (a, c) and $\text{Mach}=0.3$, $\text{Alpha}=2^\circ$ (b, d); (a, b) DOE, (c, d) calculations.

5.3.3 Pattern Search Algorithm

When designing an optimization algorithm, efforts must be made to select a method which will minimize convergence time without compromising algorithm precision and robustness. From the experimental response surface analysis (Figure 5.5a,b), there is no risk of being trapped in local maxima. Thus, a simple proprietary pattern search is devised in this study. The algorithm uses two integrated SMA actuator controllers to generate strokes within a commanded tolerance of ± 0.1 mm. The actuation speed of SMA actuators was taken into consideration in the design of the optimizer, and efforts were made to keep the pattern search trajectory as short as possible, while recording a maximum amount of data. Figure 5.6a presents the algorithm flowchart (an example of the algorithm realization is given in Figure 5.6b for Mach=0.2 and Alpha=0.5°):

- A. For a given set of flow conditions, the algorithm initially interrogates the optimized wing shape database that contains the numerically predicted strokes which give the best L/D ratio. This procedure, which represents an open-loop control approach, produces commands initiating the SMA actuators' movement towards the "First guess" point: $\delta = \{4.8; 8\}$ mm (see Figure 5.6b, $L/D = 11.73$). The trajectory between $\delta = \{0; 0\}$ and $\delta = \{4.8; 8\}$ mm is not a straight line because both SMA actuators' speeds are similar, whereas the commanded stroke displacements differ. From the aerodynamic behavior perspective, the "**unactuated**" wing profile morphs to the "**open-loop**" optimized shape.
- B. In the second step, the closed-loop control begins with the analysis of the recorded feedback revealing the point corresponding to the highest L/D ratio on the previous trajectory: "First best point", $\delta = \{4.8; 6.28\}$ mm (see Figure 5.6b, $L/D = 11.80$). A polygonal searching pattern surrounding the identified point is then delimited to verify the presence of any better L/D ratios in the vicinity. After completing the search on the polygonal pattern, the point presenting the highest objective function value is considered as the new design point, $\delta = \{3.88; 6.06\}$ mm (see "Second best point", Figure 5.6b, $L/D = 11.83$).

- C. In the subsequent iterations, the center point is translated to a new point, located farther than the current best point in the same direction (overshoot) to favor the exploration of a new design space (see the second polygon center, Figure 5.6b). With this objective, a translation factor larger than 1 is used. Thereafter, the same search procedure is repeated until no best value can be found on the new polygon. In this case, a polygon with a radius reduced by using a given contraction factor is drawn around the last best point. To avoid pattern redundancy and calculation instability, if the distance between the new and the old design points is less than the current radius, the radius will continue to decrease.
- D. When the polygon radius falls below an established minimum value, its value becomes zero and the algorithm keeps the last best point as its final point, $\delta = \{2.78; 4.46\}$ mm (see “Final point”, Figure 5.6b, $L/D = 11.94$), resulting in the “closed-loop” optimized profile.

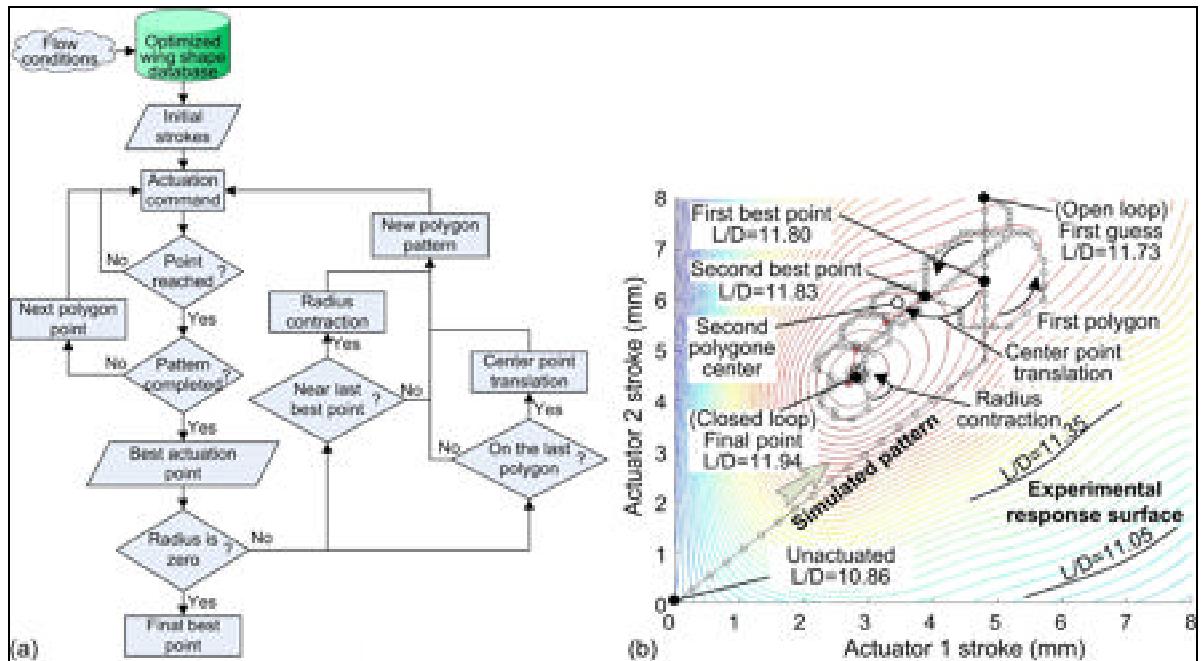


**Figure 5.6 Pattern search actuator strokes' optimization algorithm:
a) flowchart and b) simulation example for Mach=0.2 and Alpha=0.5°.**

5.3.4 Pattern Search Implementation and Calibration

The optimization algorithm is coded in Matlab software with the intention that it can be called on by the MLW closed-loop controller. The adjustment of the parameters was performed with several algorithm simulations until the convergence time was sufficiently minimized. For this task, the MLW behavior was simulated with cubic interpolation over the previously presented response surfaces obtained from the DOE procedure (Figure 5.5). Although the numerical model would have led to good results in this case, the use of experimental data to calibrate the MLW optimizer is still favored. Also, for the optimization algorithm development in the proposed control approach, at least a partial DOE was considered mandatory to ensure the validity of the numerical model to be used as an estimator.

The SMA actuation responses were simulated with two constant speeds of 0.18 and 0.08 mm/s to calculate the respective actuator stroke increase (heating) and decrease (cooling) at each time step. These speeds were defined from previous wind-tunnel runs where SMA actuators' full deployment (heating) and return (cooling) periods were 45 and 100 seconds, respectively (Georges et al., 2009). These simulations supposed a feedback sampling rate of 1Hz (time step = 1s) from what it is expected in a wind tunnel. Table 5.1 presents the retained parameters that minimized the predicted convergence time of the pattern search algorithm. In the example of Figure 5.6b, convergence time for Mach = 0.2 and Alpha = 0.5° was calculated as 3min 45s.

Table 5.1
Algorithm parameters

Initial radius (mm)	1	Stroke tolerance (mm)	0.1
Minimum radius (mm)	0.15	Translation factor	1.5
Polygon side number	8	Contraction factor	0.5

5.3.5 MLW Controller Wind Tunnel Setup with Hardware-in-the-Loop

The MLW shape optimization was performed in the IAR-NRCs $2 \times 3\text{m}$ wind tunnel with the prototype mounted vertically on the wind tunnel balance, as presented in Figure 5.1. The main balance has $\pm 0.1\%$ to $\pm 0.05\%$ full-scale measurement accuracy. This closed-circuit wind tunnel operates under atmospheric conditions with speed uniformity of $+/-0.07\%$ and 0.14% of turbulence (CNRC-IRA, 2010). Consequently, when analyzing the morphing airfoil with the aerodynamic solver XFOIL, the critical amplification factor N_{crit} was set to 7 according to the work of L. Pagès (2007). To favor two-dimensional flow over the wing, two aerodynamic fences were installed on the prototype ends. The rough balance loads used for the shape optimization were not corrected for the solid and the wake blockage, nor for the streamline curvature in the wind tunnel. A computer was used to implement the closed-loop controller built in the LabVIEW 8.6 graphical programming environment with the algorithm called through a Matlab script node. When the wind tunnel flow conditions were stabilized, the operator entered them into the controller before activating the optimizer. Then, the optimization of the MLW was performed automatically until convergence of the algorithm in a single wind tunnel run.

The viscous and the pressure forces acting over the wing and the fences' resistance in the flow stream constitute the rough aerodynamic forces (lift and drag) measured to the balance. The load signals were sampled at 5Hz by the NRC data acquisition system and received at 2Hz by the MLW controller, using a serial cable. A moving average filter using the three new values reduced the feedback signal noise from the balance, leading the algorithm to loop at 0.67Hz. Higher speed rates were proscribed to avoid computational instability. Finally, a tare was performed before the wind blew to ensure that only the aerodynamic forces would be read.

As an additional technique, a thermography IR camera targeting the active wing extrados to identify the laminar/turbulent flow transition location was monitored using an independent Matlab program. Because of the programming time constraints, human judgment was needed

to interpret the images and the transition results were entered manually into the controller interface to be used as an alternative hardware-in-the-loop. This non-automated task evidently limited the transition point location sampling rate. To carry out a proper IR investigation, pauses were introduced into the control algorithm, allowing the time for manual entry.

5.4 Wind-tunnel optimization results

To supply sufficient data for post-wind tunnel analysis, the MLW shape optimization controller was tested under four aerodynamic flow conditions labeled from -A- to -D- in Table 5.2. This table contains the measured aerodynamic performance of three wing profiles: 1) unactuated; 2) open-loop optimized using numerical model prediction; and 3) closed-loop optimized.

Table 5.2
Wind-tunnel MLW shape optimization results

Flow condition	Profile	δ_1 (mm)	δ_2 (mm)	L/D	$\Delta(L/D)$	Xtr (x/c)	ΔXtr	Convergence time	
								Wind tunnel	Simulated
-A- Mach 0.275 Alpha 0.5°	Unactuated	0.00	0.00	11.08	---	26%	---	---	---
	Open	5.21	7.85	12.19	10.0%	56%	30%	0min 35s	0min 44s
	Closed	4.87	7.09	12.26	10.6%	57%	31%	4min 18s	2min 27s
-B- Mach 0.2 Alpha 0.5°	Unactuated	0.00	0.00	10.70	---	30%	---	---	---
	Open	4.80	7.83	11.76	10.0%	62%	32%	0min 20s	0min 44s
	Closed	4.74	6.46	11.97	11.9%	61%	31%	3min 52s	3min 45s
	Closed IR	3.88	6.04	11.78	10.1%	63%	33%	7min 37s	---
-C- Mach 0.275 Alpha -1°	Unactuated	0.00	0.00	7.84	---	36%	---	---	---
	Open	2.24	4.16	8.92	13.7%	65%	29%	0min 17s	0min 23s
	Closed	2.94	3.61	8.94	15.0%	66%	30%	4min 13s	2min 7s
-D- Mach 0.3 Alpha 0.5°	Unactuated	0.00	0.00	10.77	---	26%	---	---	---
	Open	5.40	7.84	11.90	10.4%	57%	31%	0min 20s	0min 44s
	Closed	5.40	7.79	11.98	11.2%	57%	31%	4min 13s	2min 16s
	Closed IR	4.58	7.27	11.91	10.6%	59%	33%	14 min	---

5.5 Discussion

The comparison between the open- and closed-loop approaches is performed based on performance and robustness, with a consideration for the laminar flow regime improvement. For investigation purposes, two optimization cases with transition point location (IR-measured x_{tr}) as a feedback signal (Closed IR) instead of the balance L/D ratio are presented and discussed. Before going deep into discussion, the MLW controller's behavior in the wind tunnel is examined first.

5.6 MLW controller wind-tunnel behavior

Search pattern

To verify the behavior of the MLW controller in the wind tunnel, the search pattern for the aerodynamic flow conditions -A- (Mach=0.275 and Alpha=0.5°) is presented in Figure 5.7a with three profiles of interest: 1) unactuated, $\delta = \{0; 0\}$; 2) open-loop optimized, $\delta = \{5.21; 7.85\}$ mm; and 3) closed-loop optimized, $\delta = \{4.87; 7.09\}$ mm. The evolution of the wind-tunnel balance forces, including the L/D feedback signal, is presented in Figure 5.7b along with the actuators' stroke variations. Similarly, prior-to-test simulation results corresponding to this flow case are presented in Figure 5.7c,d. The simulated polygonal shape of the pattern associated with the SMA actuators' heating and cooling phases is experimentally observed. When analyzing the evolution of the feedback forces in relation to variations of the actuators' strokes, the feedback variations are larger in both cases during the first seconds following the start of morphing, when the wing profile is modified from the unactuated shape to the open-loop optimized shape. Also, for both experimental and calculated cases, when the "First guess point" is reached, L/D signal fluctuations start decreasing until the convergence is reached. An adequate agreement of both search patterns (experimentation and simulation) gives credence to the proposed control approach performance. All of the flow cases tested reached convergence but, in some cases, with patterns presenting greater divergences from those simulated from the response surface. To explain these discrepancies, analysis of the feedback signal stability was considered mandatory.

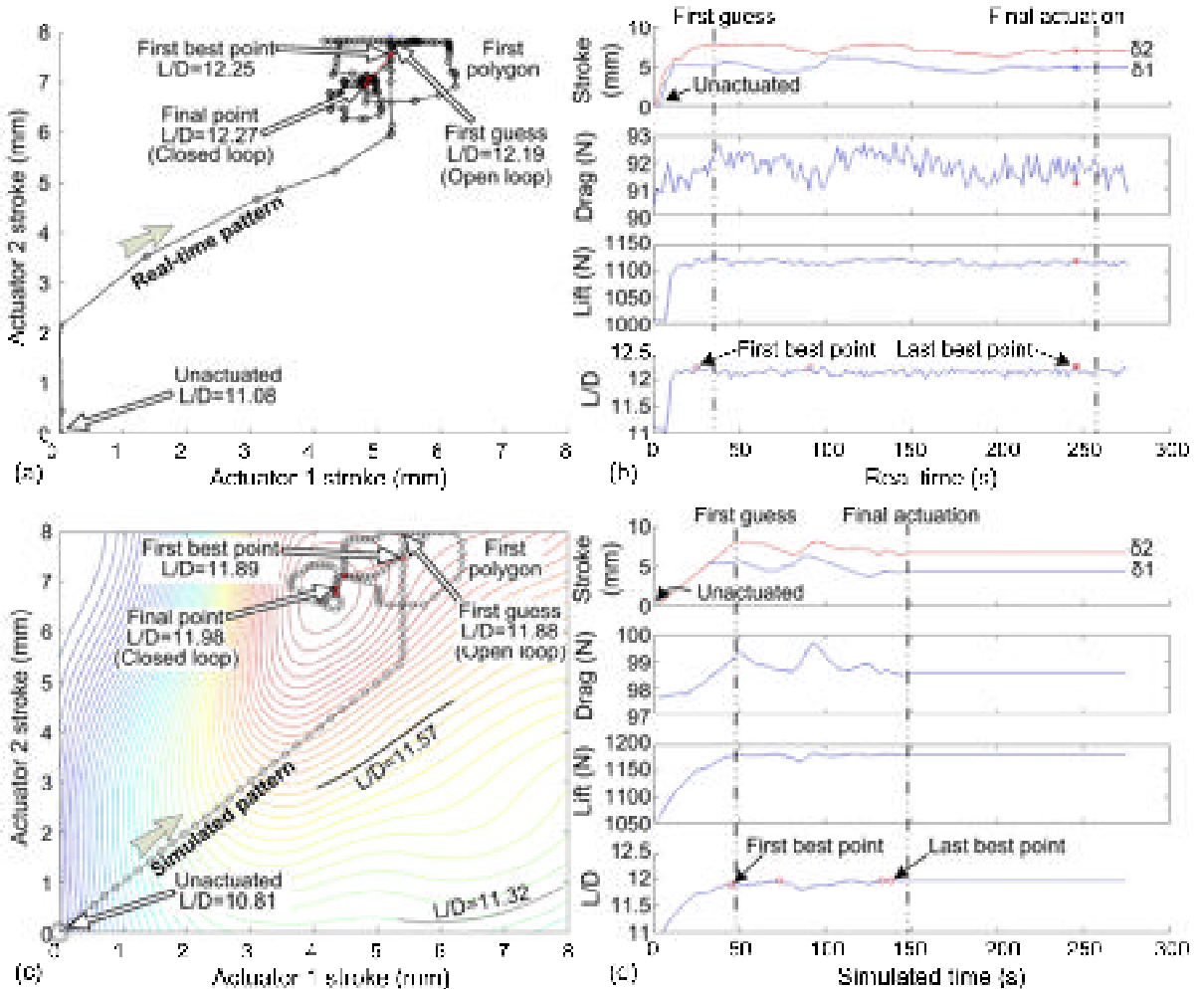


Figure 5.7 Stroke optimization for Mach=0.275 and Alpha= 0.5°:
(a,c) resulting pattern search and (b,d) performance change upon actuation;
(a,b) experimental results and (c,d) numerical prediction using response surfaces.

Feedback signal

Although a moving-average filter was used, significant wind tunnel balance noise can be observed when comparing the experimental curves (Figure 9b) to the simulated ones (Figure 9d). Given that the sampling rate available in the wind tunnel was too low to adequately process the feedback signal, the feedback noise hampered the closed-loop control capabilities because the signal peaks can force the optimization algorithm to stop prematurely. Over 60 seconds of steady flow conditions (Mach0.3 and angle of attack 0.5), the lift-to-drag ratio presented a maximum variation of $\pm 0.76\% L/D$ in respect to the mean value of 10.77. The

signal noise comes from the balance precision, variations in flow velocity, test section vibration and electromagnetic interference.

In fact, contrary to the DOE procedure for which the balance forces can be averaged over a realistic period of time, the closed-loop control approach is not well-suited for noise removal. Hopefully, this undesirable phenomenon may have negligible impacts on the MLW controller performance, as the noise level remains constant over the duration of the entire wind-tunnel test. Consequently, the maximum L/D ratio recorded is subject to be higher (12.27 instead of 11.98, Figure 5.7) as compared to previous DOE tests. The other sources of discrepancy between the simulations and the experiments are evoked here in order of importance:

- The values used to build the response surfaces of the lift-to-drag ratio at Mach 0.275 and Alpha 0.5° were linearly interpolated between the Mach 0.25 ($L/D = [10.55 \text{ to } 11.97]$) and Mach 0.30 ($L/D = [10.81 \text{ to } 12.05]$) experimental response surfaces, which could cause a maximum error of 1.5% ($\pm 0.15 L/D$).
- Between the wind-tunnel tests used to build response surfaces and those intended to test the proposed closed-loop control strategy, the prototype was disassembled and re-assembled for maintenance purposes. These manipulations included flexible and rigid structures of the MLW as well as of the actuator transmission mechanisms. Before and after the prototype's disassembly and reassembly, a maximum 0.1 mm shift in the zero actuator's position was experimentally measured by a profilometer. From the experimental response surface analysis, such a shift would have resulted in a maximum 0.5% (0.05 L/D) variation in terms of the MLW's aerodynamic response.
- Minor dissimilarities in the wind-tunnel setups from one prototype entry to another could have had an impact on the results, but this impact cannot be quantified. For example, when turning the rotating table, the weight and displacement of the connective wires could have affected the balance load despite a tare procedure that was routinely performed for each angle of attack. On the other hand, even though the dynamic pressure in the wind tunnel may also present slight differences from one test to another for the

same targeted Mach number, the L/D ratio, being insensible to small dynamic pressure variations, should not have been affected.

Response time

Finally, the last reported discrepancies between experiment and simulation are in relation to the response time. In one example, even though the trajectories of both search patterns appear similar, the closed-loop approach required 4 min 18 s to converge experimentally, almost double that of the predicted 2 min 27 s (see Table 5.2). In another (contrary) example, only 34s were necessary to reach the first experimental guess point (open-loop) as compared to the 44s predicted from simulations. These differences can be explained by the SMA actuators' response. On one hand, the experimental SMA heating rate was indeed voluntarily increased to reduce wind-tunnel time occupancy (causing overshoot in some cases). On the other hand, the simulated SMA behavior neglected the thermomechanical hysteresis that induces an inactive time lag when changing the stroke direction of the actuators. In sum, better modeling of the SMA behavior would result in better calibration of the algorithm parameters. Although these discrepancies led to a longer convergence time than was expected, the proposed optimization method is more than seven times faster than the response surface evaluation used by the DOE approach (which takes about 30 min). Moreover, from the flow cases tested, the flow case -B- ($Mach=0.2$ and $\text{Alpha}=0.5^\circ$) holds the speed record with a first best point reached after only 10s, while the pattern search reached the first guess after 20s (see Table 5.2). Then, along the subsequent polygon search, no better actuation configuration was found, resulting in the shortest convergence time of 3min 52s, eight times faster than a response surface evaluation.

Note that in the framework of our common CRIAQ7.1 project, A. V. Popov et al. (2009) used Kulite pressure transducers to obtain a feedback on the laminar flow extension over upper wing surfaces. This purely hardware-in-the-loop approach, using a mixed climbing-meta-heuristic optimization algorithm, required about 18 minutes for the MLW to converge to an optimized shape, which was intended to maximize the laminar flow over the wing. In comparison, the control approach proposed in this work appears to be more than four times

faster, demonstrating the advantage of the specially-devised optimization algorithm, which also relies on numerical model predictions.

5.6.1 Open-loop versus closed-loop

Lift-to-drag ratio improvement

To compare the open-loop (“first guess” morphed profile based on numerical modeling) and closed-loop (morphed profile after convergence) performances, Table 5.2 shows that the actuator strokes resulting from the closed-loop control are very close to those predicted by the coupled aero-structural open-loop numerical model. For actuator 1, the difference between closed- and open-loop strokes is encompassed between -0.7 and 0.34 mm, which corresponds to -8.75 to 4.25% of the full stroke. For actuator 2, this difference is 0.05 to 1.37 mm (0.61 to 17.13% of the full stroke). Furthermore, for the flow case -D-, the numerically and closed-loop optimized actuation strokes are almost similar. These observations demonstrate, more thoroughly than previous works (Coutu et al., 2009a), the excellent prediction capabilities of the numerical model.

Despite these small differences in actuator strokes, the closed-loop approach demonstrates its slight advantage in respect to the open-loop approach as far as the L/D ratio increase being significant over the feedback signal noise, as in flow case -B-. In evaluating all the cases presented in Table 5.2, the relative L/D ratio increase (using the unactuated profile value as reference) varies from 10.6 to 15% for the closed-loop approach compared to 10.0 to 13.7% for the open-loop approach. This apparently modest L/D ratio improvement obtained with a closed-loop controller may represent substantial fuel economy for an airplane on a long cruise-flight mission. On the other hand, since the closed-loop control takes more time than the open-loop, and when the actuators’ energy consumption is a factor in the energy balance, open-loop control may be more beneficial for short-range missions. Thus, the overall MLW efficiency is dependent on the control approach used and should be studied more extensively, including the evaluation of SMA actuators’ energy consumption.

MLW controller robustness

The comparison between the open and closed-loop approaches can also be performed in respect to another important criterion in a control system, robustness. Generally, robustness implies the capability of a system to respond accurately despite any (possible) perturbation. An experimental investigation of the MLW controller's robustness was performed with the combined perturbation of the flow conditions and the feedback signal. The perturbed flow condition consisted in the application of Mach 0.275 with an off-design angle of attack of -2°. Under these flow conditions, noise dominated the balance response even more because the lift and drag forces were lower. Given that no numerically optimized strokes (open-loop commands) existed for this particular flow case, a set of initial strokes corresponding to the closest flow condition (Mach=0.275, Alpha=-1°) was utilized instead. The resulting pattern search is presented in Figure 5.8a, and it illustrates the ability of the closed-loop control algorithm to converge near the “approximate first guess” point even under unanticipated flow conditions. On the other hand, when the test was repeated for the same flow conditions, but with another initial point, $\delta = \{2.49; 3.84\}$ mm, the resulting search pattern ended with a different point (Figure 5.8b). In this case, for the repeated experiments, the maximum L/D ratios were 5.45 for the first experiment vs 5.43 for the second experiment, which corresponds to a 0.56% difference in *L/D* value. This discrepancy confirms the limited robustness of the closed-loop control approach in the presence of significant feedback signal perturbations.

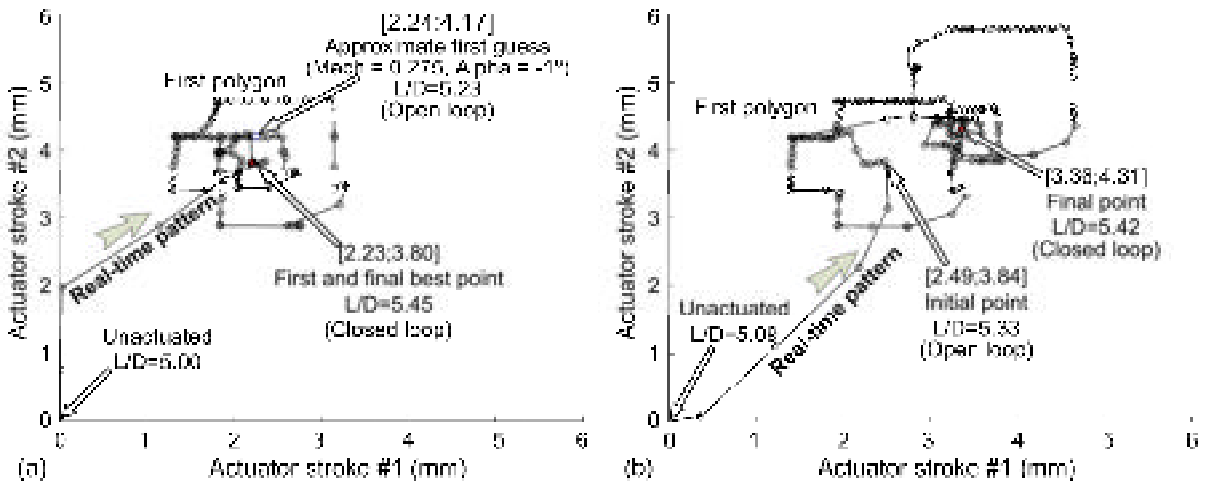


**Figure 5.8 Stroke optimization for Mach=0.275 and Alpha=-2°:
(a) first and (b) second try.**

Laminar flow improvement

To support the present experimentations, IR visualization was used to compare the locations of the laminar/turbulent flow transition occurring on the MLW upper surface for different optimized profiles. A sharp temperature gradient separating the high-temperature white zone (Figure 5.9b, for example) and low-temperature dark zone outlines the transition location. The transition detection method is based on the differences in laminar and turbulent heat transfer coefficients and is accentuated by the artificial (heating) increase of model-air flow temperature differences using scene projectors (see Figure 5.1). This detection became possible because of the significant emissivity of the flexible skin coating, in addition to the low thermal conductivity of the composite material.

Figure 5.9a displays a picture of the MLW with the flexible extrados portion in black ($x/c < 0.74$), where the region of the extrados measured by the IR camera is surrounded by the gray frame. The temperature image measured at $M=0.275$ and $\text{Alpha}=0.5^\circ$ for the unactuated shape is shown in Figure 5.9b, for which the transition was located at $x/c=24\%$.

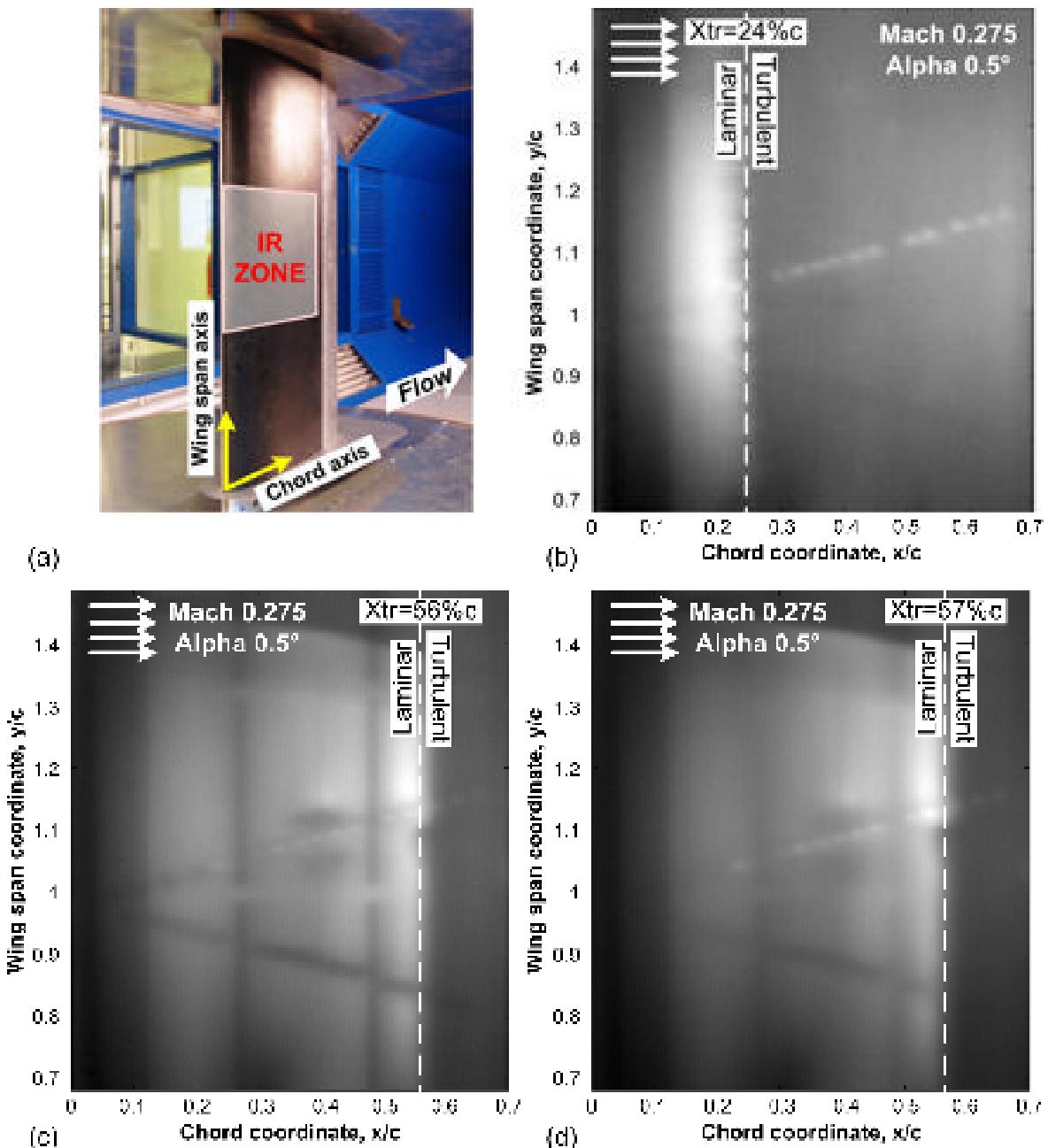


Figure 5.9 Transition point detection using (a) IR thermography visualization over the active extrados for: (b) unactuated shape $\delta = \{0; 0\}$; c) open-loop optimization $\delta = \{5.21; 7.85\}$ and d) closed-loop optimization $\delta = \{4.87; 7.09\}$.

Figure 5.9c,d show the transition location image resulting from the open- and closed-loop optimizations, respectively. The transition point location moves to $x/c=56$ and $x/c=57\%$,

respectively, a difference within the $\pm 0.5\%c$ error margin that does not show the advantage of the closed loop approach compared to the open-loop. A similar tendency for all aerodynamic flow conditions can be observed in Table 5.2, when it is known that for the flow case -B- ($Mach=0.2$ and $Alpha=0.5^\circ$), the values come from human observation of the instantaneous IR visualization, with an error margin of $\pm 1\%c$.

5.6.2 Objective Function: L/D vs x_{tr}

Envisioning a real aircraft application, it is worth noting the interrelation between the L/D improvement and the laminar flow extension. To verify the reciprocity of this relation, the optimization of the MLW was performed using the transition point location measured by the IR camera as a feedback parameter. These extra wind-tunnel tests were performed for two flow conditions, $Mach=0.2$ and $Mach=0.3$ with $Alpha=0.5^\circ$ (flow conditions -B- and -D-), with the results presented in Table 5.2. Figure 5.10 presents the resulting pattern searches for flow condition -B-, considering the L/D ratio (Figure 5.10a,b) and the transition point location (Figure 5.10c,d), respectively, as feedback parameters.

The similarity of both patterns is clear, with a slight difference between the final points: L/D optimized $\delta = \{4.74; 6.46\}$ mm and x_{tr} optimized $\delta = \{3.88; 6.04\}$ mm. Differences appear when observing the feedback evolution in Figure 5.10b,d. The L/D feedback is faster than that of the x_{tr} , as expected, because the human interpretation of the IR camera images required manual controller entry.

The closed-loop optimized profile using the transition point location as feedback allows a supplementary laminar flow regime extension of $2\%c$ as compared to the L/D feedback. The L/D of the IR closed-loop optimized profile ranges between the values corresponding to the open- and closed-loop L/D -feedback optimized profiles. With the same trend observed for flow case -D- in Table 5.2, the efficiency of the MLW shape optimization using a laminar flow extension feedback is demonstrated.

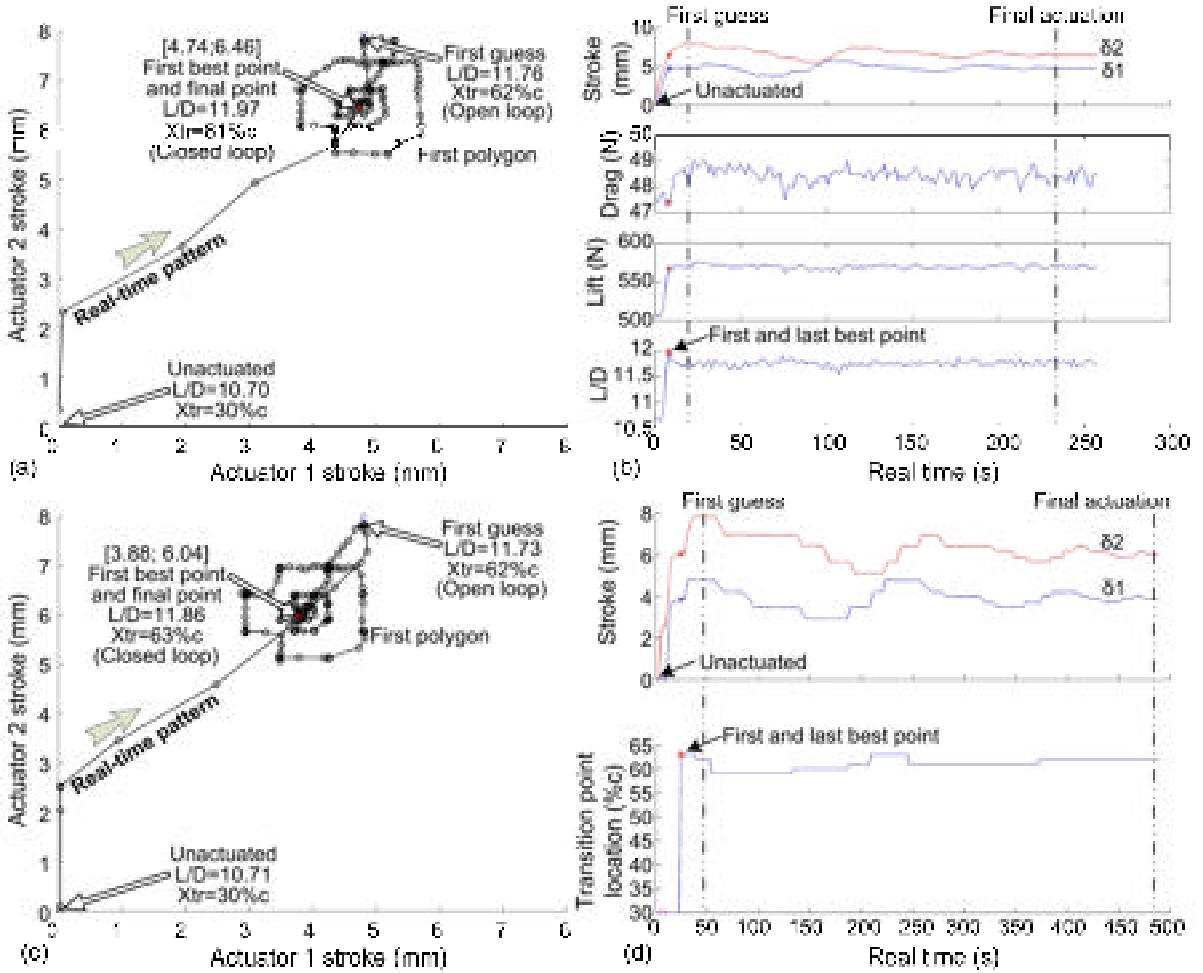


Figure 5.10 Stroke optimization for $Mach=0.2$ and $\Alpha=0.5$ using two different feedback signals: (a, b) L/D from balance and (c, d) Xtr from IR; (a, c) resulting pattern search and (b, d) performance change upon actuation.

5.7 Conclusion

The optimization of the MLW was achieved using a novel control approach combining the advantages of the DOE, numerical modeling and hardware-in-the-loop techniques. The controller was proven to be efficient and robust. The aero-structural numerical model used as an estimator by the controller was presented with reference to past works. The results of the wind tunnel DOE testing were presented in the form of response surfaces representing the MLW's aerodynamic behavior. These data showed the numerical model's limitation in

relation to three-dimensional flow effects, and thus justified the need to introduce a wind-tunnel hardware feedback in the control loop. DOE response surfaces were used to devise an appropriate optimization algorithm and to adjust the parameters. The MLW controller development concluded with a description of the wind tunnel setup involving closed-loop control using the wind-tunnel balance L/D ratio as a feedback signal.

In the second section of the paper, the MLW controller results were presented and compared. The experimental pattern search converged successfully, similar to what was expected from the simulation using the DOE response surfaces. From the MLW L/D ratio and laminar flow extension over the upper surface feedbacks, the closed-loop control demonstrated its slight advantage over the numerically-optimized strokes commanded in open loop. Also, using an IR camera as an alternative hardware in the loop, the reciprocity between the laminar flow improvement and the L/D enhancement was experimentally verified.

In summary, the inclusion of both wind-tunnel hardware and aero-structural model data in the control loop ensures morphing wing efficiency (low convergence time) and control redundancy (two control strategies). If flow conditions are unknown, and no numerical model estimation (first guess) is available, the MLW controller will still be able to optimize the morphed shape using the hardware to close the loop. On the contrary, if flow conditions are known but the hardware feedback becomes unavailable, the MLW controller will rely upon the numerical model prediction to optimize the morphed shape in an open-loop control. The combination of the open- and closed-loop control strategies seems to be the best approach to build a dependable MLW control system.

5.8 Recommendations

Envisioning a real aircraft application, the methodology developed in this paper could be extended to a larger scale with the implementation of additional hardware feedbacks in the control loop to evaluate the complete aerodynamic behavior of the aircraft. Given that the interconnection between the laminar flow and the L/D enhancement has been experimentally

verified, an MLW control-loop using a laminar flow regime indicator feedback could also be applied on a real aircraft. To this end, arrays of high sampling-rate pressure sensors on the wing extrados (Popov et al. 2009) or some IR-based techniques to measure the instantaneous laminar flow extension could be used. Attention should be paid to the MLW moment coefficient, which was neglected in this study, but which has a significant impact on aircraft control. Ultimately, the MLW controller could be used conjointly with an aircraft autopilot system with sufficient feedback and control parameters to ensure a steady flight regime whatever the MLW shape. In this ideal case, the feedback to close the loop of the MLW controller could be the one directly related to the MLW's objective: instantaneous aircraft fuel consumption.

Before applying the MLW concept to a real aircraft, some future work is recommended to facilitate the MLW controller development and improve its performance. It is recommended to examine the possibility of performing a self-tuning of the optimization algorithm parameters with the wind tunnel hardware in the loop. With the development of this method, the DOE tests will not be mandatory and the overall wind-tunnel time occupancy needed to develop such a morphing controller will be reduced. Another advantage of algorithm parameters' self-tuning is to allow a better adjustment by directly taking into account the SMA actuators' hysteresis phenomena. Also, regarding the problematic feedback signal noise observed in our MLW closed-loop control tests, a slave computer is recommended to allow higher-rate signal sampling and treatment. As a final recommendation, 3D LASER scanning or visual image correlation could be used to measure the morphed shape of the MLW subjected to aerodynamic loading in a wind tunnel. The results could serve to improve the numerical model and allow better understanding of the aero-structural interaction. The next logical step to this research would be determining the MLW's real benefit when applied to an aircraft, considering the extra weight/complexity/power consumption. This study should be performed for different flight missions to ensure that the additional power consumption caused by the use of the closed-loop controller as compared to the open-loop controller would be less than any fuel economy resulting from deploying the former.

5.9 Acknowledgments

The authors acknowledge the contributions of Thomas Georges and Brian Jahraus to the LabView programming, and they would like to thank project leader Prof. Ruxandra Botez and Andrei Popov for supporting the experimental validation of the proposed control strategy. The authors also express their appreciation to the Consortium for Research and Innovation in Aerospace in Quebec (CRIAQ), the Natural Sciences and Engineering Research Council of Canada (NSERC), Bombardier Aerospace, and Thales Canada for their financial support. The authors acknowledge G.-H. Simon, from the Thales Group as the project initiator.

5.10 References

- Boria, F., Stanford, B., Bowman, S., Ifju, P. 2009. "Evolutionary Optimization of a Morphing Wing with Wind-Tunnel Hardware in the Loop," *AIAA Journal*, 47(2):399-409.
- Botez, R.M., Molaret, P. and Laurendeau, E. 2007. "Laminar flow control on a research wing project presentation covering a three year period," *2007 Canadian Aeronautic and Space Institute Annual General Meeting*, Toronto, Ont., Canada, 25-26 April.
- Braslow, A. L. 1999. "A history of suction-type laminar-flow control with emphasis on flight research," *Monographs in aerospace history*, No 13. Washington (DC): NASA history Division, 78 p.
- CNRC-IRA., "2 m x 3 m Wind Tunnel: Technical Specifications," National Research Council Canada, *web site*: <http://www.nrc-cnrc.gc.ca/eng/facilities/iar/2x3/technical.html>.
- CLEANSKY. 2008. "What is the Clean Sky JTI?," *web site*: http://www.cleansky.eu/index.php?arbo_id=35#top.
- Coutu, D., Brailovski, V., Terriault, P. 2010. "Optimized design of an active extrados structure for an experimental morphing laminar wing," *Aerospace Science and Technology Journal*, Article in press, 5 April 2010 (doi: 10.1016/j.ast.2010.01.009)
- Coutu, D., Brailovski, V., Terriault, P. 2009. "Aero-Structural Model for Morphing Laminar Wing Optimization in a Wind-Tunnel," submitted to *Journal of Aircraft*, December.

- Flightglobal. 2006. "Boeing unveils plans for trailing edge variable camber on 787 to reduce drag, save weight," web site: <http://www.flightglobal.com/articles/2006/06/12/207172/boeing-unveils-plans-for-trailing-edge-variable-camber-on-787-to-reduce-drag-save.html>.
- Gilyard, G. B., Georgie J. and Barnicki, J. S. 1999. "Flight test of an adaptive configuration optimization system for transport aircraft," *NASA technical memorandum* 206569, Edwards, Calif., 18 p.
- Georges, T., Brailovski, V., Morellon, E., Coutu, D., Terriault, P. 2009. "Design of shape memory alloy actuators for morphing laminar wing with flexible extrados," *ASME Journal of Mechanical Design*, 131(9):091006-1 – 091006-9. (doi:10.1115/1.3160310).
- Hetrick, J. A., Osborn R. F., Kota, S., Flick, P. M., Paul, D. B. 2007. "Flight testing of Mission Adaptive Compliant Wing," *48th AIAA/ASME/ASCE/AHS/ASC Structures, Structural Dynamics, and Materials Conference*, Waikiki, HI, USA, April 23-27th.
- Jacobsen, M. and Ringertz, U. T. 2009. "Performance optimization of flexible wings using multiple control surfaces," *International Forum on Aeroelasticity and Structural Dynamics*, 21-26 June, Seattle, Washington, 15 p.
- Levinsky, E. S. and Palko R. L. 1982. "Tests of an improved, computer-controlled, self-optimizing, variable-geometry wing," *AIAA 12th Aerodynamic Testing Conference*, Williamsburg, VA, USA, Paper 82-0599.
- Pagès, L., "Maximisation de la laminarité d'un profil d'aile par optimisation de la forme de l'extrados," Master Dissertation, Mechanical Dep., Ecole Polytechnique de Montreal, Montreal, Quebec, Canada, 2007
- Popov, A., Botez, R.M., Mamou, M., Mebarki, Y. 2009a. "Real Time Morphing Wing Optimization in Wind Tunnel", submitted to *AIAA Journal of Aircraft*, September.
- SADE. 2008. "SADE - Smart High Lift Devices for Next Generation Wings," web site: http://www.smr.ch/sade/sade_public/home.html.
- Sainmont, C., Paraschivoiu, I., Coutu, D., Brailovski, V., Laurendeau, E., Mamou, M., Mébarki, Y., Khalid, M. 2009. "Boundary Layer Behaviour on a Morphing Airfoil; Simulation and Wind Tunnel Tests," *Canadian Aeronautic and Space Institute AERO09 conference*, Kanata, Canada.
- Skalecky, J. 2008. "CLEEN Planned Solicitation," *CLEEN Market Research Conference*, 20 p., online 14 April 2010: http://www.faa.gov/news/conferences_events/2008_market_research_conference/materials/media/CLEENPlannedSolicitation.pdf.

Strelec, J. K., Lagoudas, D. C., Khan, M. A., Yen, J. 2003. "Design and implementation of a shape memory alloy actuated reconfigurable airfoil," *Journal of Intelligent Material Systems and Structures*, 14(4-5):257-273. (doi:10.1177/1045389X03034687)

CONCLUSION

La préoccupation environnementale et l'augmentation du coût du pétrole nourrissent l'intérêt envers les innovations technologiques comme celles des ailes adaptatives. Dans le cadre du projet CRIAQ 7.1 visant à prouver la faisabilité du concept d'aile laminaire adaptive, les travaux de cette thèse ont permis la conception de la structure active et l'exploitation adéquate de son caractère adaptatif en soufflerie subsonique.

Conception de la structure active

Le choix de la meilleure configuration de structure active a été réalisé à l'aide d'une méthodologie de conception optimale tenant compte de l'interaction aéro-structurale. Pour ce faire, une optimisation multi-objective fut conduite à l'aide d'un modèle structural d'éléments finis et d'un solveur aérodynamique. La configuration résultante constituée de 4 plis et de 2 actionneurs s'est avérée offrir un compromis bien équilibré entre la rigidité et la souplesse si l'on en croit les résultats obtenus en soufflerie.

Exploitation de la structure active

Les outils numériques mis en place dans les travaux de conception ont ensuite été couplés afin d'être employés à l'exploitation du caractère adaptatif de l'aile laminaire en soufflerie subsonique. La comparaison des résultats expérimentaux et des prédictions numériques ont pu mettre en évidence le comportement 2D du modèle numérique à l'égard du comportement 3D de l'écoulement.

Ainsi, afin de s'assurer que le plein potentiel de l'aile adaptative puisse être exploité, les profils ont été optimisés en temps réel dans la soufflerie à l'aide de la rétroaction des forces aérodynamiques mesurées à la balance. Pour assurer la robustesse et l'efficacité de la méthode, l'algorithme d'optimisation a été conçu et ajusté pour cette application à l'aide de la modélisation expérimentale. Également, le modèle aéro-structural fut utilisé pour fournir une première estimation du profil optimal, réduisant ainsi le temps de convergence de l'algorithme.

En somme, les connaissances développées dans cette thèse seront utiles pour quiconque veut appliquer le concept de l'aile adaptative sur un avion réel. Dans cette lancée, la prochaine section fait état des aspects de la recherche qui mériteraient d'être approfondis davantage dans une éventuelle poursuite de ces travaux.

RECOMMANDATIONS

Dans la poursuite éventuelle de ces travaux de recherche, l'analyse des résultats présentés dans cette thèse permet de formuler les recommandations suivantes concernant le cahier des charges, la conception de l'aile adaptative et l'exploitation de la structure active.

1. Le cahier des charges :

- a) les caractéristiques complètes de l'avion devraient être connues : fiche technique, géométrie, masse et centrage, gestion de l'espace à l'intérieur des ailes, conditions de vol pour chacune des étapes des différentes missions;
- b) les conditions d'opération de la structure devraient être déterminées expérimentalement au besoin : pressions à l'intérieur et à l'extérieur de l'aile, chargements critiques, température, rayonnement ultra-violet, gel et dégel, humidité, vibration, fréquence d'utilisation;
- c) vu la ressemblance des résultats obtenus d'un nombre de Mach à l'autre, la matrice des conditions de l'écoulement devrait comporter un nombre minimal de conditions d'écoulement;
- d) les facteurs de sécurité et la vie en fatigue des éléments structuraux devraient être considérés.

2. La conception de l'aile adaptative :

- a) le profil de base utilisé devrait être optimisé sur les conditions de l'écoulement à l'étude afin que les gains obtenus lors de l'adaptation du profil soient réalistes;
- b) la méthodologie de conception pourrait être répétée avec plus de variables de design afin d'obtenir une solution plus raffinée. Par exemple, pour un nombre d'actionneur donné, la position de ces derniers le long de la corde pourrait être déterminée par l'optimiseur. Il en va de même pour le nombre de plis de la structure qui pourrait être variable dans la direction de la corde;
- c) advenant de la possibilité de réaliser les calculs en parallèle sur plusieurs ordinateurs, le modèle couplé aéro-structural pourrait dès lors être utilisé à cette étape;

- d) les profils résultant de l'optimisation multidisciplinaire présentée au chapitre 4 de cette thèse pourraient être considérés comme profils cibles;
 - e) pour chacune des configurations de structure active évaluées sur l'ensemble des conditions de l'écoulement, une optimisation locale est encouragée pour s'assurer du caractère optimal de chaque profil cible utilisé;
 - f) la compatibilité de la solution structurale avec les composantes internes de l'aile, comme les réservoirs d'essence par exemple, devrait être vérifiée attentivement;
 - g) la performance globale de l'avion devrait être considérée et non seulement celle du profil adaptatif;
 - h) la conception devrait tenir compte du procédé de mise en forme et du plan d'entretien.
3. L'exploitation de l'aile adaptative laminaire :
- a) le système de contrôle devrait être redondant, efficace et robuste. L'efficacité serait attribuable à l'utilisation de prédictions numériques permettant une adaptation rapide, alors que la robustesse serait assurée par une rétroaction permettant l'optimisation en temps réel du profil adaptable;
 - b) des techniques pour évaluer en vol l'efficacité aérodynamique de l'avion devraient être développées. Il serait intéressant d'explorer l'utilisation de la consommation instantanée en carburant pour des conditions de vol constantes ou encore l'utilisation des données d'un système de navigation ultra précis;
 - c) en cas de défaillance électrique ou mécanique, l'aile adaptative devrait pouvoir retourner naturellement au profil de base et y demeurer;
 - d) un système d'actionnement avec fonction de blocage devrait permettre le maintien d'une forme de profil optimale entre deux phases de modification du profil sans consommation d'énergie;
 - e) la modification du profil pourrait être réalisée par un seul actionneur lié à une transmission capable de découpler les déplacements aux lignes d'actions selon une relation proportionnelle adéquate.

Du point de vue de la mise en application de l'aile laminaire adaptative, il est primordial qu'un bilan énergétique approfondi soit réalisé. En effet, le calcul de l'économie nette en carburant doit tenir compte de la consommation de l'énergie, des frais d'installation et d'entretien ainsi que du poids additionnel lié à l'utilisation de cette innovation technologique. Il serait également intéressant d'étudier la faisabilité d'une aile adaptative qui pourrait être utile non seulement en vol de croisière mais également lors du décollage et de l'atterrissage. Pour ce faire, l'aile adaptative devrait être en mesure de faire varier sa surface portante afin de pouvoir remplacer les systèmes hypersustentateurs actuels. Ultimement, l'aile adaptative se verra confier toutes les fonctions qu'assument pour l'instant les surfaces articulées conventionnelles. C'est alors que les bénéfices nettement plus importants sauront encore mieux justifier les efforts et moyens nécessaires à l'adoption du concept de l'aile adaptative sur les avions de demain.

ANNEXE I

EXPERIMENTAL VALIDATION OF THE 3D NUMERICAL MODEL FOR AN ADAPTIVE LAMINAR WING WITH FLEXIBLE EXTRADOS

D. Coutu, V. Brailovski, P. Terriault, C. Fischer

École de technologie supérieure, 1100 rue Notre-Dame Ouest,
Montréal, Québec, Canada, H3C 1K3

Cette annexe présente un article publié à l'« International Conference on Adaptive Structure
and Technologie ». Ottawa, Canada, 3-5 oct. 2007.

Experimental validation of the 3D numerical model for an adaptive laminar wing with flexible extrados

D. Contu, V. Brailovski^a, P. Terrault, and C. Fischer

^a Department of Mechanical Engineering, École de technologie supérieure,

* Corresponding author: 1100 Notre-Dame St. West, Montreal, Canada, H3C 1K3
Tel: 1 (514) 396-8594, Fax: 1 (514) 396-8530, E-mail: vladimir.brailovski@etsmtl.ca

ABSTRACT

Wing drag reduction poses a real challenge in aerospace engineering. At the subsonic speed level, drag reduction can be achieved by increasing laminar flow over the wing. This work focuses on the development and validation of the numerical model of an experimental adaptive wing with improved laminar flow. The wing is composed of a rigid structure forming intrados and wing-box. Flexible extrados and actuators located inside the wing-box. The extrados profile is controlled by two individually controlled actuators placed along the wing chord and acting normally to the chord. The flexible extrados is made of a woven carbon/Kevlar hybrid composite designed to allow greater flexural compliance in the chord-wise than in the span-wise direction. To allow the subsequent optimisation of the adaptive wing structure, a structural shell model of the flexible extrados is built using the ANSYS finite element software. The model takes into account the following variables: (1) reinforcement type, properties and stacking sequence, (2) laminate thickness and curvilinear radius, (3) boundary conditions representing the interaction between flexible and rigid wing structures, and (4) extrados-actuator coupling conditions (location, direction, force and stroke). An adaptive wing prototype has been built to verify the predicted structural response. The experimental validation of the structural model is performed using tensile and three-point bending tests followed by testing of the entire wing structure with a laboratory experimental bench.

Keywords: laminar adaptive wing, drag reduction, 3D finite element modeling, hybrid composite

1. INTRODUCTION

Drag reduction over an airfoil poses a real challenge that has attracted significant attention in the aerospace research community. Up until now, the literature has included discussions of two main methods used for altering the flow dynamics over an airfoil: energizing of the boundary layer [1] and modifying the airfoil profile [2-5]. The second approach, partially realized in the works of Chandrasekara et al [3], Baroo et al [4], and Munday et al [5] modifies respectively the leading edge, intrados or extrados of an airfoil to extend the flight envelope, increase lift and avoid laminar flow separation. This work aims to delay the backward transition between laminar and turbulent flow over the airfoil profile using flexible skin partially covering the airfoil extrados. To optimize the design of this flexible skirt, which is made of a laminate composite material, the finite element modeling (FEM) approach is used. The adaptive wing with improved laminar flow is composed of the rigid structure (forming intrados and wing-box), the flexible extrados, the compensation cart lever spring and the actuators located inside the wing-box, as presented in figure 1.

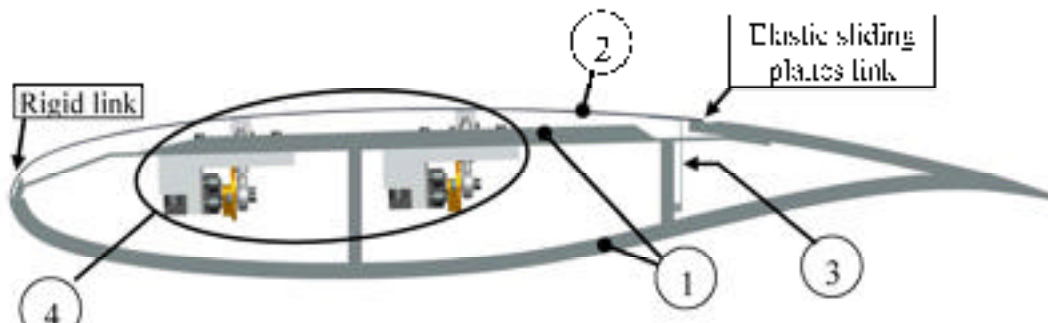


Figure 1. Conceptual design of an improved laminar flow adaptive wing using flexible extrados

To resist potentially high aerodynamic forces, the leading edge of the flexible extrados is firmly attached to the rigid structure. The other extremity of the flexible extrados is linked to a compensation cantilever spring that creates an elastic joint to accommodate extrados shaping and to maintain aerodynamic continuity between the flexible and rigid parts of the wing.

Three main objectives must be taken into account in designing the flexible extrados:

1. The wing profile should be modified according to CFD optimization calculations while maintaining uniformity of the span-wise shape changes.
2. The flexible extrados should be attached to the rigid wing-box structure such as to compensate for geometry variations, while ensuring aerodynamic continuity.
3. The flexible extrados should be connected to the actuators in a manner ensuring global shape modifications.

These general design objectives can be translated into the following technological objectives:

1. The material used to manufacture the extrados should allow the precise control of its structure and properties. In this respect, a laminate composite material is the best solution because it can be tailored to suit each task by varying the stacking sequence, the orientation, and the in-plane extent of the composite reinforcement; the material can then be adapted for a compliant structure that needs to exhibit specific shape changes under action.
2. Ultimately, both the material and the technology used to process it may be approved in accordance with existing standards for aviation materials and processes.

Given these premises, finite element modeling (FEM) can assist in the design of the flexible extrados because it allows the designer to predict flexible extrados shape variations based on loading and boundary conditions. Also, the laminate structure can be optimized in order to meet the following performance criteria: (a) conformity of the modified wing geometry with the theoretical profiles resulting from CFD calculations, and (b) compactness and lightness. This paper thus discusses the validation of the finite element model built to assist in the realization of the adaptive wing, with improved laminar flow using a flexible extrados.

2. FEM OF THE FLEXIBLE EXTRADOS

ANSYS, commercial finite element analysis software, is used to build a 3D numerical model of the flexible extrados. For validation purposes, the flexible extrados is compressed between 1 and 64% of a 500 mm length chord constant profile, and forms a < 10 mm span wing (figure 2).

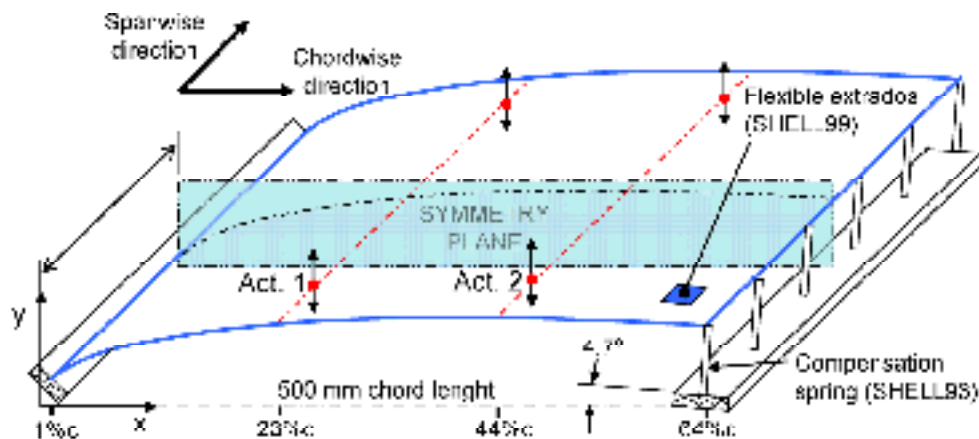


Figure 2. Flexible extrados schematics with boundary and loading conditions.

Using symmetry conditions, a 205 mm half span is modeled using Shell99 elements. This 8-node layered structural shell models the laminate made from a series of plies with orthotropic material properties. Furthermore, 3 cantilever springs are modeled at the right end of the extrados using 8-node Shell93 elements to represent an elastic link between the flexible and rigid extrados parts. Actuation forces are distributed over 9.5mm x 19mm rectangular areas representing connection zones between the actuators and the flexible structure. The definitions and properties of each ply are presented in the following section.

The flexible extrados structure is modeled through tripped meshing. To perform a convergence study, 1mm displacement is applied to the structure at a distance corresponding to 23% of the chord length for different mesh densities. For each analysis, the reaction force is reported in respect to the number of element (figure 3). A 716 quadrilateral elements mesh is the best compromise between CPU time calculation and results accuracy for subsequent analyses.

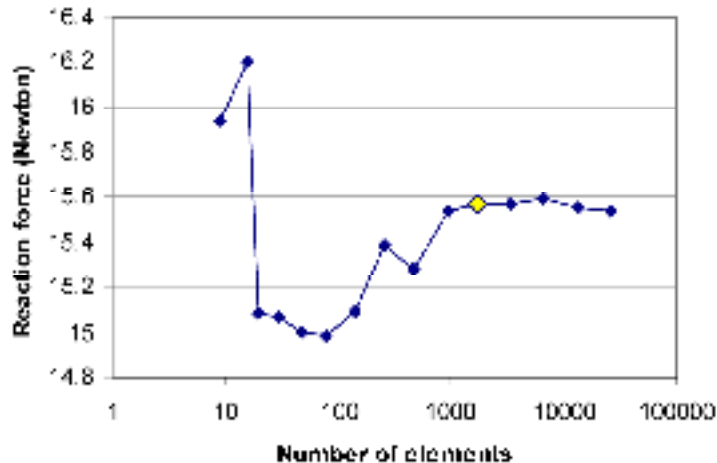


Figure 3: Convergence study to determine the number of elements.

Furthermore, the model validation is performed by comparing the calculated and experimentally observed behaviors of the composite under two loading modes: (a) simple loading in tension and 3-point bending, to ensure the proper modeling of the laminate structure and its

constituents, and (b) complex loading of the flexible extrados made of the same material, connected to the rigid wing structure, and deformed by two sets of locally applied actuation forces (figure 2).

3 COMPOSITE MATERIAL MANUFACTURING, CONSTITUENTS AND STRUCTURE

3-1 Manufacturing

All laminates created for this study were formed through *Vacuum Assisted Resin Transfer Molding* (VARTM), a process which uses a vacuum to infuse resin into the reinforcement. It provides appropriate and repeatable mechanical properties, and allows the possibility of creating complex shapes. VARTM produces lower VOC (volatile organic compound) emissions than traditional vacuum bagging, while having lower set-up costs as compared to autoclave-process prepreg systems.

Testing was undertaken first to ensure the quality of the process. Matrix burnoff measurements were also conducted according to ASTM D 3171 [6]. The coefficient of variation of the fibre content was found to be smaller than 3% for all specimens tested.

3-2 Plies - constituents and characterization

Two different plies are selected to form the extrados laminate, and are presented in figure 4. The 2 x 2 twill woven Kevlar/Carbon fibre hybrid is used in the chord-wise direction, where flexibility is needed for profile modification. The low-modulus unidirectional carbon fibre is used span-wise, in which case rigidity is preferred in order to ensure profile uniformity (see figure 2). A Huntsman 8602 Reninfusion low-viscosity epoxy resin system is used. This polymer matrix is well adapted to the VARTM process due to its low viscosity of 175 cP. However, this does not compromise its cured mechanical properties, as is confirmed by the mechanical testing of the laminate.

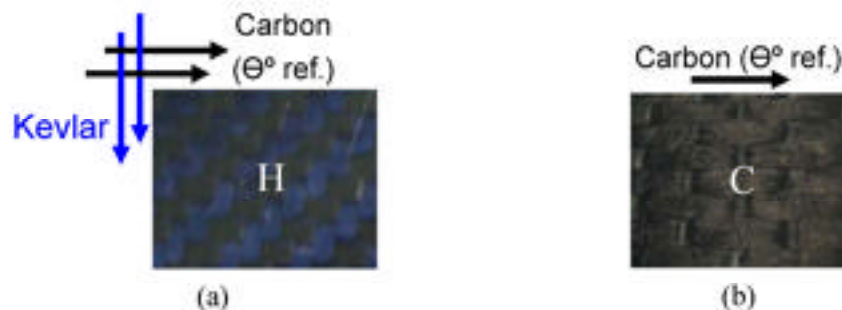


Figure 4. (a) 2x2 twill woven Kevlar/Carbon fibre hybrid (H); (b) Unidirectional carbon fibre

To calibrate the finite-elements model, tensile testing was successfully conducted according to ASTM3039 [7] and ASTM3518 [8] using 3 specimens for each ply type. The resulting average (Avg), standard deviation (SD) and coefficient of variation (CV) of each elastic constant are listed in table 1. Simplifications were made for other elastic constants listed in table 2, considering that they have a minor impact on the flexural response of the composite. The axis number 1 in the Carbon/Kevlar cloth is defined as the longitudinal axis of the carbon fibres.

Table 1. Measured elastic constants

	Const.	Avg [GPa]	SD [GPa]	CV (%)	Test method
Carbon/Kevlar Hybrid	E_1	32.9	0.7	2.2%	ASTM D3039
	E_2	17.1	0.3	1.7%	ASTM D3039
	P_{12}	0.12	0.026	22%	ASTM D3039
	G_{12}	2.1	0.031	1.5%	ASTM D3518

Table 2. Approximated elastic constants

	Const.	Value	Source
Carbon/Kevlar Hybrid	E_3	E_2	carbon
	G_{23}	G_{12}	C/K
	G_{13}	G_{12}	C/K
	PR_{23}	0,01	-
	PR_{13}	0,01	-

Unidirectional Carbon	E_1	99.9	2.3	2.3%	ASTM D3039
	E_2	5.5	0.4	7.2%	ASTM D3039
	P_{12}	0.25	0.03	10.4%	ASTM D3039
	G_{12}	3.2	0.1	3.7%	ASTM D3518

Unidirectional Carbon	E_1	E_2	carbon
	G_{23}	G_{12}	carbon
	G_{13}	G_{12}	carbon
	PR_{23}	0,01	-
	PR_{13}	0,01	-

3.3 Structure of the laminate

The 3- and 4-ply laminate structures shown in Figure 5 were used for validation. Following analyses of the resulting ply thicknesses, some corrections were made in order to account for the woven/unidirectional reinforcement and mould contact interfaces.



Figure 5. 3- and 4-ply laminates

4. MECHANICAL BEHAVIOUR OF THE LAMINATE UNDER SIMPLE TESTING MODES

These validation tests are aimed at verifying the ability of the models to take into account the reinforcement type, plies orientation and number.

4-1. Tensile tests

Tensile tests were performed on 3- and 4-ply laminates for three different fibre orientations (0°, 45° and 90°). The measured extensional moduli were found to be consistent with those predicted numerically, as shown in Figure 6. The comparison results showed some discrepancies for the 0° and

45° orientations, and the 0° experimental modulus may have been lowered because the low 15mm coupon width amplified fibre misalignment errors.

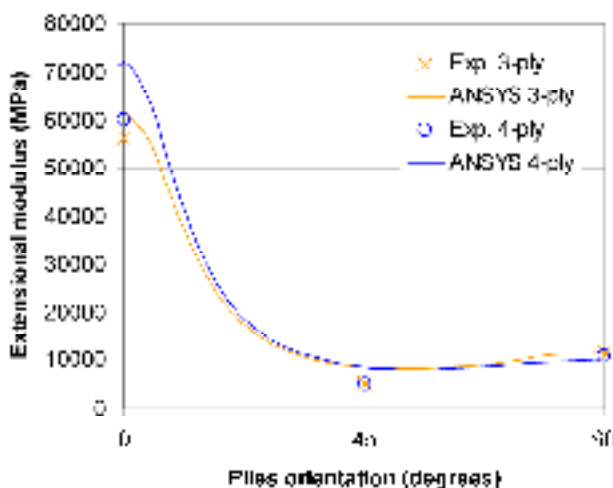


Figure 6. Laminar extensional modulus according to plies orientation and number

4-2. Three-point bending

Three point bending is performed on the 3 and 4 ply laminates. A customized three point bending fixture shown in figure 7, with a distance of 152.4 mm between two support lines is mounted on an MTS 858 Mini Bionix testing machine to receive 200 x 200 mm plate specimens. The load is applied by a 9.5 mm radius nose in order to avoid microbuckling fibre damage. Bending tests involving deflections of up to 10 mm are repeated for two orthogonal axes (0° and 90°), and the results are presented in figure 8 along with those predicted by the numerical model.

It can be concluded from the results obtained that the ANSYS numeric model provides good estimations of the bending stiffness for the experimental conditions tested. The bending stiffness was underestimated when the carbon fibre was solicited (0°) and overestimated when the Kevlar fibre was solicited (90°). One error source, the thickness value (t) of each ply of the laminate must be considered. In fact, the bending response (E_b) is very sensitive to the plate thickness, as the following material strength equation illustrates: $E_b = \frac{m t^3}{48 r^3}$.



Figure 7. Three-point bending test fixture

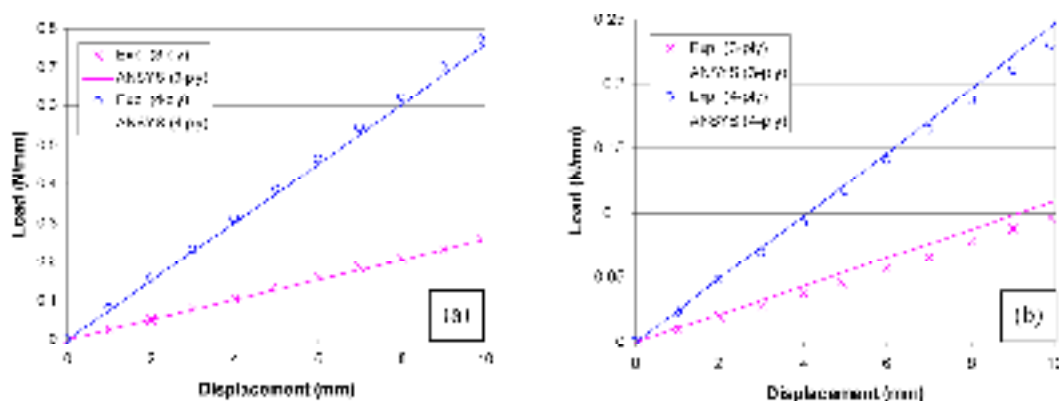


Figure 8. Normalized load deflection diagrams for (a) 0° bending direction, (b) 90° bending direction

5. MECHANICAL BEHAVIOR OF THE FLEXIBLE EXTRADOS SUBMITTED TO ACTUATION FORCES

Given that the finite-elements model has been successfully validated for simple loading modes (tension and three point bending), the validation is pursued by comparing numerical and experimental results of the flexible extrados submitted to actuation forces.

5-1. Laboratory testing bench for adaptive wing with flexible extrados

The adaptive-wing laboratory bench is presented in figure 9, with the profile digitizing facility located above the flexible extrados model. Using a LabView interface, a mobile laser displacement sensor measures the profile shape for a given actuation state. Both actuation lines are loaded through two actuator points for a total of four, as presented in figure 10. Deadweights are used either with or without pulleys to generate upward or downward loadings.

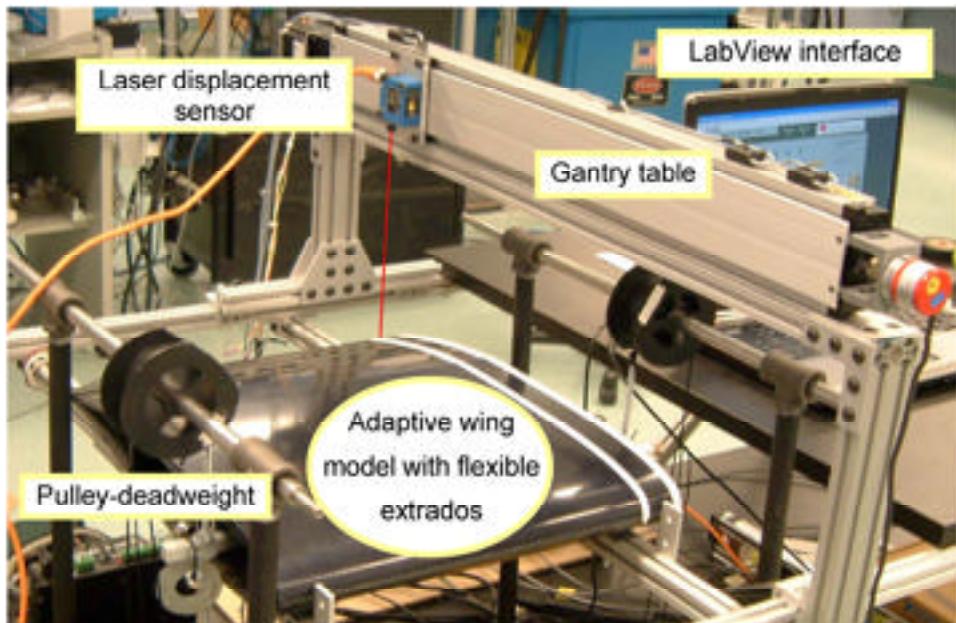


Figure 9. Adaptive wing model installed on the test bench

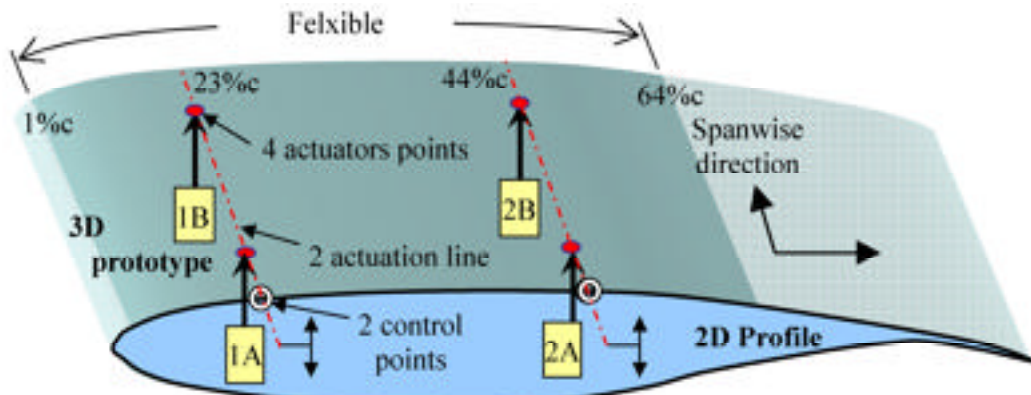


Figure 10. Wing prototype with flexible extrados

5-2. Activated extrados response

The flexible extrados uses the 3-ply laminate previously defined in figure 5, with the span direction taken to be the stacking sequence reference orientation. To gradually increase the profile thickness, the load applied at each actuation point is incremented by 2.45N from -4.9N (- signifies downward loading) to 14.7N. The load deflection diagrams presented in figure 11 were obtained using a laser displacement sensor located directly above the actuator points. The proximity between ANSYS predictions and the experiments give confidence in the numerical model to establish functional requirements for actuators.

The respective global geometrical changes for -1.9 and 11.7 N loads were obtained when scanning the airfoil profile for the 1st and 2nd actuation lines (figure 12). For an upward deflection of

over 6 mm, the difference between the calculated and the experimentally measured test is did not exceed 10%. This concordance shows the ability of the numerical model to be used to design flexible wing capable of matching the theoretical profiles resulting from CFD calculations.

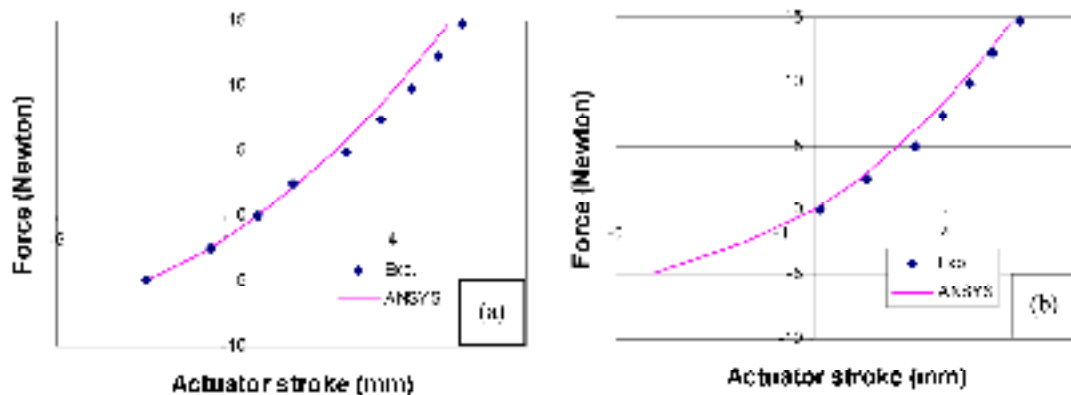


Figure 11. Load displacement diagrams: (a) 1st actuation line; (b) 2nd actuation line

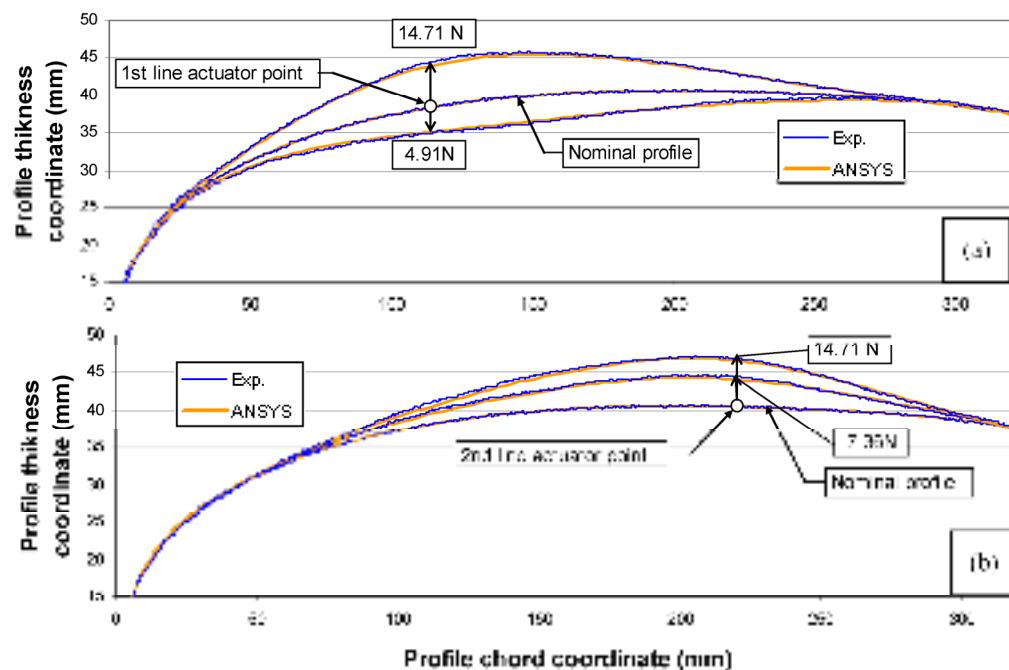


Figure 12: Experimental and computed profile shape changes for (a) 1st and (b) 2nd actuation lines

6. CONCLUSIONS

As can be seen in the experimental results, the ANSYS numerical model of the composite structure forming the flexible extrados of an adaptive wing can predict its behaviour under actuation. Using this model allows future optimization work to be conducted to optimize design variables in

order to achieve specific computed wing profiles for different flow conditions, while minimizing the overall weight of the wing. To that end, a numerical tool will be developed to quantify the concordance of the shape profile obtained by mechanical modeling with that calculated through the CFD. Furthermore, aerodynamic pressure will be considered in the numerical optimization leading to an improved laminar adaptive wing. Stress distribution is another concern that will receive attention in future works in order to ensure the integrity of the whole wind tunnel prototype.

ACKNOWLEDGEMENTS

The authors would like to thank CRIAQ, NSERC, Bombardier Aerospace and Thales Canada for their financial support as well as to acknowledge G.-H. Sirur from Thales for initiating this project and S. Rodriguez and T. Georges for their assistance in experimentations.

REFERENCES

1. Gilmanis, J.L., L.W. Trabu, and O.K. Redioutis. *A new class of synthetic jet actuators-Part II: Application to flow separation control*. Transactions of the ASME, Journal of Fluids Engineering, 2005, pp. 377-387.
2. Weissberg, V., I. Snikmaner, and A.K. Green. *The application of shape memory alloy actuators in adaptive structures*. Proceedings of 10th International Conference on Adaptive Structures and Technologies (ICAST 99), 11-13 Oct. 1999, 2000; pp. 229-236.
3. Chandrasekhar, M.S., et al. *Design and development of a dynamically deforming leading edge airfoil for unsteady flow control*. Proceedings of the 1997 17th IEEE International Congress on Instrumentation in Aerospace Simulation Facilities, ICASF, Sep 29-Oct 2 1997; pp. 132-140.
4. Bauer, A., B.B., Branchaw, N., Ostry, B., Pearsall, J., Perlman, G., Selsam, J.. *Morphing Wing Mo33*, 2003, Technical report, University of Colorado at Boulder, 102 pages.
5. Muniakay, D. and J. Jacob (2001). *Active control of separation on a wing with cambered camber*. Paper presented at the 39th AIAA aerospace sciences meeting and exhibit, 10 pages.
6. ASTM D3517-99, Standard Test Methods for Constituent Content of Composite Materials.
7. ASTM D3039/D3039M-00 (2000). Standard Test Method for Tensile Properties of Polymer Matrix Composite Materials.
8. ASTM D3518/D3518M 94(2001). Standard Test Method for Li Plate Shear Response of Polymer Matrix Composite Materials by Tensile Test at $\pm 45^\circ$ Laminate.

ANNEXE II

PROMISING BENEFITS OF AN ACTIVE-EXTRADOS MORPHING LAMINAR WING

D. Coutu, V. Brailovski, P. Terriault

École de technologie supérieure, 1100 rue Notre-Dame Ouest,
Montréal, Québec, Canada, H3C 1K3

Cette annexe présente une note d'ingénierie publiée dans le
« Journal of Aircraft », vol. 46, no. 2, mars-avril 2009, pp. 730-731.

Promising Benefits of an Active-Extrados Morphing Laminar Wing

Daniel Couris,¹ Vojtěch Brnávský,² and Patrick Tessier^{1,2}

¹*École de Technologie Supérieure,
Montréal, Québec H3C 1K3, Canada*

DOI: 10.2514/6A-2005-7

Nomenclature

c	sweep chord, mm
E_{act}	energy from the actuators, J
E_{red}	energy saved from the wing morphing, J
M	Mach number
p_{∞}	dynamic pressure, Pa
S	wing surface area, m ²
t	time duration, s
V_{∞}	
x	distance from the aerofoil leading edge, mm
x_p	transition point location from the aerofoil leading edges, mm
α	angle of attack, deg
ΔC_d	drag coefficient reduction during wing morphing
ρ_s	air density, kg/m ³

L Introduction

IN AIR transport, drag reduction is often a synonym of energy saving because the energy consumption depends on the engine thrust related to equilibrate the plane drag. Among innovative solutions, morphing technology [1] is well suited to achieve wing drag reduction. The CRISO (Consortium for Research and Innovation in Aerospace in Québec) 7.1 project aims to study the feasibility of a morphing wing capable of reducing drag through laminar flow regime enhancement [2]. Because the project's credibility relies on the overall energy performance, the mechanical work required from actuators to modify the wing profile and to improve the flow laminarity should be less important than the energy saved from the drag reduction. This paper presents a simplified efficiency analysis of such a laminar morphing wing as a path to further economic impact evaluations.

II. Design of the Morphing Wing

The morphing wing prototype is designed to be capable of modifying its extrados profile for a series of distinct flow conditions

Received 29 April 2005; revised version received 10 January 2006. Copyright © 2006 by the American Institute of Aeronautics and Astronautics, Inc. All rights reserved. Copies of this paper may be made for personal or internal use, on the condition that the copier pay the \$10.00 per copy fee to the Copyright Clearance Center, Inc., 222 Rosewood Drive, Danvers, MA 01923; include the code 0731-686X/06 \$10.00 in correspondence with the CCC.

1P.-E. S. degree, Mechanical Engineering.

²Professor, Mechanical Engineering, 1100 Notre-Dame Street West, vbrnavsky@etec.etsmtl.ca (Corresponding Author).

Professor, Mechanical Engineering.

encompassing seven Mach numbers ($M = 0.2$ to 0.45 , incrementally 0.025) and seven angles of attack ($\alpha = -1$ to 2 deg, incremented by 0.5 deg), which gives a total of 19 flow cases. The concept relies on an active composite structure resembling to a rigid wing body, as presented in Fig. 1. The modification of the initial profile occurs when shape memory alloy (SMA) actuators located inside the wing box apply induced cyclic displacements to the flexible extrados. The overall stiffness and integrity of the experimental wing is provided by the rigid intrados. The root and rear edges of the flexible extrados are connected to the rigid intrados in such a way that ensures joint to joint continuity, vacuum relates clamps lifelines, and sustains aerodynamic forces. It results in a flush-glass joint near the leading edge and a sliding plane link at the aft end, including a compensation spring placed between flexible and rigid structures. Finite element method sensitivity analyses identified the number of actuators and the number of carbon/Kevlar plies constituting the flexible structure as the main input/design variables. A total of 48 design arrangements were considered: 8 possible actuator configurations (from 0 to 7 actuators) and 6 possible ply configurations (from 3 to 8 plies). Considering maximization of the laminar flow rate, wing morphing and minimization of the skin energy required for this morphing as two design objectives, a multicriteria optimization led to the selection of a 4-ply, 2-actuator design arrangement of the active structure [3].

III. Morphing Laminar Wing Efficiency

A. Mechanical Work Provided by the Actuators

The 3D finite element model of the active structure is built in ANSYS software using SHELL98 elements for the flexible structure and S-H8R4A5 for the compensation leaf spring with locked rotation around the y axis, to ensure slope profile continuity. Figure 2a presents a 2D cross section of the model. For each flow case, to enhance the laminar flow regime, previous CFD analyses [5] provided optimized displacements at each actuator point and the corresponding 2D pressure distributions over the morphed extrados. The resulting force-displacement envelopes for both actuators covering all flow cases are presented in Fig. 2b, in which the solid and dashed rectangles correspond to the actuators located closer to the leading (act 1) and trailing (act 2) edges, respectively. The actuator force is normalized against a meter of span. It can be observed that the actuators are always in pull (or retarding) mode, as the aerodynamic suction forces prevail on the forces needed to deform the flexible extrados for all the flow cases. From the mechanical design point of view, having a unique operating mode appears to be an advantage, because one-way actuators can be used instead of two-way actuators. It is assumed that the actuators do not consume energy when the optimized shape is maintained (they are mechanically locked in this position) and that they are activated only when they return the structure to the reference profile. As an example, the actuation cycle for the flow case $M = 0.375$ and $\alpha = 1.5$ deg is presented in Fig. 2c. From the analysis idealized actuation paths 1 and 2, the mechanical mechanical work required to return the structure from the morphed profile close to the reference profile can be evaluated as 5.1 and 5.2 J, respectively, with a total of $E_{\text{act}} = 8.3$ J/m of the wing span.

B. Energy Saving from Drag Reduction

To evaluate energy saving from drag reduction, both reference and morphed profiles are analyzed by the boundary layer solver XFOIL



Fig. 1 Conceptual design of the morphing laminar wing.

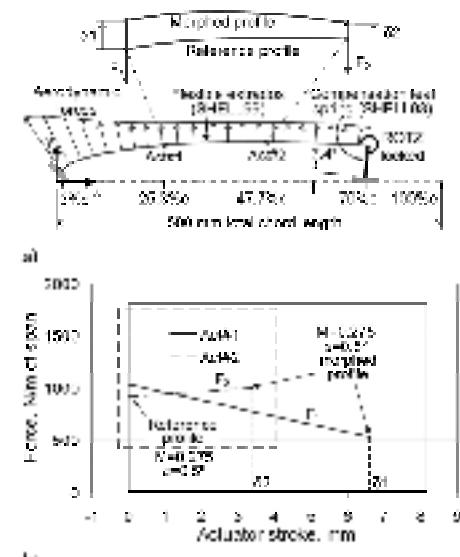


Fig. 2 Structural simulation: (a) numerical model of the native structure, using ANSYS software and (b) working envelope of the morphing wing.

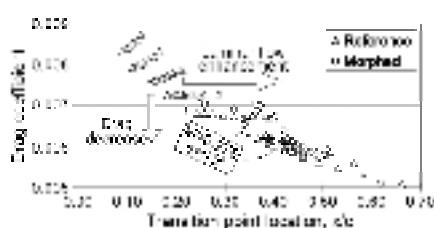


Fig. 3 Drag coefficient reduction due to laminar flow regime enhancement using the morphing laminar wing.

0.36 [6], the drag coefficients of the laminar-turbulent flow transition point x_t are calculated for each flow case (Fig. 3). It is clear that the effect of the laminar flow enhancement (backward move of the transition point) causes significant drag reduction. For example, for the case of $M = 0.771$ and $\alpha = 0.5^\circ$ (reg. 0 transition point) for the reference profile (located at $x_t/c = 0.22$ with a drag coefficient of 0.0073) is pushed back to $x_t/c = 0.42$ (with a drag coefficient of 0.0051) when the actuators deform the flexible camber and the optimized profile is reached.

Let us suppose that the wing profile morphs from the reference to the optimized profile and that the flight conditions corresponding to

this latter profile do not change over a given period of time t . The energy saved from drag reduction can then be evaluated as follows:

$$E_{\text{saved}} = \Delta C_d \cdot q_\infty \cdot S \cdot V_\infty \cdot t \quad (1)$$

Consider now a morphing wing with 0.5 m of chord and 1 m of span ($S = 0.5 \text{ m}^2$) installed on an aircraft flying with an angle of attack $\alpha = 0.5^\circ$ (reg. 1 mm) ($\delta = 60^\circ$) at a constant speed ($M = 0.771$ and $\alpha = 0.5^\circ$, $p = 1013.3 \text{ Pa}$, and $V_\infty = 93.7 \text{ m/s}$). If this wing now morphs to an optimized laminar profile, a laminar regime enhancement from 0.22 to 0.42, t_c will result in more than a 15% drag decrease (from 0.0073 to 0.0051). Given these parameters, more than 16.7 kJ of energy per minute of flight can be saved. To obtain this economy, only 8.5 J of actuators' work input will be needed, which represents a tremendous potential gain.

IV. Conclusions

A finite element structural model of the active structure has been developed and an aerodynamic solver was used for the active structure efficiency evaluation. This preliminary analysis shows promising results that need to be validated through subsequent wind tunnel testing. This evaluation, though very simplistic, covers the path to further analyses that should take more parameters into account (e.g., type of airframe and its aero efficiency, weight of the actuators and their energy supply systems, reliability, manufacturing and maintenance cost, flight condition envelope, and frequency of morphing).

Acknowledgments

The authors would like to thank Conseil for Research and Innovation in Aerospace (Québec-CRIAQ), Natural Sciences and Engineering Research Council (NSERC), Rénier Inc. Aerospace, and Thales Canada for their financial support that made this research possible. The authors acknowledge G. H. Simon from Thales as the project initiator.

References

- Thill, C., Leduc, L., Daudé, L., Peter, K., and Weare, R., "Morphing Skins," *The Aerospace Journal*, Vol. 112, No. 1129, Mar. 2006, pp. 110–129.
- Brown, R. M., Medina, P., and Léveillé, D., "Morphing Flow Control for a Research Wing Project: Instabilities During a Three Year Period," 2007 Canadian Aerospace and Space Institute Annual General Meeting (CD ROM), Kanata, ONT, Canada, 25–26 Apr. 2007.
- Gauvin, T., Brzilewski, V., Come, D., and Tremblay, P., "Design Diagram for Linear SMA Actuators Integrated in a Morphing Wing Structure," *SMAS2007*, International Organization for Shape Memory and Superelastic Technologies, San Jose, CA, Dec. 2007, pp. 13–16.
- Come, D., Brzilewski, V., and Tremblay, P., "Optimal Design of an Active Structure for an Experimental Morphing Laminar Wing," *Aerospace Technology and Science* (submitted for publication).
- Faiss, L., Iacob, O., and Panazhchenko, I., "Optimized Laminar Flow Control on an Airfoil Using the Adaptive Wall Technique," 2007 45th Congress of the 19th Annual General Meeting (CD-ROM), Turin, Italy, 21–26 Apr. 2007.
- Graa, M., and Gaitonde, M. B., "Vortex-Deformation Analysis of Transonic and Low Reynolds Number Aerodynamics," *AIMA Journal*, Vol. 25, No. 3, 1987, pp. 1547–1555.
doi:10.2514/6-0789

LISTE DE RÉFÉRENCES BIBLIOGRAPHIQUES

- ACARE. 2001. *EUROPEAN AERONAUTICS: A VISION FOR 2020: Meeting society's needs and winning global leadership*. Coll. « Report of the group of personalities », Luxembourg: European Communities, 26 p.
- ACARE. 2009. « About ACARE: terms of reference ». In *The Advisory Council for Aeronautics Research in Europe website*. En ligne. <<http://www.acare4europe.com/html/tor.asp>>. Consulté le 14 avril 2010.
- Aéro-Montréal. 2010. « Communiqué de presse: Aéro Montréal se réjouit de l'annonce du gouvernement québécois de soutenir l'innovation aérospatiale ». En ligne. 2 p. <<http://www.gaiapresse.ca/images/nouvelles/15937.pdf>>. Consulté le 14 avril 2010.
- AirForce. 2007. *Mission Adaptive Compliant Wing*. Coll. « Air Force SBIR/STTR Innovation Story », AF98-180, Dayton (OH): Air Force SBIR Program, 2 p.
- Anderson, J. D. 2001. *Fundamentals of Aerodynamics*, 3^e édition. Coll. « Aeronautical and Aerospace Engineering ». Boston: McGraw-Hill Higher Education, 892 p.
- ATA. 2008. « Annual Crude Oil and Jet Fuel Prices ». In *Air Transport Association, Economics, Data and Analysis*. En ligne. <<http://www.airlines.org/Economics/DataAnalysis/Pages/AnnualCrudeOilandJetFuelPrices.aspx>>. Consulté le 16 avril 2010.
- Benkemoun, L. 2006. *Validation du comportement aérodynamique du profil WTEATE1*. Coll. « Rapport interne du projet CRIAQ 7.1 », Montréal: École de technologie supérieure, 10 p.
- Bernhard, R. J. 2005. « PARTNER: Partnership for air transportation noise and emissions reduction ». *TR News Magazine*, septembre-octobre 2005, n° 240, p. 10.
- Boria, F., B. Stanford, S. Bowman and P. Ifju. 2009. « Evolutionary Optimization of a Morphing Wing with Wind-Tunnel Hardware in the Loop ». *AIAA Journal*, vol. 47, n° 2, p. 399-409.
- Braslow, A. L. 1999. *A history of suction-type laminar-flow control with emphasis on flight research*. Coll. « Monographs in aerospace history », Numéro 13. Washington (DC): NASA history Division, 78 p.
- Brusati, M. 2007. « The Aeronautics Joint Technology Initiative “Clean Sky” ». En ligne. 18 p. <http://ec.europa.eu/research/transport/pdf/marco_brusati_en.pdf>. Consulté le 10 avril 2010.

- Campanile, L. F. and S. Anders. 2005. « Aerodynamic and aeroelastic amplification in adaptive belt-rib airfoils ». *Aerospace Science and Technology*, vol. 9, n° 1, p. 55-63.
- Campanile, L. F. and D. Sachau. 2000. « The belt-rib concept: a structronic approach to variable camber ». *Journal of Intelligent Material Systems and Structures*, vol. 11, n° 3, p. 215-24.
- Chandrasekhara, M. S., L. W. Carr, M. C. Wilder, M. C. Paulson and C. D. Sticht. 1997. « Design and development of a dynamically deforming leading edge airfoil for unsteady flow control ». In *Proceedings of the 1997 17th IEEE International Congress on Instrumentation in Aerospace Simulation Facilities, ICIASF*, (Pacific Grove, CA, USA, Sep 29-Oct 2 1997), p. 132-140. Piscataway, (NJ): IEEE.
- CLEANSKY. 2008. « What is the Clean Sky JTI? ». In *The CLEANSKY website*. En ligne. <http://www.cleansky.eu/index.php?arbo_id=35#top>. Consulté le 14th April 2010.
- CNRC-IRA. 2006. « 2 m x 3 m Wind Tunnel: Technical Specifications ». In *Le site du Conseil National de Recherche du Canada : Institut de Recherche en Aérospatiale*. En ligne. <<http://www.nrc-cnrc.gc.ca/fra/installations/ira/2x3/techniques.html>>. Consulté le 10 mai 2010.
- Coutu, D., V. Brailovski, V. Demers and P. Terriault. 2006. « The design diagram for optimal shape memory alloys (SMA) linear actuators ». In *Proceedings of 10th International Conference on New Actuators - ACTUATOR 2006*. (Bremen, Germany, 14-16 June 2006). Bremen : Messe Bremen GMBH.
- Coutu, D., V. Brailovski, P. Terriault and C. Fischer. 2007. « Experimental validation of the 3D numerical model for an adaptive laminar wing with flexible extrados ». In *Proceedings of 18th International Conference on Adaptive Structures and Technologies (ICAST '07)*. (Ottawa, Canada, 3-4-5 Oct. 2007,
- CRIAQ. 2006. « Amélioration de l'écoulement laminaire sur une voilure aéroélastique ». In *Le site du Consortium de Recherche et d'Innovation en Aérospatiale du Québec*. En ligne. <http://www.criaq.aero/Recherche/Ronde_2/7_1_vf.html>. Consulté le 18 février 2010.
- Dion, B., M. Lamoureux and S. Langevin. 2007. « Projets de recherche en partenariat confirmés entre mai 2006 et avril 2007 ». *L'ÉTS @ 360°*, Été 2007, n° 1, p. 8.
- Eggleston, B., R. J. D. Poole, D. J. Jones and M. Khalid. 1987. « Thick Supercritical Airfoil with Low Drag and Natural Laminar Flow ». *Journal of Aircraft*, vol. 24, n° 6, p. 405-411.
- Enviro.aero. 2008. « Technologie ». In *Le site Enviro.aero*. En ligne. <<http://fr.enviro.aero/innovation-technologique.aspx>>. Consulté le 14 avril 2010.

FlexSys_Inc. 2003. « Adaptive Leading and Trailing Edge Flaps ». In *Flexsys Inc. website*. En ligne. <<http://www.flxsys.com/Projects/MACW/Leading%20Edge/>>. Consulté le 25 février 2009.

GARDN. 2009. « Groupement Aéronautique de Recherche et Développement en eNvironnement ». En ligne. 2 p. <http://www.gardn.org/LinkClick.aspx?fileticket=2H8qSpky2dk%3d&tabid=36&language=f_r-CA>. Consulté le 14 avril 2010.

GIEC. 1992. *Climate Change 1992: The Supplementary Report to the IPCC Scientific Assessment*. Coll. « 1992 Supplementary Reports », Cambridge (Royaume-Uni): Groupe d’experts intergouvernemental sur l’évolution du climat, 200 p.

GIEC. 1999. *Aviation and the Global Atmosphere: summary for policymakers*. Coll. « IPCC special report », ISBN: 92-9169-. Geneva, Switzerland: Intergovernmental Panel on Climate Change, 12 p.

Hetrick, J. A., R. F. Osborn, S. Kota, P. M. Flick and D. B. Paul. 2007. « Flight testing of Mission Adaptive Compliant Wing ». In *Collection of Technical Papers - 48th AIAA/ASME/ASCE/AHS/ASC Structures, Structural Dynamics, and Materials Conference*, (Waikiki, HI, États-Unis, April 23-27th 2007), p. 92-109. Reston, VA: America Institute of Aerospace and Astronautics.

IATA. 2009. « The IATA Technology Roadmap Report, 3rd Edition ». En ligne. 50 p. <http://www.iata.org/NR/rdonlyres/8FC59023-919D-4719-8CEE-F20FF1BAB181/0/Technology_Roadmap_May2009.pdf>. Consulté le 10 mars 2009.

ICAO. 2009. *Résumé des délibérations: note présentée par le secrétariat*. Coll. « Réunion de haut niveau sur l’aviation internationale et les changements climatiques », HLM-ENV/09-WP/1. Montréal: Organisation de l’aviation civile internationale, 6 p.

Info.effeserre.free.fr. 2005. « Le forçage radiatif ». In *Le site d’information sur l’effet de serre !* En ligne. <http://info.effetserre.free.fr/Phenomene/Forcage_Radiatif.html>. Consulté le 21 mai 2010.

Levinsky, E. S. and R. L. Palko. 1982. « Tests of an improved, computer-controlled, self-optimizing, variable-geometry wing ». In Williamsburg, VA, USA, p. 215-223. AIAA (CP822).

Liebeck, R. H. and A. I. Ormsbee. 1970. « OPTIMIZATION OF AIRFOILS FOR MAXIMUM LIFT ». *Journal of Aircraft*, vol. 7, n° 5, p. 409-415.

Mackworth-Praed, B. 1990. *Aviation : the pioneer years*, Londre, (R-U): Studio Editions, p. 320.

- Mankins, J. C. 2009. « Technology readiness assessments: A retrospective ». *Acta Astronautica*, vol. 65, n° 9-10, p. 1216-1223.
- Morellon, É. 2010. « Développement d'actionneurs en alliage à mémoire de forme pour un prototype d'aile d'avion adaptative ». Mémoire de maîtrise en génie mécanique, Montréal, École de technologie supérieure, 114 p.
- Musée de l'air et de l'espace. 1992. *Pionniers du ciel*, Paris: Atlas p. 128.
- NASA. 1976. « F-111 TACT in flight ». In *Dryden Flight Research Center Photo Collection*. En ligne. <<http://www.dffrc.nasa.gov/Gallery/Photo/F-111TACT/HTML/ECN-5033.html>>. Consulté le 2 April 2010.
- Pagès, L., O. Trifu and I. Paraschivoiu. 2007. « Optimized laminar flow control on an airfoil using the adaptable wall technique ». In *2007 AERO Conference and 54th Annual General Meeting*. (Toronto, Ont., Canada, 24-26 avril 2007).
- Pingstone, A. 2007. « The position of the leading edge slats on an airliner (Airbus A310-300) ». In *Le site Wikipedia: dispositif hypersustentateur*. En ligne. <http://fr.wikipedia.org/wiki/Fichier:Wing_slat.600pix.jpg>. Consulté le 8 avril 2010.
- Rutherford, D. and M. Zeinali. 2009. « Efficiency Trends for New Commercial Jet Aircraft, 1960 to 2008 ». En ligne. 20 p. <http://pre2010.theicct.org/documents/ICCT_Aircraft_Efficiency_final.pdf>. Consulté le 10 mars 2010.
- Skalecky, J. 2008. « CLEEN Planned Solicitation ». En ligne. 20 p. <http://www.faa.gov/news/conferences_events/2008_market_research_conference/materials/media/CLEENPlannedSolicitation.pdf>. Consulté le 14 avril 2010.
- Strelec, J. K., D. C. Lagoudas, M. A. Khan and J. Yen. 2003. « Design and implementation of a shape memory alloy actuated reconfigurable airfoil ». *Journal of Intelligent Material Systems and Structures*, vol. 14, n° 4-5, p. 257-273.
- Transport Canada. 1998. *Manuel de Pilotage: avion*, 4 éd. Montréal, (Qc): Les Éditions de l'Homme, p. 237.
- Trifu, O. 2007. *Optimization of the upper side of the WTEATE1 airfoil*. Coll. « Rapport interne du projet CRIAQ 7.1 », Montréal: École Polytechnique de Montréal, 5 p.